Institute of Agricultural Sciences in the Tropics (Hans-Ruthenberg-Institute) (490)

University of Hohenheim

Crop Water Stress Management

Prof. Dr. Folkard Asch

Photosynthesis, quantum requirements, and energy demand for crop production in controlled environments

Dissertation

submitted in fulfilment of the regulations to acquire the degree "Doktor der Agrarwissenschaften"
(Dr.sc.agr. / Ph.D. in Agricultural Sciences)

to the

Faculty of Agricultural Sciences

presented by

Marc Schmierer

Stuttgart

2020

This thesis titled 'Photosynthesis, quantum requirements, and energy demand for crop production in controlled environments' was accepted as a doctoral dissertation in fulfilment of the requirement for the degree "Doktor der Agrarwissenschaften" by the Faculty of Agricultural Sciences at the University of Hohenheim on 10 June 2020.

Date of oral examination: 10 June 2020, Hohenheim

Examination Committee

Head of Committee: Prof. Dr. Uwe Ludewig

First Examiner and Supervisor: Prof. Dr. Folkard Asch

Second Examiner: Prof. Dr. Mathias Becker

Third Examiner: Prof. Dr. Joachim Müller

Table of contents

I

List of Figures

List of Tables

Summary

In this work, energy costs for LED (light emitting diodes) lighting of a virtual plant stand exhibiting C3-photosynthesis have been calculated via a model considering the quantum demand to build-up dry matter and energy efficiency of state-of-the art LEDs. Optimistic and pessimistic scenarios have been calculated by taking into account uncertainties regarding the H^+/ATP stoichiometry of photosynthesis and different management strategies for indoor plant production. Energy costs were between 265 and 606 kWh for a production cycle ranging over 100 days and resulting in 2500 g dry matter per square meter for the optimistic and the pessimistic scenario respectively. The conversion efficiencies from electrical energy to energy bound in phytomass at the end of the production cycle were 2.07 % and 4.72 % (pessimistic and optimistic scenario, respectively). This was lower than the theoretical maximum values calculated for C3 plants that are given as 9.5 % in the literature. However, when the losses that occur during the conversion from electrical energy to light energy were excluded and only the efficiency of the conversion from incident light energy to phyto-energy was calculated, values increased to 4.0 and 9.1 %. The differences between the optimistic and the pessimistic scenario was caused by decreased photorespiration via carbon dioxide fertilization, which increased the conversion efficiencies by 38 %, followed by different assumptions about the H^+ requirement for ATP production (34 %) and an increased rate of active absorption of light energy (24 %). Considering cumulative as well as feedback effects of all of the mentioned parameters, the conversion efficiency in the optimistic scenario was 2.3 times higher than in the pessimistic scenario. A system for measuring gas-exchange of whole plants or plant stands was developed in order to be able to investigate and improve the above mentioned management strategies in the future. CO_2 sensors and temperature and humidity sensors were used to detect water loss and CO_2. Readily available off-the-shelf electronic and mechanical materials were used in order to build a low-cost system that can be used in high throughput experiments. The results indicate that around 90 % of the transpirational water was detected by the system. We conclude that parts of the transpirational water condensed on the surfaces thus not leaving the chamber. When checking the accuracy of the H_2O and CO_2 sensors using an industry quality infrared gas analyser (IRGA), we found significant deviations from the values given by the IRGA and used this data for calibration of the CO_2 sensors. The responses of the CO_2-sensors were also linearly coupled to the H_2O concentrations (about -0.1 % ppm CO_2 / ppm H_2O). A regression analysis was performed and the coefficients were used to correct the sensor readings. Since LEDs exhibit a higher energy-to-light ratio when operated at lower light levels, we tested a very small growing gibberellin (GA) deficient super dwarf rice genotype in a climate chamber experiment under different illumination levels and different levels of nitrogen supply to assess its suitability for crop production in artificial environments. A 25 % reduction in illumination lead to a 75 % reduction in yield, mainly due to a 60 % reduction in formed tillers and 20 % reduction in kernel weight, and an 80 % reduction in illumination caused total yield loss. Whereas leaf area under reduced illumination was significantly lower, only marginal changes in the dimensions of single leaves were observed. Photosynthesis at growing light conditions was not different between control plants and

plants under 75 % illumination. This was explained by a higher photochemical efficiency under lower light conditions and a reduced mesophyll resistance. Therefore, we conclude that this genotype is an interesting candidate for crop production in vertical plant production systems, especially because of its short stature and the absence of shade avoidance mechanisms, such as leaf elongation, that would complicate production in small-height growing racks under low-light conditions. Nitrogen concentrations of 2.8 and 1.4 mmol L^{-1} in the nutrient solution lead to no differences in plant growth. We conclude that a nitrogen concentration of 1.4 mmol L^{-1} is sufficient for this genotype under the light intensities that were applied here. A software tool for simulations of photosynthesis in the python programming language was developed. The software implements a classical Farquhar-von Caemmerer-Berry (FvCB) model of leaf photosynthesis coupled with a model for the estimation of stomatal behaviour dependent on environmental conditions. We want to emphasize that the use of such models is essential to understand the complex interactions between plant growth, leaf photosynthesis and the environment. Knowledge on those relationships is the key to improve the efficiency of plant production in controlled environments.

Zusammenfassung

In dieser Arbeit wurden die Energiekosten für LED-Beleuchtung (Licht emittierende Dioden) eines virtuellen C3 Pflanzenstandes mit Hilfe eines Modells berechnet, das einerseits den Quantenbedarf für den Aufbau von pflanzlicher Trockenmasse und andererseits die Energieeffizienz von modernen LEDs berücksichtigt. Optimistische und pessimistische Szenarien wurden unter Berücksichtigung von Unsicherheiten bezüglich der H^+/ATP-Stöchiometrie der Photosynthese und verschiedener Managementstrategien für die Pflanzenproduktion in kontrollierten Umwelten berechnet. Die Energiekosten lagen zwischen 265 und 606 kWh für einen Produktionszyklus von 100 Tagen Länge und einem finalen Ertrag von 2500 g Trockenmasse pro Quadratmeter für das optimistische bzw. pessimistische Szenario. Die Umwandlungswirkungsgrade von elektrischer Energie in in Phytomasse gebundene Energie am Ende des Produktionszyklus betrugen 2,07 % und 4,72 % (pessimistisches und optimistisches Szenario). Dies war niedriger als die theoretischen Höchstwerte, die für C3-Pflanzen berechnet und in der Literatur mit 9,5 % angegeben werden. Wenn man jedoch die Verluste, die bei der Umwandlung von elektrischer Energie in Lichtenergie auftreten, ausschließt und nur die Effizienz der Umwandlung von einfallender Lichtenergie in Phytoenergie berechnet, stiegen die Werte auf 4,0 und 9,1 %. Die Unterschiede zwischen dem optimistischen und dem pessimistischen Szenario wurden durch eine verminderte Photorespiration durch Kohlendioxiddüngung verursacht, die die Umwandlungseffizienz um 38 % erhöhte, gefolgt von unterschiedlichen Annahmen über den H^+-Bedarf für die ATP-Produktion (34 %) und einer erhöhten Rate der aktiven Absorption von Lichtenergie (24 %). Berücksichtigt man sowohl kumulative als auch Rückkopplungseffekte aller genannten Parameter, war der Umwandlungswirkungsgrad im positiven Szenario 2,3 Mal höher als im pessimistischen Szenario. Ein System zur Messung des Gasaustausches von Pflanzen oder Pflanzenbeständen wurde entwickelt, um die oben genannten Managementstrategien in Zukunft zu untersuchen und zu verbessern. CO_2-Sensoren sowie Temperatur- und Feuchtigkeitssensoren wurden zur Messung von Wasserverlust und der CO_2 Aufnahme eingesetzt. Es wurden handelsübliche elektronische und mechanische Materialien verwendet, um ein kostengünstiges System zu entwerfen, das in Hochdurchsatzexperimenten eingesetzt werden kann. Die Ergebnisse zeigen, dass etwa 90 % des Transpirationswassers durch das System erfasst wurden. Wir schließen daraus, dass Teile des Transpirationswassers auf den Oberflächen kondensierten und somit das System nicht verließen. Bei der Überprüfung der Genauigkeit der H_2O- und CO_2-Sensoren mit einem Infrarot-Gasanalysator (IRGA) in Industriequalität fanden wir signifikante Abweichungen von den durch den IRGA angegebenen Werten und verwendeten diese Daten zur Kalibrierung der CO_2-Sensoren. Die Reaktionen der CO_2-Sensoren waren ebenfalls linear an die H_2O-Konzentrationen gekoppelt (ca. -0,1 % ppm CO_2 / ppm H_2O). Eine Regressionsanalyse wurde durchgeführt und die Koeffizienten wurden zur Korrektur der Sensorwerte verwendet. Da LEDs ein höheres Energie zu Licht-Verhältnis aufweisen, wenn sie bei niedrigeren Lichtstärken betrieben werden, testeten wir einen sehr kleinen wachsenden Gibberellin (GA) defizienten Super-Zwergreis-Genotyp in einem Klimakammerexperiment unter verschiedenen

Beleuchtungsstärken und unterschiedlicher Stickstoffzufuhr, um seine Eignung für den Pflanzenbau in künstlichen Umgebungen zu beurteilen. Eine 25 %ige Verringerung der Beleuchtung führte zu einer Ertragsreduzierung von 75 %, hauptsächlich aufgrund einer 60 %igen Verringerung Anzahl an geformten Bestockungstrieben und einer 20 %igen Verringerung des Korngewichts. Eine 80 %ige Verringerung der Beleuchtung verursachte einen Gesamtverlust bezüglich Kornertrag. Während die Blattfläche unter reduzierter Beleuchtung deutlich geringer war, wurden nur marginale Veränderungen in der Morphologie der Blätter beobachtet. Die Photosyntheseleistung in den jeweiligen Wachstumsbeleuchtungsstärken unterschied sich nicht zwischen Kontrollpflanzen und Pflanzen unter 75 % Beleuchtung. Dies wurde durch eine höhere photochemische Effizienz unter geringeren Lichtbedingungen und eine reduzierte Mesophyllresistenz erklärt. Daher kamen wir zu dem Schluss, dass dieser Genotyp ein interessanter Kandidat für die Pflanzenproduktion in Vertikalen Pflanzenproduktionssystemen ist, insbesondere wegen seiner kleinen Statur und dem Fehlen von Mechanismen zur Schattenvermeidung, wie z.B. Blattverlängerungsreaktionen, die die Produktion in niedrigen Produktionssystemen unter Schwachlichtbedingungen erschweren würden. Stickstoffkonzentrationen von 2,8 und 1,4 mmol L^{-1} führten nur zu marginalen Unterschieden im Pflanzenwachstum. Wir kommen zu dem Schluss, dass eine Stickstoffkonzentration von 1,4 mmol L^{-1} bei den hier angewandten Lichtintensitäten für diesen Genotyp ausreichend ist. Es wurde ein Software-Tool zur Simulation der Photosynthese in der Programmiersprache Python entwickelt. Die Software implementiert ein klassisches Farquhar-von-Caemmerer-Berry (FvCB)-Modell der Blattfotosynthese, gekoppelt mit einem Modell zur Abschätzung der stomatären Leitfähigkeit in Abhängigkeit von den Umweltbedingungen. Wir möchten betonen, dass die Verwendung solcher Modelle wesentlich ist, um die komplexen Wechselwirkungen zwischen Pflanzenwachstum, Blattfotosynthese und Umwelt zu verstehen. Kenntnisse über diese Beziehungen ist essentiell bezüglich der Erhöhung der Effizienz von Pflanzenproduktion in künstlichen Umwelten.

1. General Introduction

1.1. Background

The success of green revolution technologies after their introduction in the 1960s led to a massive increase in rice production in tropical Asia. In the following 40 years, expansion of growing areas and continuing technological improvements, especially the ongoing development of high yielding varieties that are robust against pests and diseases rendered it possible for the global rice production to keep up with population growth and changing food habits (Khush, 2005). However, the world population is predicted to reach 9.5 billion people in 2050, requiring a yearly increase in world rice production of more than 1 % (Normile, 2008; Rosegrant et al., 1995; United Nations, 2019). Since urbanization and land degradation will lead to a severe reduction in growing area in the coming decades, more rice must be produced on less land. In fact, rice yields have remained stagnant since the late 1990s and maximum on-farm yields do still not exceed 10 t/ha (Peng et al., 2009) and technologies like F_1-Hybridization or genetic engineering are being developed to break this so called 'yield barrier' (Jeon et al., 2011; Khush, 2005).

A different approach to deal with the increasing pressure on the global growing area are so called vertical, or controlled environment farming technologies. These technologies describe the production of plants in multi-storage facilities implementing high-level technologies for climate control, nutrient supply, and artificial lighting. The major advantage of such buildings is the higher land-use ratio since plants are produced on multiple storages. In the literature, such systems are often envisaged as hermetically sealed closed-loop systems thus requiring much less pesticides than free-air agriculture and exhibiting higher water- and nutrient-use efficiencies since waste, transpirational water and residual materials could be recycled and reinjected into the system (Banerjee and Adenaeuer, 2014; Despommier, 2011). Further benefits mentioned are lower risks of diseases and disasters. However, current implementations of vertical farms are far from that level of technological advancement and the available data suggests that the carbon footprints of these systems is much larger than compared to conventional free-air agriculture including up to 80 times higher energy demands (Beacham et al., 2019). However, in a feasibility study on rice production in plant factories, Yamori and Zhang (2014) summarized that such systems can play an important role in the future, especially in areas where environmental conditions are difficult and when the production of biopharmaceuticals by means of genetically engineered rice is considered. Moreover, due to economic reasons, currently operating systems are only used for the production of vegetables but the word's vegetable production covers only 4 percent of the global growing area compared to over 40 percent used for cereal production (Food and Agriculture Organization of the United Nations, 2018). Hence, to apply controlled vertical environment farming as a tool to reduce pressure from the global cropland, new technologies must be developed allowing energy efficient production of major cereals like rice in indoor growing facilities. Since there

is not much literature on cereal production in controlled environment farms, potential problems as well as costs and yields must be investigated and respective research instruments must be identified.

1.2. Potential yield and energy demand

Plants absorb sunlight and use its energy to assimilate CO_2 from the atmosphere into sugars in order to build up biomass and cover costs for respiration. In the field, the energy contained in a plant stand at the end of a cropping period ranges between 4 and 6 percent of the solar energy that reached the covered area during the same period (Loomis and Amthor, 1999). This is usually termed 'radiation use efficiency' (RUE). However, more than half of that energy cannot be converted to biomass since it is simply outside the photosynthetic active spectrum (PAR, 400 – 700 nm), meaning that the photon energy is either too high or too low to drive photosynthesis (McCree, 1972). Those losses can relatively easily be prevented by the use of Light Emitting Diodes (LEDs) that emit light in wavelengths exclusively inside the photosynthetic active spectrum. Further losses (~ 5 %) in free-air agriculture raise from reflection and transmission processes (Zhu et al., 2008). This means that sunlight is either not captured by the plant stand but absorbed by the soil or the plants reflect that radiation. Transmission processes occur mainly in the early development period when leaf area index (LAI) is small and thus ground cover is low. Technical systems that allow a dynamic adjustment of the planting density during the growing period could be used to keep these losses low. Losses due to reflection could be lowered by the use of wavelengths that are relatively weakly reflected by leaves, e.g. blue and red as it is already implemented in state of the art LED-panels for greenhouse and indoor production (Poulet et al., 2014). Further, light that is reflected or transmitted by the canopy could partly be recycled by covering floor, walls, and ceilings with highly reflecting surfaces.

Photorespiration causes further reductions in RUE. Photorespiration is the process of oxygen (O_2) assimilation during the light-independent reaction of photosynthesis and is usually considered a protection strategy during conditions of high light intensities and low CO_2 concentrations inside the leaf that can occur e.g. during hot and dry days (Bauwe et al., 2010) as a result of low stomatal conductance. Since O_2 is assimilated instead of CO_2 during photorespiration it is usually considered a constraint regarding productivity of a magnitude of around 20 % of the total carboxylation processes (Amthor, 2010). Because photorespiration is a function of the CO_2 concentration in the leaf, CO_2 fertilization is used in modern greenhouses to supress photorespiration and to increase productivity. This is an essential technical feature for any indoor plant production system.

Information about the energy demand for growth is important for the design of high efficiency indoor plant production systems. While the mechanistic process of photosynthesis and its stoichiometry is relatively well described (von Caemmerer and Farquhar, 1981), there are still some uncertainties concerning e.g. the H^+ demand for ATP production, the carbon costs for growth or maintenance

respiration (Loomis and Amthor, 1999). These uncertainties should be considered when estimating the energy demand for indoor plant production.

1.3. Measuring canopy gas exchange

Optimizing environmental factors for plant production is essential for establishing efficient indoor plant production systems. Optimization strategies should target on minimizing input costs in terms of light supply, thermal, and humidity management of the air and maximizing outputs in terms of yield. Since plants respond strongly to environmental factors, measuring photosynthesis and transpiration in real time is an essential tool for estimating the effects of e.g. different light environments. Such systems have been described formerly in the literature (Muller et al., 2009; van Iersel and Bugbee, 2000; Wünsche and Palmer, 1997). These systems usually utilize industry-quality equipment for data acquisition and logging, resulting in relatively high system costs. During the last years, low-cost physical computing platforms such as Arduino and single board computers like the Raspberry PI became popular among electronic enthusiasts and scientists. In science, these systems are widely used for several applications like monitoring air quality (Ali et al., 2016), robotics (Candelas et al., 2015) and control applications (Sobota et al., 2013). These systems could be extremely useful in plant physiology since they can easily control simple CO_2-sensors that are available for less than 100 € and combined temperature and humidity sensors (~20 €).

1.4. Model crops

Model organisms are an extremely useful tool in biology. In plant physiology genetics for example, major breakthroughs on questions about stress biology or genetic regulation of metabolic regulations have been achieved by research on the model plant *Arabidopsis thaliana* (Van Norman and Benfey, 2009). In rice science, the variety IR64 that was developed in 1985 by the International Rice Research Institute (IRRI) has been widely used as a check variety in a large number of experiments (Mackill and Khush, 2018). In 1999, Bugbee (Bugbee, 1999) suggested to develop model crops specifically for spaceflight experiments. The background of this idea is the fact that experimental units on space missions such as the International Space Station (ISS) are extremely space limited due to high costs of transport of materials into an earth orbit. The idea resulted in the development of several super-dwarf crops, amongst others peas (Romagnano et al., 2010), wheat (Bugbee et al., 1999) and rice (Frantz et al., 2004). The identified rice genotype was a gamma-ray mutant from the Konoshita Collection (Kinoshita and Shinbashi, 1982) that exhibits a maximum plant height of about 20 cm. Such crops are not only useful for space flight experiments but also for experiments on earth when available space is limited. This could be the case in e.g. climate chamber experiments or when measuring whole-plant photosynthesis in cuvettes. Hence, those super- dwarf crops could be interesting model crops for research targeting the optimization of light and climate conditions for indoor plant production systems. However, especially in the case of the GA-deficient super-dwarf rice it is unclear whether its peculiar

morphological characteristics affect the possibility to generalize experimental results obtained with this genotype.

Even though light is the energy source for photosynthesis and thus growth, it has been shown in several studies that higher irradiances do not necessarily result in higher growth rates and higher yield. In a study on rice for example, a reduction of growing light intensity from 1000 µmol m^{-2} s^{-1} PAR to 350 µmol m^{-2} s^{-1} did not lead to lower growth rates or lower rates of light saturated photosynthesis (Makino et al., 1997). The authors explained this finding to whole-plant morphological changes, especially a drastic reduction of starch and sucrose in leaves resulting in a higher leaf-area ratio that allowed for a much more efficient use of fixed carbon. However, this study also included several nitrogen levels and several light-nitrogen interactions were found. Leaf area of plants grown under 350 µmol m^{-2} s^{-1} for example was larger when nitrogen concentrations in the nutrient solution were 0.5 or 2 mM but was smaller compared to plants grown under 1000 µmol m^{-2} s^{-1} when N-concentration was as high as 8 mM.

On the other hand, in a multi genotype study, Wang et al. (2015) found that grain yield significantly dropped for all investigated genotypes when shading of 53% was applied. Further in a study about rice growth in vertical farms Yamori and Zhang (2014) summarized that even though higher light supply usually increases yield, light use efficiency (defined as g grain yield / kmol irradiated light) may be lower under lower light supply. This could be of importance when the economics of a vertical farm is of interest, since especially LEDs are more energy efficient when operating under lower light levels. Thus, reduction in light intensity could increase both the energy efficiency of the lighting system as well as the light use efficiency of the plant stand. This management strategy could easily be tested with the above mentioned super-dwarf rice genotype since a respective experiment could be carried with a low demand in growing space. Since Yamori and Zhang (2014) have pointed out that the size of a normal rice plant is one of the major constraint for growing rice in a state-of-the-art multi-level rack as they are used in current plant factories that produce vegetables, an extremely short growing rice genotype could be another interesting management strategy.

1.5. Modelling tools

The process of photosynthesis interacts with a couple of control mechanisms of the leaf, especially the dynamic responses of stomatal aperture to environmental conditions. This is usually taken into consideration by so called coupled models (Medlyn et al., 2011). Coupled models link the classic Farquhar-von Caemmerer-Berry model of photosynthesis with parametric models that describe the response of stoma to environmental conditions and photosynthesis itself. These models are essential for understanding plant-environment interactions. and They also help increasing radiation- and water-use efficiency since they offer insights in the complex response mechanisms of stomatal control and the

photosynthetic machinery to changes in environmental factors such as light, air humidity, and CO_2-concentration, which are fully controlled in indoor plant production systems and, thus, can be set to optimal values in terms of production efficiency.

The python programming language has become one of the worlds most used programming language since its introduction in 1995 (Oliphant, 2007; Van Rossum and Drake Jr, 1995) and has been used in many research fields ranging from astronomy to symbolic algebra (Meurer et al., 2017; Robitaille et al., 2013). An open-source implementation of a coupled model in python would allow easy integration of other modules e.g. symbolic math or available algorithms for control and feedback control systems thus decreasing the complexity and length of the source code. Further, such an implementation could in turn be integrated into models of higher scale, like ecosystems or, in this case, controlled environment farms.

1.6. Objectives

Hardly any literature exists on growth of major cereals like rice in controlled environments for staple food production. The main objective of this research is therefore to estimate the energy demand of such a production system and to develop research tools and strategies to optimize the efficiency and output for the specified systems. The specific objectives are:

- To estimate the energy demand for LED lighting systems for one production cycle of a major crop like rice
- To develop a low-cost system for measuring canopy photosynthesis under controlled environmental conditions that can be used to test optimization strategies for plant production regarding the light and atmospheric conditions
- To test a super-dwarf rice genotype for its suitability a model crop for research on controlled environment agriculture and to test its responses to low light levels and different nitrogen concentrations in the nutrient solution
- To implement a coupled A-g_s model in the Python programming language that can be used to elucidate complex plant-photosynthesis-environment interactions

Ali, A.S., Zanzinger, Z., Debose, D., Stephens, B., 2016. Open Source Building Science Sensors (OSBSS): A low-cost Arduino-based platform for long-term indoor environmental data collection. Build. Environ. 100, 114–126.

Amthor, J.S., 2010. From sunlight to phytomass: on the potential efficiency of converting solar radiation to phyto-energy. New Phytol. 188, 939–959.

Banerjee, C., Adenaeuer, L., 2014. Up, Up and Away! The Economics of Vertical Farming. J. Agric. Stud. 2, 40.

Bauwe, H., Hagemann, M., Fernie, A.R., 2010. Photorespiration: players, partners and origin. Trends Plant Sci.

Beacham, A.M., Vickers, L.H., Monaghan, J.M., 2019. Vertical farming: a summary of approaches to growing skywards. J. Hortic. Sci. Biotechnol.

Bugbee, B., 1999. Engineering plants for spaceflight environments. Gravitational Sp. Biol. Bull. 12, 67–74.

Bugbee, B., Koerner, G., Albrechtsen, R., Dewey, W., Clawson, S., 1999. "USU-Apogee" Wheat - Registration. Dwarf Crop.

Candelas, F.A., García, G.J., Puente, S., Pomares, J., Jara, C.A., Pérez, J., Mira, D., Torres, F., 2015. Experiences on using Arduino for laboratory experiments of Automatic Control and Robotics. IFAC-PapersOnLine 48, 105–110.

Despommier, D., 2011. The vertical farm: controlled environment agriculture carried out in tall buildings would create greater food safety and security for large urban populations. J. für Verbraucherschutz und Leb. 6, 233–236.

Food and Agriculture Organization of the United Nations, 2018. World food and agriculture : statistical pocketbook 2018. Rome, Italy.

Frantz, J.M., Pinnock, D., Klassen, S., Bugbee, B., 2004. Characterizing the Environmental Response of a Gibberellic Acid–Deficient Rice for Use as a Model Crop. Agron. J. 96, 1172–1181.

Jeon, J.-S., Jung, K.-H., Kim, H.-B., Suh, J.-P., Khush, G.S., 2011. Genetic and Molecular Insights into the Enhancement of Rice Yield Potential. J. Plant Biol. 54, 1–9.

Khush, G.S., 2005. What it will take to Feed 5.0 Billion Rice consumers in 2030. Plant Mol. Biol. 59, 1–6.

Kinoshita, T., Shinbashi, N., 1982. Identification of Dwarf Genes and Their Character Expression in

the Isogenic Background. Japanese J. Breed. 32, 219–231.

Loomis, R.S., Amthor, J.S., 1999. Yield potential, plant assimilatory capacity, and metabolic efficiencies. Crop Sci. 39, 1584–1596.

Mackill, D.J., Khush, G.S., 2018. IR64: a high-quality and high-yielding mega variety. Rice 11.

Makino, A., Sato, T., Nakano, H., Mae, T., 1997. Leaf photosynthesis, plant growth and nitrogen allocation in rice under different irradiances. Planta 203, 390–398.

McCree, K., 1972. The action spectrum, absorptance and quantum yield of photosynthesis in crop plants. Agric. Meteorol. 9, 191–216.

Medlyn, B.E., Duursma, R.A., Eamus, D., Ellsworth, D.S., Prentice, I.C., Barton, C.V.M., Crous, K.Y., De Angelis, P., Freeman, M., Wingate, L., 2011. Reconciling the optimal and empirical approaches to modelling stomatal conductance. Glob. Chang. Biol. 17, 2134–2144.

Meurer, A., Smith, C.P., Paprocki, M., Čertík, O., Kirpichev, S.B., Rocklin, M., Kumar, Am., Ivanov, S., Moore, J.K., Singh, S., Rathnayake, T., Vig, S., Granger, B.E., Muller, R.P., Bonazzi, F., Gupta, H., Vats, S., Johansson, F., Pedregosa, F., Curry, M.J., Terrel, A.R., Roučka, Š., Saboo, A., Fernando, I., Kulal, S., Cimrman, R., Scopatz, A., 2017. SymPy: symbolic computing in Python. PeerJ Comput. Sci. 3, e103.

Muller, J., Eschenroder, a, Diepenbrock, W., 2009. Through-flow chamber CO_2/H_2O canopy gas exchange system—Construction, microclimate, errors, and measurements in a barley (Hordeum vulgare L.) field. Agric. For. Meteorol. 149, 214–229.

Normile, D., 2008. Reinventing Rice to Feed the World. Science 321, 330–333.

Oliphant, T.E., 2007. Python for scientific computing. Comput. Sci. Eng. 9, 10–20.

Peng, S., Tang, Q., Zou, Y., 2009. Current Status and Challenges of Rice Production in China. Plant Prod. Sci. 12, 3–8.

Poulet, L., Massa, G.D., Morrow, R.C., Bourget, C.M., Wheeler, R.M., Mitchell, C.A., 2014. Significant reduction in energy for plant-growth lighting in space using targeted LED lighting and spectral manipulation. Life Sci. Sp. Res. 2, 43–53.

Robitaille, T.P., Tollerud, E.J., Greenfield, P., Droettboom, M., Bray, E., Aldcroft, T., Davis, M., Ginsburg, A., Price-Whelan, A.M., Kerzendorf, W.E., Conley, A., Crighton, N., Barbary, K., Muna, D., Ferguson, H., Grollier, F., Parikh, M.M., Nair, P.H., Günther, H.M., Deil, C., Woillez, J., Conseil, S., Kramer, R., Turner, J.E.H., Singer, L., Fox, R., Weaver, B.A., Zabalza, V.,

Edwards, Z.I., Azalee Bostroem, K., Burke, D.J., Casey, A.R., Crawford, S.M., Dencheva, N., Ely, J., Jenness, T., Labrie, K., Lim, P.L., Pierfederici, F., Pontzen, A., Ptak, A., Refsdal, B., Servillat, M., Streicher, O., 2013. Astropy: A community Python package for astronomy. Astron. Astrophys. 558, A33.

Romagnano, J., Mills, E., Bugbee, B., 2010. 'Earligreen' a Super-Dwarf Pea Cultivar for Use in Controlled Environment Research. Dwarf Crop.

Rosegrant, M.W., Sombilla, M.A., Perez, N., 1995. Global food projections to 2020: implications for investment, Food, Agriculture and the Environment Discussion Paper No. 5. IFPRI, Washington, DC.

Sobota, J., Pǐsl, R., Balda, P., Schlegel, M., 2013. Raspberry pi and arduino boards in control education. IFAC Proc. Vol. 10, 7–12.

United Nations, 2019. Selected Results of the 2019 UN World Population Projections. Popul. Dev. Rev. 45, 689–694.

van Iersel, M.W., Bugbee, B., 2000. A multiple chamber, semicontinuous, crop carbon dioxide exchange system: design, calibration, and data interpretation. J. Am. Soc. Hortic. Sci. 125, 86–92.

Van Norman, J.M., Benfey, P.N., 2009. Arabidopsis thaliana as a model organism in systems biology. Wiley Interdiscip. Rev. Syst. Biol. Med. 1, 372–379.

Van Rossum, G., Drake Jr, F.L., 1995. Python reference manual. Centrum voor Wiskunde en Informatica Amsterdam.

von Caemmerer, S., Farquhar, G.D., 1981. Some relationships between the biochemistry of photosynthesis and the gas exchange of leaves. Planta 153, 376–387.

Wang, L., Deng, F., Ren, W.J., 2015. Shading tolerance in rice is related to better light harvesting and use efficiency and grain filling rate during grain filling period. Field Crops Res. 180, 54–62.

Wünsche, J.N., Palmer, J.W., 1997. Portable through-flow cuvette system for measuring whole-canopy gas exchange of apple trees in the field. HortScience 32, 653–658.

Yamori, W., Zhang, G., 2014. Feasibility Study of Rice Growth in Plant Factories. Rice Res. Open Access 2, 1–6.

Zhu, X.-G., Long, S.P., Ort, D.R., 2008. What is the maximum efficiency with which photosynthesis can convert solar energy into biomass? Curr. Opin. Biotechnol. 19, 153–159.

2. Estimating the Quantum Requirements for Plant Growth and Related Electricity Demand for LED Lighting Systems

Marc Schmierer[1*], Holger Brueck[2], Folkard Asch[1], and Joachim Sauerborn[1]

1) Hans-Ruthenberg Institute of Agricultural Sciences in the Tropics, University of Hohenheim, 70599 Stuttgart, Germany 2)

2) Research Centre Hanninghof, Yara International, Dülmen

*Corresponding author: M. Schmierer (marc.schmierer@uni-hohenheim.de)

Abstract

Indoor plant production systems with artificial lighting are considered an emerging technology contributing to biomass based value webs. The viability of this concept greatly relies on the energy requirements (ER, Watt) for lighting. We estimated the ER for plant growth by calculating the conversion efficiency of electricity to light of solid-state light-emitting diodes (LED) and the quantum requirements for plant growth of a fictional plant stand producing 2 500 g of dry weight per m^2 of ground during 100 days. The quantum output (μmol s^{-1} W^{-1}) of eight LEDs of different colours varied between 0.78 for green and 2.54 for deep red. Uncertainty in the H$^+$ demand for ATP synthesis during photosynthesis, the relative portion of photorespiration and the fraction of light intercepted by plant canopies (f_{abs}) were considered in a pessimistic (PA) and optimistic (OA) approach of calculation of ER. Cumulative ER were 606 and 265 kWh m^{-2} for the PA and OA scenarios. The energy conversion efficiencies in the PA and OA scenarios were 2.07 and 4.72%. Estimates of energy savings by suppressing photorespiration and increasing f_{abs} vary between 24 and 38%. The peak daily ER were 9.44 and 4.14 kWh in the PA and OA scenarios. Results are discussed in the context of the design of lighting in indoor plant production systems and commercial greenhouses where natural fluctuation in solar radiation could be balanced by dimmable LED panels.

The 8.5 billion people living on Earth in 2030 as projected with the medium fertility variant by the United Nations (United Nations, 2019) will aggravate the threat of food shortage. Climate change (Lobell et al., 2008), regional shortfall of freshwater availability (Falkenmark et al., 1997), and the foreseeable decline in fossil oil (OECD/IEA, 2011) and high-grade rock phosphate resources (Cordell et al., 2009; Gilbert, 2009) will both amplify food insecurity and challenge presently existing concepts of food production. Rice, wheat, maize, and barley form the backbone of the global food processing value chain, and FAO estimates that annual world cereal production must increase by roughly 60% (Alexandratos and Bruinsma, 2003) to meet the projected demand in 2050. This requires extension of arable land area (including land conversion), intensification of production by an increased and more efficient use of resources, such as nutrients and water (Tilman et al., 2011), and substantial improvements in harvest, transport, and storage technologies. However, such an increase in production has to be considered in the context of the socio-economic framework conditions (Cohen, 1997) and the external costs (e.g., greenhouse gas emissions, loss of biodiversity) related to these measures (Balmford et al., 2002; Walsh, 1991).

Particularly external costs of food production stimulated concepts of plant cultivation in contained indoor systems. Research on indoor growth systems were initiated in frame of space flight missions and are, with less sophisticated control over environmental factors, going to be established in commercial factories focusing on high-value crops such as vegetables. A similar approach of plant cultivation is followed in proposed vertical farming concepts (Beacham et al., 2019; Despommier, 2011) and some authors have specifically mentioned rice as a target crop for indoor staple food production (Germer et al., 2011; Song et al., 2018). These concepts seek to illustrate the feasibility of partially substituting food production on arable land. A central feature of such visionary indoor plant production systems is the evaluation of related energy demand. Studies on energy demand have to consider energy expenditure for temperature and humidity control and lighting systems with the latter being the preponderant item of energy balance sheets for indoor plant factories.

Since the commercial release of the first red LEDs in 1968, the development of solid-state LEDs has progressed rapidly. Projections indicate that, due to energy savings, LEDs may displace all traditional lamps for general illumination within the next few decades (Haitz and Tsao, 2011). As compared with the successful implementation of solid-state LEDs in technical applications (e.g., indicator lights, room and street lighting, screens and flashlights), LED panels are still not widely used in greenhouses. While low radiant efficiency and the effects of light quality on growth and photo-morphogenesis of plants due to the few available wavelengths restricted use of first generation LEDs in greenhouses (Bula et al., 1991), current LED lighting systems for plant growth match high-pressure sodium (HPS) lamps in terms of electrical efficiency and light quality. In growth environments which exclusively rely on artificial lighting, LEDs could be a prime technology, especially since light intensity can be adjusted to the

plants' specific demand while thermal load for the plants is lower than with HPS lamps (Folta et al., 2005; Massa et al., 2008; Morrow, 2008).

Information about the plants' energy demand for growth is essential for future design of LED-based lighting systems. We present calculations of the quantum requirements for plant growth and combine this with related electric energy demand for indoor environments equipped with LED lighting. By using a standard data set of plant growth parameters, our approach allows for an approximate estimation of temporal dynamics of energy demand of LED lighting fields in indoor-growth environments.

2.1. Material and methods

Estimating cumulative electric energy requirements

The cumulative electric energy requirement (ER, Watt $(m^2$ ground)$^{-1}$) is here defined as the ratio of the quantum requirements (QR, mol quanta $(m^2$ ground)$^{-1}$) for the built-up of dry mass over time and the conversion efficiency of electricity to light (CO_{Eff}, mol quanta Watt^{-1}) and can be calculated by Eq. 1.

$$ER = QR / CO_{Eff} \qquad \text{Eq. [1].}$$

Estimating quantum requirements (QR)

QR was calculated according to Eq. 2:

$$QR = (dY * GLU_{reqG.} + Y * GLU_{reqM.}) * 0.0\overline{3} * (a + b\Phi) * (1 + 1 - f_{abs}) \qquad \text{Eq. [2],}$$

where construction costs for daily dry weight formation (dY, g DW $(m^2$ ground)$^{-1}$ day^{-1}) are expressed in glucose requirements ($GLU_{reqG.}$, g glucose (g DW)$^{-1}$). Carbon costs for maintenance respiration ($GLU_{reqM.}$, g glucose (g DW)$^{-1}$) are related to standing biomass (Y, g DW $(m^2$ ground)$^{-1}$) and $0.0\overline{3}$ is a conversion factor from g glucose to mol C considering the molar stoichiometry of carbon and glucose ($72 / 180 = 0.4$) and the conversion from g C to mol C ($0.4 / 12 = 0.0\overline{3}$). The conversion from glucose

to mol C is necessary for calculating daily QR for carboxylation which is defined by the term $(a + b\Phi)$ and depends on the relative rate of oxygenation to carboxylation (Φ). The term f_{abs} is the portion of incident light which is absorbed and used in photosynthesis by the plant canopy. E.g., with a value of f_{abs} of 0.8, the term $1 + 1 - f_{abs}$ is 1.2, indicating that QR is 20% higher than if it were in a situation of complete absorption of quanta by the plant surface.

QR was calculated for a fictional plant stand producing 2 500 g DW $(m^2 \text{ ground})^{-1}$ over 100 days. Assuming that 500 g of DW are invested in the root system (relative root allocation factor of 0.2) and the harvest index of plants is 0.5, the cumulative DW formation over the growth period represents a fictional grain yield of 1 000 g $(m^2 \text{ ground})^{-1}$. This yield level was chosen as a high productivity benchmark of field crops such as rice and wheat. QR varies over time as growth rate and chemical composition of plants change. In order to consider this, a fictional growth dynamic of a plant stand was calculated with the symmetric expolinear function suggested by Goudriaan, cited in Yin et al. (2003):

$$dY = \frac{c_m}{r_m} \, ln \, \frac{1 + e^{r_m (t - t_o)}}{1 + e^{r_m (t - t_o - w_{max}/c_m)}} \quad \text{Eq. [3].}$$

Values used were 40 for the maximum growth rate c_m, 0.2 for the maximum relative growth rate in the expolinear phase r_m, 20 for the time when linear growth begins, t_o, and 2 500 for final weight w_{max}.

Carbon costs for growth (GLU_{ReqG}) were calculated from information about ash-free heat of combustion (ΔH_C, J kJ^{-1}) of grain (18.5), stem (17.5) and root (16.5) (Amthor, 2010) according to Griffin (Griffin, 1994):

$$GLU_{ReqG} = [\, (0.06968 \, \Delta H_C - 0.065)(1 - AC) + 7.5 \, (k_N / 14.0067) \,] \, (\, 1 / E_g) \quad \text{Eq. [4],}$$

with ash content (AC, g g^{-1}) of grain (0.015) and straw (0.044) taken from Jørgensen et al. (2007). The straw data were assumed to represent those of leaf, stem and root tissue. N content (g g^{-1}), in a simplified approach, was assumed to be constant over time with values of 0.04 (leaf) and 0.02 (root, stem, grain). A k_N value (considering costs of N assimilation) of 5 (sole nitrate-N supply) and $E_g = 0.87$ were used (see (Griffin, 1994)). The assumed $GLU_{Req.}$ were 1.287, 1.219, and 1.149 g Glucose (g DW)$^{-1}$ for grain, stem and root tissue, respectively. Experimental estimates of maintenance respiration rates vary from 15-50 mg Glu g^{-1} DW day^{-1} (Loomis and Amthor, 1999). We took a value of 30 mg Glu g^{-1} DW.

Calculations of daily QR are uncertain with regard to 'true' values listed in Eq. 2. Uncertainty arises from factors which can be technically manipulated such as the environmental CO_2 concentration (variable rate of oxygenation to carboxylation, Φ) as well as the fraction of light absorbed by the plant canopy (f_{abs}). Additionally, uncertainty in QR exists as 'true' quantum costs for production of energy and reducing equivalents is not clear. This is considered by a pessimistic (PA) and optimistic (OA) approach (see Table 1 and text below).

Carbon demand for growth and maintenance is equivalent to the required rate of carboxylation, V_C per unit ground area, which can be expressed as $(a + b\Phi)$. This term quantifies the required production rates of energy- (ATP) and reducing equivalents (NAD(P)H sustaining the rates of carboxylation and oxygenation according to von Caemmerer & Farquhar (1981). The required rate of ATP consumption is $(3 + 3.5\Phi)V_C$. We assumed that either three or four H^+ are required for the synthesis of 1 ATP (Sacksteder et al., 2000). Consequently, rates of proton production were $(9 + 10.5\Phi)V_C$ or $(12 + 13.5\Phi)V_C$ in the optimistic and pessimistic approaches, respectively (Table 1). Relative rates of photorespiration (Φ) were assumed to be 0.28 or 0.05 under ambient or high atmospheric CO_2 concentrations, respectively with the ambient CO_2 concentration used in the PA scenario. The fraction of quanta which are absorbed by leaves (f_{abs}) depends on reflective properties of the leaf surface and the absorption efficiency which depends on pigment density (Evans and Poorter, 2001). An additional source of inefficient quanta absorption is the portion of ground coverage and reflective properties of the ground surface. In the OA scenario we assume a fraction of absorbed quanta of 0.95 which would represent an optimized indoor design with permanent complete ground cover and use of highly reflective material of the growth chamber inner surfaces. A value of 0.70 was assumed in the PA scenario. This value is representative for field crops which do not reach full canopy cover. In indoor systems such low values could be realized if floor or wall material is not highly reflective.

Conversion efficiency of electricity to biomass (ε; J / kJ) was calculated by dividing the cumulated energy of plant biomass by the electricity demand for LED lighting. An energy content of 18.1 kJ (g DW)$^{-1}$ (Jørgensen et al., 2007) was assumed for plant biomass.

Calculation of conversion efficiency of electricity to light of LEDs (CO$_{Eff}$)

LED suppliers usually specify the efficacy of illuminants in terms of the photometric luminous flux. For the calculation of photosynthetically active quanta (μmol PPFD m^{-2} s^{-1}), we first converted the photometric luminous flux to the physical luminous flux. The relationship between photometric and physical luminous flux is given by:

$$\Phi_v = K_m \int_{380nm}^{780nm} \frac{de^{(\lambda)}}{d\lambda} * V(\lambda)d\lambda \qquad \text{Eq. [5]},$$

where Φ_v is the photometric luminous flux in Watt, Φ_e is the physical luminous flux in Lumen for a specific wavelength λ and $V(\lambda)$ is the luminous efficiency function of the human eye (photopic) in Lumen per Watt with its highest value K_m of 683.002 l/W at a wavelength of 555 nm.

For the conversion, we determined the relative spectral power distribution $S(\lambda)$ of a LED spectra reported in specific datasheets of Osram (Osram Opto Semiconductors GmbH & Co., Regensburg, Germany). The graph of the spectral distribution from the datasheet was converted to a monochromatic image and the numerical values of the distribution were estimated by self-written software with a resolution of 1 nm. The total physical luminous flux of the LED was then calculated according to Eq 6:

$$\Phi_e = \frac{\Phi_v}{\sum_{380nm}^{780nm} K_m * V(\lambda) * S(\lambda)} \qquad \text{Eq. [6]},$$

with ϕ_v given in the specific datasheet. Subsequently, $\phi_e(\lambda)$ was calculated by multiplying the relative spectral power distribution $S(\lambda)$ for each wavelength with the formerly calculated total physical luminous flux of the illuminant.

For the calculation of photosynthetically active quanta, the photonic energy per wavelength was calculated as:

$$E = \phi * \frac{hc}{\lambda} \qquad \text{Eq. [7]},$$

where h is the Planck constant and c is the speed of light. The number of quanta per wavelength was calculated by dividing the numerical values of the power distribution for each wavelength by the dedicated photonic energy. Finally, the number of photosynthetically active quanta was calculated by integrating all photons between 400 and 700 nm.

As an example, for Cool White LEDs from the OSLON SSL (LUW CQDP (EQW)), Osram Opto Semiconductors GmbH & Co., Regensburg, Germany), the published data sheet (available on

http://www.osram-os.com) specifies a ϕ_v of 130 Lumen for test conditions of 350 mA forward current and 3.2 Volt forward voltage (1.12 Watt). The image from the graph of the typical relative spectral emission between 380 and 780 nm on page 9 of the data sheet was converted (The GIMP, The GIMP Development Team) to a monochromatic image. The image was analyzed by self-written software to obtain numerical values (in pixel) for each wavelength with a resolution of 1 nm. Next, the relative spectral power distribution $S(\lambda)$ was constructed by dividing the values for each nm by the highest value of the entire spectra. The resulting values were summed and each single value divided by the sum, thereby normalizing the spectrum to a value of one and distributing this value across the whole spectrum. In order to obtain the efficiency of the LED, we calculated Φ_v according to Eq. 5 and found $\Phi_v = 0.35$ Watt. Since this is the radiant power at 1.12 electrical Watt, the actual radiation efficiency of the LED is 0.31 Watt of radiation power per electrical Watt. Using $S(\lambda)$ again, we distributed the 0.31 Watt of radiant power that is emitted per 1 Watt electrical power via the spectrum, giving the radiant power that is emitted per nm waveband in Watt. These values can be transferred into eV s^{-1}, and the number of photons emitted per second was calculated with respect to the wavelength specific photonic energy. For example, at a wavelength of 600 nm, we found 7.54×10^{-3} μmol of photons emitted per second per Watt. The sum of all plant-usable photons between 400 and 700 nm was 1.41 μmol emitted by this LED per second per Watt.

It should be noted that the brightness values given in the datasheets are typical values measured under the specified test conditions. For detailed information about test conditions and measuring inaccuracy see footnotes 1) and 6) on page 24 of the datasheet. Due to production related fluctuations in certain LED parameters such as peak wavelength and optical flux, LEDs from a particular model are usually classified into different wavelength and brightness groups. The values presented in this paper usually refer to LEDs that are specified as 'typical' in the data sheets.

The software for the estimation of the relative spectral power distribution from the LED datasheets was written in C++. For image analysis, we used the Qimage class provided by the Qt framework version 4.7.4 (https://www.qt.io/). Binaries and source code are available from the authors on request. Information about 4 LED types and a combination from deep red and deep blue LEDs and for High Pressure Sodium (SON-T 400 W, PHILIPS, The Netherlands) are summarized in Table 2. The quantum output for LEDs was calculated for different colours and varied between 0.83 for true green and 2.64 for deep red. Calculations are presented for HPS lamps, cool white LEDs, and a combination of deep red and blue LEDs with a red:blue photon ratio of 5:1. Distribution of electrical energy between deep red and blue LEDs was 4.29:1. For the calculation of energy requirement, LED efficiency was recalculated to operating temperatures at 60° C as stated in the datasheets.

2.2. Results and Discussion

The ER of indoor plant production systems with exclusive LED lighting have not been reported so far. The cumulative ER per unit ground area with exclusive LED lighting is, according to our estimates, between 265 and 606 kWh for a growth cycle of 100 days and 2 500 g DW production (Table 3). The calculated ER can be used for dimensioning energy supply systems required to power LED lighting fields of indoor plant production units like those intensively investigated in the context of controlled environment life support systems (Bugbee, 1992) and vertical farming concepts (see Introduction).

The pronounced differences in ER between the two scenario calculations indicate that, by a combination of management practices such as CO_2 enrichment and use of reflective materials, substantial energy savings can be achieved. The peak daily ER were 9.44 and 4.14 kWh m^{-2} in the PA and OA scenarios, respectively, and were substantially lower at the beginning and end of the growth cycle. This highly dynamic ER during the growth cycle suggests that LED lighting fields should be designed to meet this variable and plant growth stage-specific energy supply. This could be a significant contribution to energy saving in greenhouses and indoor plant growth systems and could be achieved by either diming LED light field or by moving plants into demand-defined light environment supplied by LED panels in separate sectors of the indoor growth facility. This could further include the option of supplying spectrally different light composition and, by that, exploiting ontogenetic-specific photo-morphogenetic effects.

A theoretical maximum energy conversion efficiency of photosynthetically active light (400-740 nm) at the plant surface of C3 plants of 9.5% (Amthor, 2010; Zhu et al., 2008) has been derived from consideration of biophysical and –chemical principles of CO_2 assimilation. Relating the time-integrated energy accumulation of the scenario crop to the electric energy demand, the energy conversion efficiencies in the PA and OA scenarios were 2.07 and 4.72 %. These values are unavoidably lower than the theoretical maximum energy conversion efficiency due to the energy losses along the physical transformation of electricity to quanta. LEDs vary in efficiency of plant-available Watt per Watt of electricity and in CO_{Eff}, with lower values of true green LEDs and the highest in Deep Red and Blue LEDs (Table 2).

As indicated by differences in ER of the PA and OA scenarios by varying f$_{PAR}$ and the ratio of carboxylation to oxygenation (Φ), technical options are relevant for energy savings. High CO_2 environments are commercially used in order to suppress photorespiration. By reducing Φ from 0.28 to 0.05, the ER was reduced from 606 to 437 kWh m^{-2} and ε increased by 38% (Figure 2). Although high CO_2 environments appear as a feasible option for reducing energy costs and water requirements, the role of photorespiration in stress tolerance (Bauwe et al., 2010) and putative effects of CO_2 enrichment

16

on nutrient uptake and assimilation, and grain composition and quality (Erda et al., 2005; Fangmeier et al., 1999) must be considered in an integrated management approach.

The absorption of light by the plant canopy (f_{abs}) is relevant for the system's ER as an increase of f_{abs} from 0.70 to 0.95 increased ε by 24% (Figure 2). As summarized in Amthor (2010), dense canopies might absorb 90-95% of photosynthetic active radiation (PAR), but so called inactive PAR absorption by pigments not involved in photosynthetic carbon assimilation may reduce the effective absorption to a certain, yet not well quantified, extent. A value of 0.95 in the OA scenario would imply that all quanta emitted by LEDs were absorbed by leaves and that only 5% of quanta lost by conversion to heat and fluorescence. In order to minimize unproductive losses of light in greenhouses or indoor factories, plant density should be adjustable over the growth period to maximize canopy cover during the growth period. Secondly, the use of highly reflective surfaces surrounding plants can minimize losses by reflectance of plant canopies and increase the fraction of diffuse light. As shown by Tubiello et al. (1997), high levels of diffuse light can increase radiation-use efficiency (RUE) by equalizing the high and low radiation levels at the upper and lower layers of the canopy, respectively. However, given that newer findings by Brodersen et al. (2008) suggest an increase of leaf level photosynthesis under high direct light levels compared to equal irradiances of diffuse light for high light grown leaves, it seems plausible to focus on the development of an integrated lighting environment with respect to both the position of the light sources as well as to the light-directional quality. Technically, all the management options are feasible.

Temperature control is one of the major items of energy balance sheets in greenhouse and indoor plant factory management and has not been assessed in our calculations. Calculated energy requirements cannot be considered as a fixed value under variable environmental temperatures since, due to temperature effects on solubility of gases, high temperature environments will increase the quantum requirements by higher rates of photorespiration (see

Amthor (2010) for details). Although technical aspects of temperature control and related energy costs are not considered here, the relevance is not at all questioned.

Additionally, to technical options for minimizing ER, some bio-physical processes of plant growth are highly relevant to improve estimates of real ER. Firstly, the quantum requirement is under debate as electron transport in the light reaction part of photosynthesis is apparently not simply a linear transport but has a constitutive or facultative operation of cyclic electron flow. Furthermore, the costs of ATP synthesis are not clear but transport of four H^+ through the chloroplastic ATP synthase may be required per ATP with up to 12 H^+ transported into the thylakoid lumen per 8 quanta absorbed (Amthor, 2010; Sacksteder et al., 2000). In our PA and OA scenarios, 15.78 and 11.94 quanta per rate of carboxylation would be required, estimates which are higher (PA) or comparable (OA) to the estimates used by

Amthor (2010). Clarification of the quanta/ATP stoichiometry is not only of scientific interest but affects the QR and thus ER for LED based lighting systems. ER would decrease from 606 (PA) to 458 kWh m^{-2} if proton costs for ATP synthesis were lower than assumed in the PA scenario. Notably our approach differs from that usually used as we preferred the ATP- over the NADPH-limited version. By this we explicitly exclude the possibility of ATP import into the chloroplasts during the light phase and assume that the surplus of reducing equivalents is exported to the cytosol via the malate/oxalacetate shuttle (Scheibe, 2004).

Maintenance respiration is a significant component of the plant's carbon economy and conceptually reflects all carbon costs related to ensure functionality of cells in terms of membrane potentials, pH regulation, de-toxification, and repair and turnover of structure and enzymes. Though clear in a biological sense, estimates of carbon costs of maintenance are methodologically difficult but are roughly of similar cumulative glucose requirements than those invested in growth respiration over a complete growth cycle (Loomis and Amthor, 1999). In consideration of the functions supported by maintenance respiration, costs are evidently not constant per unit plant DW but expected to increase in stressful environments, with increasing N content of tissue and towards maturity. Relevance of maintenance respiration in our calculations is indicated by the peak energy demand at 73 days after sowing, while peak growth rate occurred at 52 DAS. This is due to the increasing relevance of maintenance respiration with plant age, keeping the ER at 100 DAS at high values. We likely overestimate cumulative ER in both scenarios as senescence of plant tissue and re-translocation from vegetative organs to grain will reduce ER during the generative growth phase.

2.3. Conclusions

The calculation of ER as outlined can be applied to any crop once the growth dynamics and energy content of plant organs is known, which often is the case. Unlike other lighting systems, LEDs are easily dimmable and can therefore be adjusted to the plants' demand which could substantially reduce energy costs. The basic approach of our calculations is valid for any vertical farming concept and already existing greenhouses. Relevance of our findings is highest for concepts of completely self-contained growth environments, since in traditional greenhouses the energy demand for thermal control is more relevant than energy requirements for lighting. Logically, hybrid systems with transitory supply of light through transparent surfaces will reduce the energy estimates of our study. With a more consolidated understanding of energy demand and conversion efficiency by plants, the construction of appropriate LED-based light fields should be possible. However, and as indicated by our consideration of pessimistic and optimistic approaches, the design of environmental conditions in sealed systems is far from trivial and plants are transferred into a combination of bio-physical factors (e.g., permanent light

and high CO_2) for which information is sparse in terms of presently used mechanistic plant growth models.
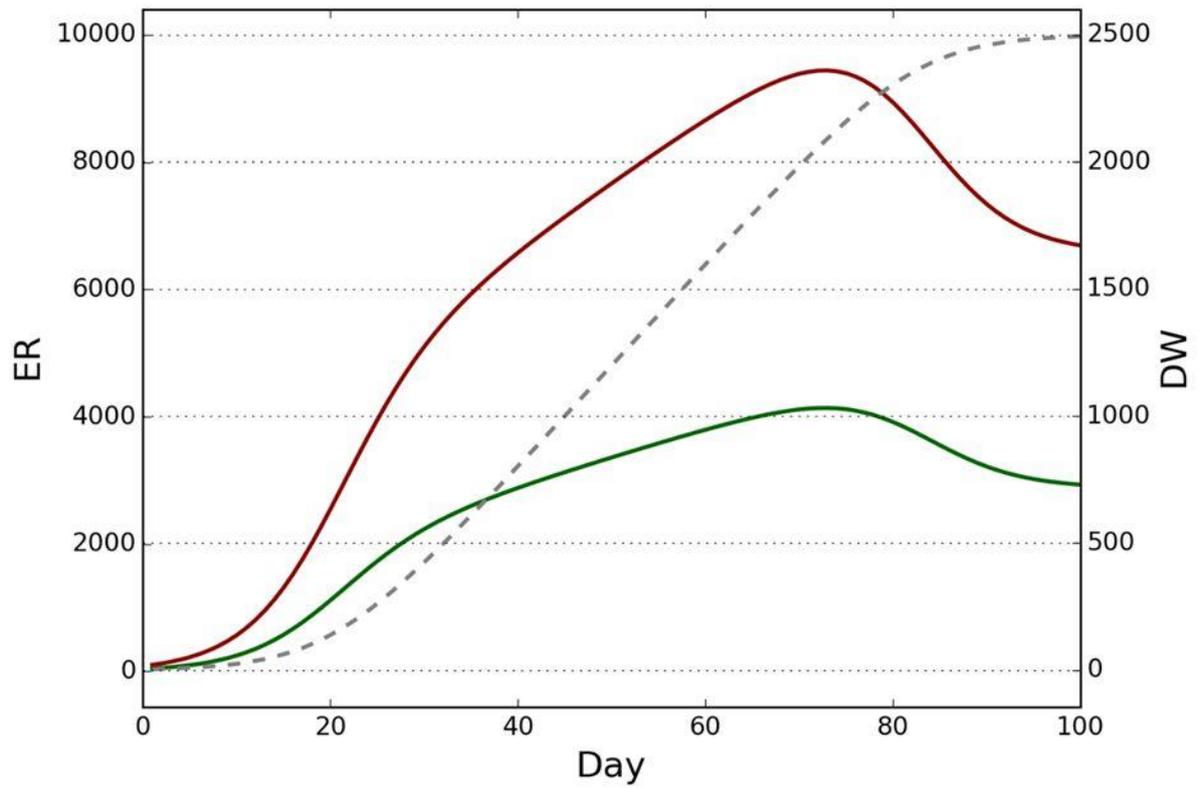
Figure 1: Temporal dynamics of dry mass formation (DW, g m-2; broken line), and energy requirements (ER, kWh (m2 ground)-1 day-1) of the fictional plant stand. ER were calculated with the optimistic (OA, green line) and pessimistic (PA, red line) approach as outlined in Table 1
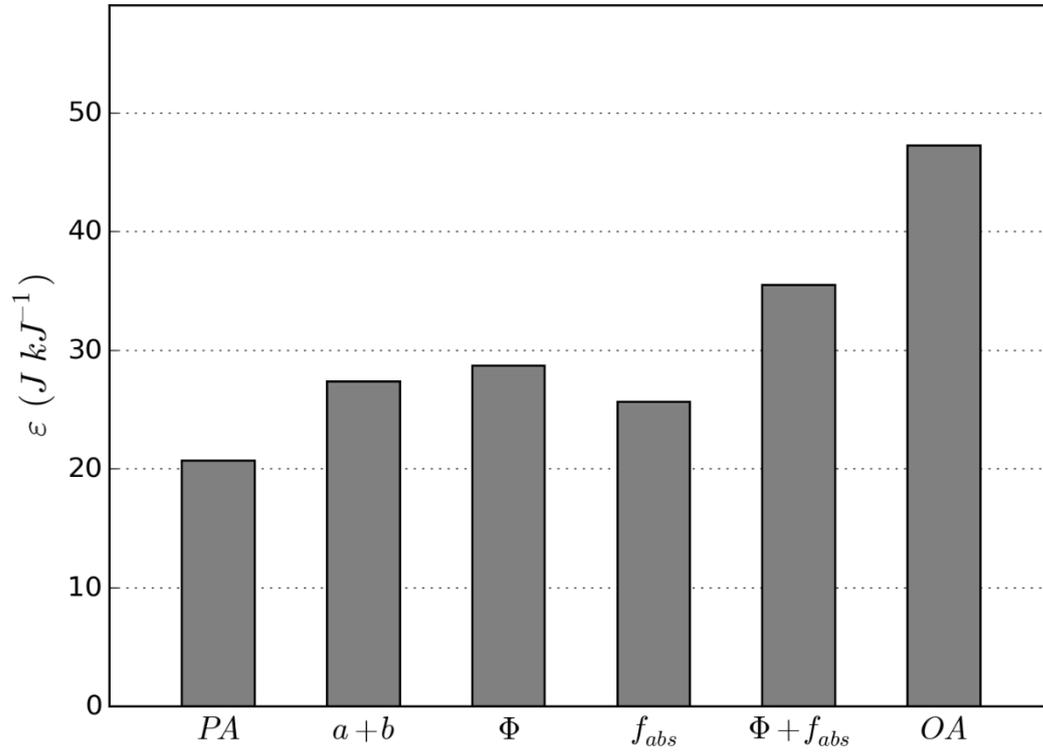
Figure 2: The energy conversion efficiencies of a fictional plant stand producing 2 500 g total DW m-2 during a growth cycle of 100 days. Calculations are based on the pessimistic approach (PA), and stepwise changes in parameters listed in Table 1 under the optimistic approach (OA), or with all parameters changed according to the OA scenario.

Table 1: Coefficients for calculating the quantum requirements (a, b), the ratio of oxygenation to carboxylation (Φ) and the fraction of light absorbed by leaves (fabs) in the pessimistic (PA) and optimistic (OA) approach.

Scenario	a	b	Φ	$f_{abs.}$
	------- dim.less. --------			
PA	12	13.5	0.28	0.70
OA	9	10.5	0.05	0.95

Table 2: Peak wavelength (λ_{peak}), efficiency (W plant available per W of electricity) and photon conversion efficiency of electricity to quanta (CO_{Eff}, 400 – 700 nm) of 5 different commercially available LEDs LEDs at typical test conditions (forward current:350 mA, temperature: 25 °C), a combination of deep red and deep blue and a High Pressure Sodium lamp (SON-T, 400 W).

Visible Color	λ_{peak}	Efficiency	$CO_{Eff.}$
	nm	W W^{-1}	µmol J^{-1}
Hyper Red	660	0.46	2.55
Blue	470	0.57	2.18
Deep Blue	451	0.50	1.89
True Green	521	0.18	0.78
Cool White	445 / 555	0.28	1.35
Hyper Red:Blue (5:1)	470 / 660	0.48	2.47
HPS (SON-T, 400 W)	n.a.	0.29	1.53

Table 3: Cumulative energy requirement (ER) for a dry weight formation of 2 500 g m^{-2} during a crop growth cycle of 100 days for plants growing in an indoor system under a the PA/ OA scenarios as described in Table 1. Calculations were based on $CO_{Eff.}$ of the a combination of deep red and blue LEDs with a red:blue photon ratio of 5:1 (Osram Opto Semiconductors GmbH & Co., Regensburg, Germany) (see Table 2).

ER	PA	a + b	Φ	f_{abs}	Φ + f_{abs}	OA
kWh m^{-2}	606	458	437	489	353	265

2.4. References

Alexandratos, N., Bruinsma, J., 2003. World agriculture towards 2030/2050: the 2012 revision. ESA Working paper No. 12-03. FAO, Rome.

Amthor, J.S., 2010. From sunlight to phytomass: on the potential efficiency of converting solar radiation to phyto-energy. New Phytol. 188, 939–959. doi:10.1111/j.1469-8137.2010.03505.x

Balmford, A., Bruner, A., Cooper, P., Costanza, R., Farber, S., Green, R.E., Jenkins, M., Jefferiss, P., Jessamy, V., Madden, J., Munro, K., Myers, N., Naeem, S., Paavola, J., Rayment, M., Rosendo, S., Roughgarden, J., Trumper, K., Turner, R.K., 2002. Economic reasons for conserving wild nature. Science 297, 950–953. doi:10.1126/science.1073947

Bauwe, H., Hagemann, M., Fernie, A.R., 2010. Photorespiration: players, partners and origin. Trends Plant Sci. doi:10.1016/j.tplants.2010.03.006

Beacham, A.M., Vickers, L.H., Monaghan, J.M., 2019. Vertical farming: a summary of approaches to growing skywards. J. Hortic. Sci. Biotechnol. doi:10.1080/14620316.2019.1574214

Brodersen, C.R., Vogelmann, T.C., Williams, W.E., Gorton, H.L., 2008. A new paradigm in leaf-level photosynthesis: direct and diffuse lights are not equal. Plant. Cell Environ. 31, 159–164. doi:10.1111/j.1365-3040.2007.01751.x

Bugbee, B., 1992. Determining the potential productivity of food crops in controlled environments. Adv. Space Res. 12, 85–95. doi:-O10.1016/0273-1177(92)90014-O

Bula, R.J., Morrow, R.C., Tibbitts, T.W., Barta, D.J., Ignatius, R.W., Martin, T.S., 1991. Light-emitting diodes as a radiation source for plants. HortScience 26, 203–205.

Cohen, J.E., 1997. Population, Economics, Environment and culture: an introduction to Human Carrying Capacity. J. Appl. Ecol. 34, 1325–1333. doi:10.2307/2405250

Cordell, D., Drangert, J., White, S., 2009. The story of phosphorus: global food security and food for thought. Glob. Environ. Chang. 19, 292–305.

Despommier, D., 2011. The vertical farm: controlled environment agriculture carried out in tall buildings would create greater food safety and security for large urban populations. J. für Verbraucherschutz und Leb. 6, 233–236. doi:10.1007/s00003-010-0654-3

Erda, L., Wei, X., Hui, J., Yinlong, X., Yue, L., Liping, B., Liyong, X., 2005. Climate change impacts on crop yield and quality with CO_2 fertilization in China. Philos. Trans. R. Soc. B Biol. Sci. 360, 2149–2154. doi:10.1098/rstb.2005.1743

Evans, J.R., Poorter, H., 2001. Photosynthetic acclimation of plants to growth irradiance: the relative importance of specific leaf area and nitrogen partitioning in maximizing carbon gain. Plant Cell Environ. 24, 755–767. doi:10.1046/j.1365-3040.2001.00724.x

Falkenmark, M., Kijne, J.W., Taron, B., Murdoch, G., Sivakumar, M.V.K., Craswell, E., 1997. Meeting Water Requirements of an Expanding World Population. Philos. Trans. Biol. Sci. 352, 929–936. doi:10.2307/56536

Fangmeier, A., De Temmerman, L., Mortensen, L., Kemp, K., Burke, J., Mitchell, R., Van Oijen, M., Weigel, H.J., 1999. Effects on nutrients and on grain quality in spring wheat crops grown under elevated CO_2 concentrations and stress conditions in the European, multiple-site experiment "ESPACE-wheat." Eur. J. Agron. 10, 215–229. doi:10.1016/S1161-0301(99)00012-X

Folta, K.M., Koss, L.L., McMorrow, R., Kim, H.-H., Kenitz, J.D., Wheeler, R., Sager, J.C., 2005. Design and fabrication of adjustable red-green-blue LED light arrays for plant research. BMC Plant Biol. 5, 1–11. doi:10.1186/1471-2229-5-17

Germer, J., Sauerborn, J., Asch, F., Boer, J., Schreiber, J., Weber, G., Müller, J., 2011. Skyfarming an ecological innovation to enhance global food security. J. für Verbraucherschutz und Leb. 6, 237–251. doi:10.1007/s00003-011-0691-6

Gilbert, N., 2009. The Disappearing nutrient. Nature 461, 716–718.

Griffin, K.L., 1994. Calorimetric Estimates of Construction Cost and Their use in Ecological Studies. Funct. Ecol. 8, 551–562. doi:10.2307/2389915

Haitz, R., Tsao, J.Y., 2011. Solid-state lighting: 'The case' 10 years after and future prospects. Phys. Status Solidi 208, 17–29. doi:10.1002/pssa.201026349

Jørgensen, J.R., Deleuran, L.C., Wollenweber, B., 2007. Prospects of whole grain crops of wheat, rye and triticale under different fertilizer regimes for energy production. Biomass and Bioenergy 31, 308–317. doi:10.1016/j.biombioe.2007.01.001

Lobell, D.B., Burke, M.B., Tebaldi, C., Mastrandrea, M.D., Falcon, W.P., Naylor, R.L., 2008. Prioritizing climate change adaptation needs for food security in 2030. Science 319, 607–610. doi:10.1126/science.1152339

Loomis, R.S., Amthor, J.S., 1999. Yield potential, plant assimilatory capacity, and metabolic efficiencies. Crop Sci. 39, 1584–1596. doi:10.1074/jbc.M908890199

Massa, G.D., Kim, H.H., Wheeler, R.M., Mitchell, C.A., 2008. Plant productivity in response to LED lighting. HortScience 43, 1951–1956.

Morrow, R., 2008. LED lighting in horticulture. HortScience 43, 1947–1950.

OECD/IEA, 2011. World Energy Outlook 2011. International Energy Agency, Paris. doi:10.1787/weo-2011-en

Sacksteder, C. a, Kanazawa, A., Jacoby, M.E., Kramer, D.M., 2000. The proton to electron stoichiometry of steady-state photosynthesis in living plants: A proton-pumping Q cycle is continuously engaged. Proc. Natl. Acad. Sci. U. S. A. 97, 14283–14288. doi:10.1073/pnas.97.26.14283

Scheibe, R., 2004. Malate valves to balance cellular energy supply. Physiol. Plant. 120, 21–26. doi:10.1111/j.0031-9317.2004.0222.x

Song, X.P., Tan, H.T.W., Tan, P.Y., 2018. Assessment of light adequacy for vertical farming in a tropical city. Urban For. Urban Green. 29. doi:10.1016/j.ufug.2017.11.004

Tilman, D., Balzer, C., Hill, J., Befort, B.L., 2011. Global food demand and the sustainable intensification of agriculture. Proc. Natl. Acad. Sci. 108, 20260–20264. doi:10.1073/pnas.1116437108

Tubiello, F., Volk, T., Bugbee, B., 1997. Diffuse light and wheat radiation-use efficiency in a controlled environment. Life Support & Biosph. Sci. 4, 77–85.

United Nations, 2019. Selected Results of the 2019 UN World Population Projections. Popul. Dev. Rev. 45, 689–694. doi:10.1111/padr.12288

von Caemmerer, S., Farquhar, G.D., 1981. Some relationships between the biochemistry of photosynthesis and the gas exchange of leaves. Planta 153, 376–387. doi:10.1007/BF00384257

Walsh, J., 1991. The Greening of the Green Revolution. Science (80-.). 252, 26–26. doi:10.1126/science.252.5002.26

Yin, X., Goudriaan, J., Lantinga, E. a., Vos, J., Spiertz, H.J., 2003. A flexible sigmoid function of determinate growth. Ann. Bot. 91, 361–371. doi:10.1093/aob/mcg029

Zhu, X.-G., Long, S.P., Ort, D.R., 2008. What is the maximum efficiency with which photosynthesis can convert solar energy into biomass? Curr. Opin. Biotechnol. 19, 153–159. doi:10.1016/j.copbio.2008.02.004

3. Design and implementation of a low-cost microcontroller based system for measuring gas exchange of plants

Marc Schmierer[1]*, Holger Brueck[2], and Folkard Asch[1]

1.) Hans-Ruthenberg-Institute ; Institute of Agricultural Sciences in the Tropics, University of Hohenheim, 70599 Stuttgart, Germany

2.) Research Centre Hanninghof, Yara International, Dülmen

*Corresponding author at: Hans-Ruthenberg- Institute - Institute of Agricultural Sciences in the Tropics, University of Hohenheim, 70599 Stuttgart, Germany. Email address: marc.schmierer@uni-hohenheim.de (M. Schmierer)

Abstract

A system for measuring plant gas exchange processes under controlled environmental conditions was designed and constructed. Rates of CO_2 uptake and water loss of plants are measured with inexpensive solid-state sensors integrated in microcontroller based sensor modules. Free open-source software libraries for all of the sensors used are available. The measurement system was implemented in a chamber system designed for open-flow measurements. A heating and cooling system as well as a humidification system was integrated allowing for measurements under controlled atmospheric conditions. Since the sensors used in this project were consumer rated, we tested their accuracy with an industry rated IRGA. For the humidity sensors, a linear deviation from the IRGA measurements with a small positive slope was found. For the CO_2-sensors, the bigger problem was the dependency of the readings on the H_2O-concentration. This dependency was linear and can be corrected for when calculating assimilation rates. Since open-flow systems require measurements in the in- and outflow, two pairs of sensors are needed. A calibration procedure is given to correct for sensor differences. Total costs for the electronic components of the sensor modules were less than 140 €. Costs for the atmosphere control system was less than 600 € but strongly depend on the desired size of the system.

Gas exchange measurements, Microcontroller, CO_2-sensors, Photosynthesis, Transpiration

3.1. Introduction

Research on gas exchange of plants dates back to the 18th century when scientists started to reveal the material and energetic origins of plant biomass. Today, gas exchange measurements are common in plant physiology and sophisticated techniques have been developed to date to determine precisely the CO_2 and vapor (H_2O) fluxes between plants and the atmosphere. Usually, these measurements are based on the detection of changes in the CO_2 or H_2O concentrations in the air surrounding a leaf or a part of a leaf enclosed in a chamber, with the analysis of the air usually performed by infrared-gas-Analyzers (IRGAs). Gas exchange measurements on leaf level have not only shown to be extremely useful in assessing the magnitude and dynamics of carbon gains and water losses of plants under varying conditions, they have also expanded our understanding of the principles of photosynthesis. For example, when combined with conceptual models of photosynthesis such as developed by von Caemmerer and Farquhar (1981), gas exchange measurements allow deep insights into the biochemistry of leaves, such as the abundance and activity of Ribulose-1,5-bisphosphate carboxylase oxygenase (RuBisCO) or the capacity of the photosynthetic electron transport chain (Long and Bernacchi, 2003).

Since photosynthesis and transpiration are strongly coupled (Medlyn et al., 2011), the quantitative assessment of both processes is critical for the quantification of matter and energy flows in ecological or agro-ecological systems (Cowan and Troughton, 1971; Medlyn et al., 2011) allowing to study the energy exchange between land surfaces covered by vegetation and the atmosphere near the earth surface.

Water fluxes in this context are often approximated via empirical evapotranspiration equations like the Penman-Monteith equation and derivatives (Allen et al., 2005; Penman, 1948), however, direct measurements of gas exchange may be necessary when calibrating parameters for new crops or genotypes. Furthermore, they are often less intrusive, simpler, and cheaper than alternative methods such as lysimetric measurements, eddy covariance, or remote sensing. However, since upscaling from leaf to field level is inevitable afflicted with errors (Jarvis, 1985), commercial off–the-shelf instruments intended for gas exchange measurements on leaf level may not be the first choice in this context. Numerous systems have been developed in the past to conduct water and carbon flux measurements for whole plants or plant communities.

Probably the earliest study in this regard was conducted by Thomas and Hill (1937), who describe a chamber-like system made up out of celluloid that was deployed over a 3.3 m^2 plot. The system was able to measure photosynthesis, respiration, and transpiration continuously over a period of several days. More recent systems are described e.g. by Garcia et al. (1990), Wünsche and Palmer (1997), and Muller et al. (2009).

While the above mentioned systems have been intended to be field deployable and respective measurements were performed usually over a period no longer then several days, several approaches have been described for long term measurements of plant canopies grown under controlled environment conditions (Bugbee, 1992; van Iersel and Bugbee, 2000). These systems are intended to host whole plant stands over a full life cycle while permanently recording gas exchange and related environmental data. Accordingly, they do not only comprise of pure sensor and data logging equipment but rather resemble entire climate chambers giving the experimenter full control over environmental parameters like temperature, humidity, CO_2 concentration, or light quality. Such systems can be used to study plant responses to environmental factors and are often used in the context artificial environment research (e.g. Cope et al., 2014).

All of the above mentioned systems use industry-quality equipment for data acquisition and logging. Usually, high accuracy IRGAs with several channels are combined with off-the-shelf data loggers resulting in system costs of several thousand euros. However, during the last years, low-cost physical computing platforms such as Arduino and single board computers like the Raspberry PI not only became popular among electronic enthusiasts but have as well found their way into research laboratories. These systems have been shown suitable for long term-monitoring of indoor air quality (Ali et al., 2016), several robotic (Candelas et al., 2015), or control applications (Sobota et al., 2013). Additionally, more and more ready-to-use sensors have become available for the consumer market, giving researchers the chance to assemble individual modules closely designed for the intended purpose.

In this study, we report the performance and accuracy of a custom build system for measuring CO_2 and H_2O fluxes from a plant canopy enclosed in an environmentally controlled test chamber. The system comprises of two printed circuit boards bearing sensors for temperature relative humidity, air pressure and CO_2 concentration and a control board for data acquisition and storage. The system was deployed in a custom-build test chamber that allowed for regulation of air humidity and temperature. The objective of the study was to develop a system for measuring transpiration and assimilation on whole plant or canopy level and to document the accuracy and reliability of the measured data.

3.2. System design considerations

At least 3 different concepts exist to measure gas exchange rates of plants: closed systems, semi-closed systems and open systems (Bugbee, 1992). Closed and semi-closed systems are sealed from the outside and the measurements are based on the depletion or enrichment of gaseous components inside. Closed systems are therefore unsuitable for long term measurements or measurements of transient systems (e.g. plant responses to sudden changes in relative humidity). This can be circumvented in semi-closed systems where gaseous components are continuously supplied or removed in order maintain a steady environment. However, both of these systems require a high leak-tightness to prevent gas fluxes between the inside and the surrounding that would falsify the measurements.

In open systems, a chamber is constantly flowed through an airstream and the calculation of gas exchange rates is based on the concentration differences between the incoming and outgoing air multiplied by the flow rate. Open systems require more instrumentation because measurements must be taken at two points. However, as pointed out by Bugbee (1992), such systems bypass the necessity for tightness as long as the inside of the chamber is maintained on a slightly positive pressure to prevent the diffusion from outside air into the system. Since we were particularly interested in stomatal responses to changes in the light environment and atmospheric water content, we decided to design an open system suitable for measurement periods as long as several hours and that simultaneously offers the possibility to adjust air humidity and temperature.

For an open system at least 2 sensor modules are needed. Further, knowledge about the flow rate through the system is necessary. Flow meters can be used for this purpose, and this is inevitable when the flow rate is changed during operation, e.g. to adjust air humidity inside the system. However, if the flow rate is kept constant, the rate of change of gas components inside the chamber after a change in the inflowing concentration of the component can be used to calculate the flow rate. This approach was described earlier by Garcia et al. (1990) and is based on the fact that the depletion and enrichment of gases inside the chamber follows an exponential convergence process. Hence, we can use the measurements taken in the incoming and outgoing air to calculate the system flow rate. It should be noted that this approach requires thorough air mixing inside the chamber to prevent dead pockets of air that would otherwise falsify the assumption of exponential convergence.

3.3. Expected turnovers and required maximum flow rate

Gas exchange measurements are prone to numerous sources of error like limited sensor accuracy, leaks, and condensation in the gas pathway to name but a few. However, for an open chamber system, total system accuracy is greatly affected by the magnitude of the differences between H_2O and CO_2 concentrations in the measured air streams, since this will ultimately affect the signal to noise ratio. The rate of change of gas components inside an open chamber system is determined by the turnovers caused by the plants and by the flow rate through the system, where a smaller flow rate will always lead to a larger depletion of CO_2 and to a higher water vapour concentration. Very high water vapour concentrations are not feasible, since they increase the chance of condensation and the transpiration rate would be underestimated by the amount of the condensate. Hence, the flow rate should be chosen to be as small as possible but as high as necessary. However, without data on hand, estimation of gas exchange rates can be difficult since they depend on a couple of environmental and biological conditions.

Prior to this research, we run a numerical simulation for estimating the changes of CO_2 and H_2O concentrations caused by a fictional plant stand with a leaf area of 4 m^2 in a chamber of a volume of 2 m^3. A light intensity inside the chamber of about 700 µmol PAR m^{-2} s^{-1} was assumed, resulting in an

assimilation rate of 10 µmol s^{-1} m^{-2} leaf. Based on experiences from leaf gas exchange measurements, this value appeared reasonable for a crop like e.g. rice or wheat. A semi-mechanistic model was used for the calculation of stomatal conductance (Medlyn et al., 2012). This was done in order to map the interaction between in-chamber humidity, CO_2 concentration and stomatal conductance itself, since these parameters are strongly coupled to each other. Table 4 gives an overview about the impact of different flow rates on the concentration changes of CO_2 and H_2O inside the chamber when the chamber is flowed through with air of either 50 % or 25 % humidity. If the air source is as dry as 25 %, a flow rate of 20 g s^{-1} is enough to limit relative humidity to 65 %. However, the expected ΔCO_2 is then just 44 ppm and this is possibly not enough to detect smaller changes in assimilation performance of the plant stand, especially with consumer-rated CO_2 sensors intended for this research. Following the values in Table 4, flow rate could be reduced to 10 g s^{-1}, thus increasing ΔCO_2 to about 80 ppm and relative humidity to 81 %, a value where condensation is still unlikely. Although this is just a rough estimate, we can see that the expected flow rates are of a magnitude that can be achieved with standard 12- Volt Ventilators, given the availability of relative dry air. For this purpose, rotating dryers can be used as they provide sufficient output rates.

Table 4: Assumed changes in relative humidity and CO_2 concentration caused by a fictional plant stand with 4 m^2 leaf area in a 2 m^3 chamber at different flow rates and with inflow air of different relative humidity levels. T is the time constant of the system specifying the time after about 63 % of the chamber air is exchanged. CO_2 concentration of the inflowing air is assumed to be 400 ppm and temperature 30 °C.

rH (%)	flow rate (g s^{-1})	T (s)	rH (converged) (%)	ΔCO_2 (ppm)
	5	400	98	167
50	10	200	90	79
	20	100	79	44
	5	400	96	168
25	10	200	81	79
	20	100	65	44

3.4. Electronic design of the sensor and control modules

Sensor modules

Temperature, relative humidity, carbon dioxide concentration, and air pressure were measured by two sensor platforms. The sensor platforms were made out of a 1-layer printed circuit board (PCB) with dimensions of 100 mm x 125 mm. Electronic components like integrated circuits, resistors, capacitors, etc. were soldered directly to the PCB. Sensors were connected pluggable via pin headers to allow for replaceability. The sensor boards were not cased. However, in order to prevent excessive radiation load from the lights and to guarantee high ventilation of all sensor components, the sensor boards were located 10 cm inside the PVC fittings tubes that routed the airstreams in and out of the chamber.

Air temperature and relative air humidity were measured by a HYT-221 digital temperature and humidity module (IST AG). According to the datasheet, the module uses an integrated PTAT (proportional to absolute temperature current) source for temperature measurement with an accuracy of 0.2 K between 0 and 60 °C, and a capacitive polymer humidity sensor with an accuracy of 1.8% rH at 23 °C between 0 and 90 % rH. Resolution is 0.01 °C for temperature and 0.01 % rH. Data is accessible via an I^2C interface (NXP Semiconductors, 2012).

Carbon dioxide concentrations were measured with a diffusion type NDIR (nondispersive infrared sensor) CO_2-Sensor (K-30, CO_2Meter, Inc., Ormond Beach, FL, USA). Accuracy is given as 3% of the reading. This corresponds to ±6 ppm for a CO_2 concentration of 400 ppm. The sensor provides several analogue outputs a well as I^2C and ModBus communication interfaces for digital data acquisition. Care has to be taken not to use the self-calibration feature (Automatic Baseline Correction, ABC) of the module. This feature is activated by default and automatically adjusts the reference for 400 ppm (fresh air value) to the lowest value measured during the last 7.5 days. In an application like the one described here where CO_2 is constantly depleted by a plant stand, this would corrupt the calibration and thus any further measurements. This feature should be deactivated and a span calibration procedure at 0 and 400 ppm CO_2 should be performed instead. Both procedures are described in the module's I^2C manual, available from the manufacturer. For measurement of air pressure, we used a Bosch BMP-085 Barometric Pressure sensor.

Data acquisition from the sensors was performed by an Atmega 48-P microcontroller (Microchip Technology). All sensors were connected to the I^2C-Bus interface of the microcontroller. Data connection to the control unit was provided via a CAN-Bus interface consisting of a MCP 2515-I/P CAN-Bus Controller and a MCP 2551-I/P CAN Transceiver (Microchip Technology). Sensor Data were updated once a second.

Inter-electrical connection was complicated by the fact that some of the components were not 5 V tolerant (BMP-085), others were 5 V tolerant but required an I^2C-Bus level of 3.3 V (K-30), and others

required a minimum operation voltage of 4.5 V (MCP 2551-I/P). Therefore, the CAN-Bus components, the microcontroller, and the K-30 were supplied with 5 V and all the other sensors with 3.3 V. Additionally, an I^2C -bus level translator and repeater (PCA9516, NXP Semiconductors) had to be used as an I^2C-Hub between the microcontroller and the sensors. 5 V was provided by the control unit and 3.3 V were provided on-board from a LM-317 linear voltage regulator (Texas Instruments). Since linear voltage regulators and other electrical components can generate a significant amount of excessive heat, care should be taken that sensors are unaffected. In this application, the sensors were prearranged relative to the airstream.

Data acquisition and control modules

A second microcontroller module was designed to collect and save data from the sensor modules and to control optional actuators such as heating or cooling elements, ventilators, and lights. Additionally, the module should be able to send real time data as well as stored data to a personal computer. Like the sensor modules, the board consisted of a single layer PCB with dimensions of 125 x 200 mm. The main components of the board were an Atmega 32P as the central microcontroller (Microchip Technology), two 24C512 EEPROMs (STMicroelectronics) providing an overall of 65,536 bytes of memory, a CAN-Bus interface equivalent to that of the sensor modules, and an UDN2981 (Allegro Microsystems) serving as an 8 channel high side output switch for controlling heating, cooling and humidification subsystems. For serial data transfer to a PC, both UART pins from the microcontroller (RXD and TXD) as well as GND and V+ were routed to a 4-pin connector that was intended to be connected to an UART to USB adapter. Circuit design and routing was performed with the open source electronic design automation software KiCad (Version 2013.07.07 (available at http://kicad-pcb.org/).

Table 5: Description of parts and quantity, part number, manufacturer and costs (€) for the control and sensor modules. Costs refer to the total number of parts.

Description	quantity	Part number and Manufacturer	Total costs (€)
Control unit			
Microcontroller	1	ATMEGA32-16PU, Microchip Technologies	6.6
Memory	2	24C512, STMicroelectronics	4
CAN-Bus controller	1	MCP 2515-I/P, Microchip Technologies	1.8
CAN transceiver	1	MCP 2551-I/P, Microchip Technologies	1
Voltage regulator	1	LM317, Texas Instruments	0.3
Output driver	1	UDN2981, Allegro MicroSystems	1.1
Sensor units			
Microcontroller	2	Atmega 48-P, Microchip Technologies	1.8
CO2-Sensor	2	K-30, CO2 Meter, Inc.	80
Humidity-/Temperature-sensor	2	HYT 221, IST AG	25
Pressure-sensor	2	BMP085, Bosch Sensortec	8
CAN-Bus Controller	2	MCP 2515-I/P, Microchip Technologies	1.8
CAN Transceiver	2	MCP 2551-I/P, Microchip Technologies	1
I^2C-bus level translator	2	PCA9516, NXP Semiconductors	2.5
Total			134.9

3.5. Deployment of the system in a climate regulated test chamber

Test chamber set-up

The gas exchange measurement system described here consists of a chamber with total inner dimensions of 138*156*100 cm (Figure 3). The chamber was subdivided in two compartments. The rear compartment had inner dimensions of 138*156*18 cm and served as a mixing chamber for adjustment of the temperature and the water vapour content of the incoming air. The front compartment with dimensions of 138*156*84 cm was illuminated and represented the actual cuvette that contained the plants during measurement.

Plywood plates with a thickness of 2 cm were used as construction material. To prevent the absorption of water vapour by the material, the plates were wrapped in 2 layers of standard black and white foil before assembly. A final layer of high reflection foil (Diamond ECO, Easy Grow Ltd., Grimsby, UK) was applied to minimize light reflection losses at the chamber surfaces. After assembly, the chamber was insulated with polystyrene boards and eventually covered with black and white foil.

The mixing chamber and the cuvette were connected with a 20 cm section of a PVC fitting 10 cm in diameter mounted in the middle of the separating wall 5 cm below the ceiling. A radial ventilator (FAN-ML 120-12H, Sunonwealth Ltd., Kaohsiung, Taiwan) was mounted to the connection pipe via an adapter and pushed air from mixing chamber into the cuvette section. During operation, the negative pressure created by the fan drew air from an air inlet at the rightmost top of the mixing chamber. To reduce fluctuations of water vapour and CO_2 concentration in the incoming air, the air inlet was connected to a flexible aluminium duct that took air from outside the building at approximately 3 m height. Air left the chamber through a 7.5 cm diameter PVC pipe located at the bottom of the backside of the cuvette section that protruded 50 cm into the chamber.

For heating of the air in the mixing chamber, generic 3 mm resistive wire (Cu Ni 44) with a resistance of 0.069 Ω m^{-1} was wrapped 23 times to a coil with an inner diameter of 40 mm providing a heating power of approximately 630 W at 12 V. The coil was fixed on a steel-sheet and screwed onto a 4 cm thick heat-insulating tile that was mounted on the back wall of the mixing chamber. The heating module was ventilated by a generic 80 mm PC-ventilator.

For cooling, four 154 Watt peltier elements (TEC1-12710, Hebei I.T. Co.,Ltd., Shanghai, China) were used. Each peltier element was fixed between 2 aluminium plates (12 cm x 12 cm x 2cm) and on each aluminium plate a CPU heatsink, including a ventilator, (HPK-10025EA, Evercool Thermal Co., Taiwan) was mounted. The peltier elements, the aluminium plates, and the heat sinks were thermally coupled with heat transfer paste. 4 holes were cut into the backside of the mixing chamber and the cooling modules were placed on top of them with the cold side of the peltier elements facing inside the chamber.

Another heating module, analogue to that in the mixing chamber, was installed in the cuvette. It was ventilated by an off-the-shelf table fan (20 cm diameter) that was mounted at the ceiling for thorough air mixing. Air speed inside the cuvette ranged from 1 m s^{-1} at 1 m height (above canopy) to 0.2 m^{-1} at the bottom of the chamber.

All heating elements and as well as the peltier elements were connected to power 70 Ampere N-MOSFETS (IRL3705N, International Rectifier Co.) to allow for power regulation from the control module.

An ultrasonic nebulizer (Fogstar 300, Seliger GmbH) was used to control the water vapor content of the incoming air. The nebulizer was placed on a swimming ring that was located in a 30 L tank outside the chamber. The tank was half-filled with distilled water and connected to the mixing chamber by 2 PVC tubes. A fan in the mixing chamber established an air flow through the tank, with a magnitude according to the humidification demand. For this purpose, another power MOSFET was connected ahead of the fan to provide an interface with the control module.

4 custom build LED panels were installed through slots at the ceiling. They were cooled by CPU-heat sinks that were located outside of the chamber. The LED panels supplied a total light intensity of about 500 µmol PAR m^{-2} s^{-1} at the bottom of the chamber.

Hardware integration and software control

The sensor module that was intended to measure the incoming air was located inside the PVC tube that connected the mixing chamber and the cuvette section. A second one was located in the PVC tube that depicted the air outlet. The CAN-ports of both modules were connected to the control module by twisted pair cables. The control module as well as the power supply units were located outside the chamber.

The outlet driver of the control module was connected to the power MOSFETs of the peltier and the heating elements in the mixing chamber and to the heating elements in the cuvette section.

The control module accessed the data from the sensor modules once per second. Temperature, relative humidity and pressure data were recalculated to specific humidity (sH, mass H$_2$O mass-1 air) according to:

$$sH = \frac{0.622 * VP}{p - 0.378 * VP} \tag{1}$$

where p is the barometric pressure of air and VP is the partial pressure of water vapor calculated as:

$$VP = rH * 6.1094 * e^{\left(\frac{17.625 * T}{T + 243.04}\right)} * (1.00071 * e^{0.0000045 * p}) \tag{2}$$

where rH is the relative humidity measured, T is temperature in °C, and p is the barometric pressure of the air. The rightmost part of the equation is a correction factor for pressure as proposed by Alduchov and Eskridge (1996). For calculation of transpiration and assimilation rates, the control board averaged data of the parameters of the incoming air for a 60 s interval and stored them at the end of the interval together with single point data from outgoing air parameters measured at the end of the interval. According to the user settings, power over the heating and cooling elements was regulated via pulse-width-modulation. Pulse width was adjusted via a PID (proportional integral derivative) controller implemented in software. Specific humidity instead relative humidity was used as the control value for adjusting water vapour content of the incoming air because it is less dependent on temperature. This has the benefit that the PID control loop of the humidification subsystem operates more independently from the control of the temperature control subsystem and that deviations from the stetted temperature, for example caused by sudden changes in the ambient temperature, do not induce disturbances or oscillations in the humidity control.

The software for the microcontrollers was written in the C programming language. Atmel Studio 5.0 (Microchip Technologies) was used for software development.

Calibration procedure and measurements

The absolute accuracy of the readings of the sensor boards were tested with a newly calibrated Infra-Red Gas Analysator (IRGA) from a photosynthesis measurement device (GFS-3000, Heinz Walz GmbH, Effeltrich, Germany). The sensor boards were placed into a plastic box that was connected via tubes to the air outlet of the machine. The Box was closed and flooded with air of different composition from the GFS-3000. When conditions in the box were stable, the values were recorded and water vapor concentration or CO_2 content of the air was changed. Finally, regression analyses were performed to display the deviations between the readings of the sensor boards and the IRGA.

To be able to correct for the relative deviations between the sensors, an additional calibration procedure was performed before every measurement. For this purpose, the chamber was heated up for approximately 30 minutes. Subsequently both sensor modules were placed next to each other in a plastic box. The plastic box had open sides but was covered from above to prevent radiation caused biases (see manual for the K-30 CO_2 sensor). During the next 15 to 20 minutes temperature, relative humidity and CO2 content were altered to cover a range of values that were later used for measuring and correcting the bias between the respective sensors on both of the sensor boards. The success of the calibration procedures was checked by running measurements in an empty chamber, where transpiration and assimilation are expected to be 0.

Measurements incorporating plants usually took between 1 and 8 hours. We used the system to quantify responses of a rice stand to different levels of air humidity over a full growing cycle, the specific

humidity of the incoming air was changed approximately every 30 minutes or when gas exchange reached steady state (see Figure 4).

Calculation of flow rate, transpiration and assimilation rates

Flow rate through the system was calculated by measuring the change of the water vapour concentration inside the empty chamber after changing the water vapour concentration in the incoming air. Air mixing in the chamber can be modelled as an exponential decay process:

$$N_t = N_{end} + (N_{start} - N_{end}) * e^{-t/\tau} \tag{3}$$

where N_t is the concentration of the component in question after a time t has passed, N_{end} is the concentration of the component at the end of the convergence process (in our case the concentration of a component in the inflowing air that will finally determine the concentration in the chamber), N_{start} is the concentration of the component inside the chamber at the beginning of the process and τ is the time constant of the process. With increasing time, the rightmost term of equation 3 will approach zero, and N_t will finally equal N_{end}. τ can be calculated by dividing the chamber volume by the flow rate and indicates the amount of time after a fraction of $\frac{1}{e}$ (~63 %) of the chamber air is exchanged. If the flow rate is unknown, we can solve equation 1 for τ and calculate the system flow rate based on the measurements taken before (N_{start}), during (N_{end}) and after (N_t) the interval t.

Assimilation and transpiration rates can be calculated by multiplying the differences in the concentrations of H_2O and CO_2 between the inflowing and the outflowing air with the flow rate through the chamber. Additionally, when dealing with high transpiration rates like it is the case for this research, the outflow is greater than the inflow due to the addition of water vapour by the plants. While this can easily be corrected for as described by von Caemmerer and Farquhar (1981), the major drawback of this approach is that it is only valid if the gas exchange rates by the plants are in steady state and as long as the gas concentrations of the air entering the chamber are constant. To circumvent this limitation, we use equation 3 for modelling the gas concentrations for an empty chamber were transpiration and assimilation were absent. In our case, N_{end} corresponds to the concentration of a gas component in the incoming air. If we know the concentration of a gas component inside the chamber at the beginning of a time interval t, and the concentration of the component inside the chamber after the time interval we can calculate the concentration of the component in the incoming air:

$$N_{end} = \frac{e^{\frac{t}{\tau}} * N_t - N_{start}}{e^{\frac{t}{\tau}} - 1} \tag{4}$$

For calculating transpiration and assimilation rates, the control unit recorded CO_2 and H_2O concentrations inside the chamber every 60 seconds. Further, the CO_2 and H_2O concentrations in the incoming air were measured and averaged over the entire interval. Equation 4 was then used for

calculating the actual concentrations of CO_2 and H_2O entering the chamber, were N_{start} is the point data measured inside the chamber at the beginning of the interval and N_t is the point data measured inside the chamber at the end of the interval. The differences between the modeled and the measured gas concentrations in the incoming air were then used for calculating transpiration rates by the plants according to von Caemmerer and Farquhar (1981):

$$E = \frac{sH_{out} - sH_{in}}{1 - sH_{out}}$$
(5)

with sH indicates specific humidity. The denominator is a correction term for the efflux of water vapour. Assimilation was calculated respectively.

3.6. Results

Absolute accuracy of the sensors was checked by exposing the sensor boards to air with known H_2O and CO_2 concentrations provided by the GFS-3000. Both of the humidity sensors on each of the sensor boards showed similar deviations from the actual H_2O concentration. When recalculated to the mole fraction, the regression values found for the sensors were 1.143 * *ppm H_2O* -1244 and 1.133 * *ppm H_2O* – 1348 respectively. Both regressions were strongly linear with R^2 values of 0.99. For air that holds approximately 20000 ppm H_2O (e.g. 30° C and 50 % relative Humidity), this would result in a difference of about 270 ppm H_2O. For a flow rate of about 10 g s^{-1}, the resulting error in the calculated transpiration rate would be about 0.1 mmol H_2O per second. The resulting error for high transpiration rates (e.g. 9 mmol s^{-1} for a plant stand with 3 m^2 leaf and an average transpiration rate of about 3 mmol m^{-2} s^{-1}) the resulting relative error would thus only be slightly over 1 %. However, for smaller turnovers, these errors could be significant.

The absolute errors determined for the K-30 CO_2 sensors were smaller when a span calibration was performed prior to the measurements, but we found that the response was strongly coupled to the H_2O concentration (about -0.1 % ppm CO_2 / ppm H_2O). We therefore took this interaction into account in the calculation of the assimilation rate.

Prior to each measurement, both sensor modules were placed into the chamber next to each other and recorded data from air with changing H_2O and CO_2 concentrations. Linear regressions were performed to correct for deviations between the sensor pairs. The success of this method was checked by running measurements in an empty chamber for periods of about 1.5 hours. The calculated transpiration rates were as small as ±0.01 mmol s^{-1} with a standard deviation of 0.1 mmol s^{-1}. Measured assimilation rates were ±0.1 μmol s^{-1}, with standard deviations of 1.2 μmol s^{-1}.

We used the system to record gas exchange response of a rice stand to different levels of water pressure deficits from tillering to ripening. An example data set is shown in Figure 5:. When we counterchecked the transpiration data calculated from the sensors with water loss measured with balances, we found

that the sensors were able to detect approximately 90 % of the transpired water. The accuracy tended to be smaller for higher transpiration rates. An explanation could be condensation that took place when the air inside the chamber got very humid.

3.7. Summary

We designed a measurement system for monitoring plant gas exchange processes under controlled environmental conditions. Assimilation and transpiration rates were measured with inexpensive solid state sensors integrated in microcontroller based sensor modules. Such modules can easily be designed on basis of widespread physical computing platforms like Arduino or raspberry Pi and free open-source software libraries for all of the sensors used are available. The measurement system was implemented in a simple chamber system designed for open-flow measurements that additionally allowed for controlling air humidity and temperature.

Since the sensors used in this project were consumer rated, we tested their accuracy with an industry rated IRGA. For the humidity sensors, a linear deviation from the IRGA measurements with a small positive slope was found. For the CO_2-sensors, the bigger problem was the dependency of the readings on the H_2O-concentration. However, since this dependency was linear, it can be corrected for when calculating assimilation rates. To correct for differences between the sensor pairs that measure the inflowing and outflowing air respectively, a sensor comparison in the same air should be performed every time before the measurements. Total costs for the electronic components of the sensor modules were less than 140 €. Hardware costs the chamber system was less than 600 € and here the costs strongly depend on size of the system and the respective power class of the power supply and heating and cooling elements.

We conclude that building a canopy-gas-exchange measurement system with sufficient accuracy to measure gross photosynthesis and transpiration of a plant stand is possible with off-the-shelf material that are nowadays available for a relative low price. The electronics do not have to be completely self-assembled and developed. Instead, standard systems like *Arduino* and single board computers like the *Raspberry PI* could be used, as they have been already shown helpful in scientific applications. Our system is scalable and the described electronics and software can be applied in smaller systems designed for measuring single-plant gas-exchange. The low costs would allow a higher number of experimental units and thus offer the possibility of high throughput experiments screening different combinations of environmental and light quality/direction parameters at the same time.

Table 6: Parts used for the test chamber setup.

Description	quantity	Part number and Manufacturer	Total costs (€)
Peltier elements	4	TEC1-12710, Hebei I.T. Co., Ltd.	40
Heat sinks	8	HPK-10025EA, EVERCOOL Thermal Co.	200
Resistance wire	1	Generic, NA	5
Ultrasonic nebulizer	1	Fogstar 300, Seliger GmbH	60
power MOSFETs	16	IRL3705N, International Rectifier Co.	20
Switching power supply	2	HRP-600-12, Mean Well Enterprises Co.	250
Miscellaneous (ventilators, cable, plugs, wire terminators, etc.)			20
Total			575
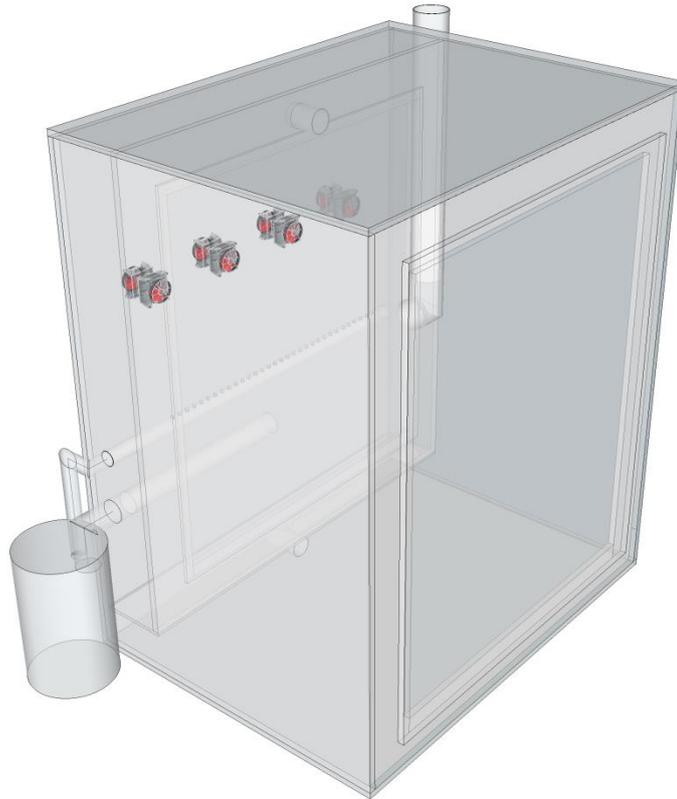
Figure 3: Chamber system used to test the custom build gas exchange measurement system. Air enters the mixing chamber at the back. Before entering the cuvette section, humidity can be added by a ultrasonic nebulizer located in a water tank. Temperature of the air in the mixing chamber can be adjusted by peltier elements or a heating element at the rear side of the chamber. A ventilator at the separating wall pushes the air from the mixing chamber into the cuvette section. Located at the ceiling (not shown for reasons of clarity) are a ventilator for air mixing, another heating element and LED elements for light supply. Air leaves the cuvette section at the rear side.
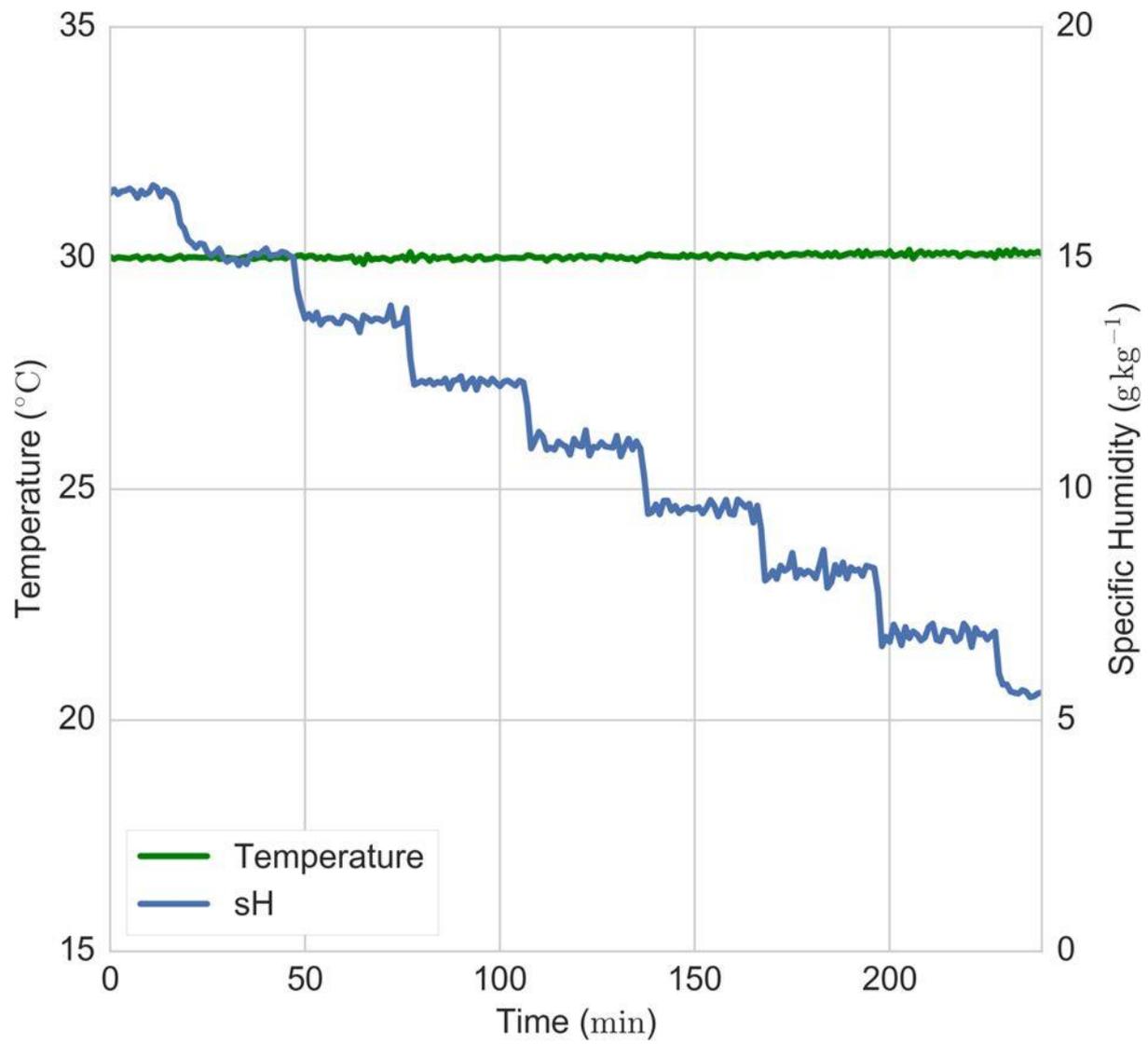
Figure 4: Temperature in the cuvette section of the chamber and specific humidity (sH) of the air entering the chamber.
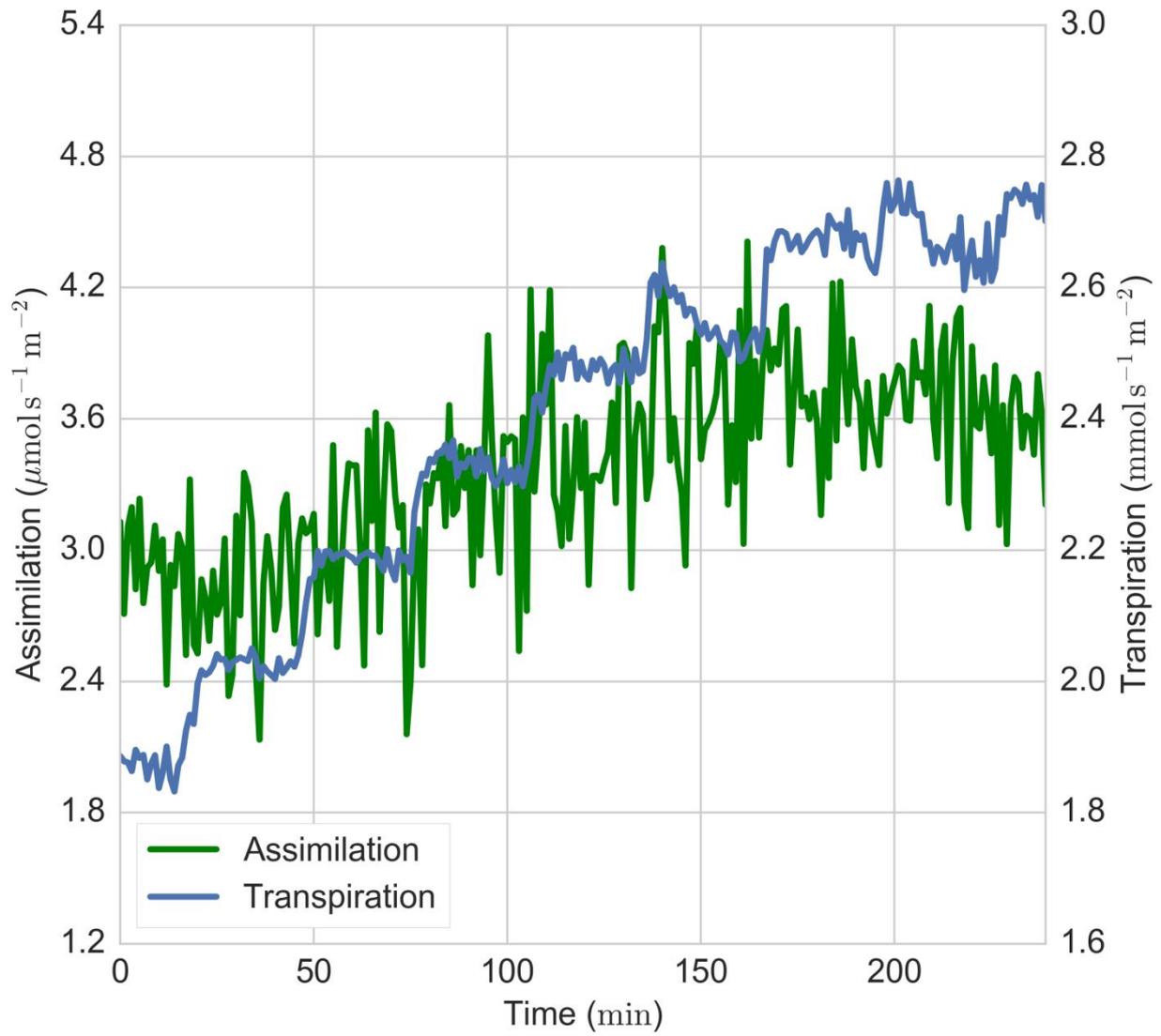
Figure 5: Transpiration and assimilation rates of a rice stand grown in pots (24 plants, total leaf area ~2.6 m²). Changes in transpiration rate are induced by changing the humidity of the incoming air.

3.8. References

Alduchov, O.A., Eskridge, R.E., 1996. Improved Magnus Form Approximation of Saturation Vapor Pressure. J. Appl. Meteorol. 35, 601–609. doi:10.1175/1520-0450(1996)035<0601:IMFAOS>2.0.CO;2

Ali, A.S., Zanzinger, Z., Debose, D., Stephens, B., 2016. Open Source Building Science Sensors (OSBSS): A low-cost Arduino-based platform for long-term indoor environmental data collection. Build. Environ. 100, 114–126. doi:10.1016/j.buildenv.2016.02.010

Allen, R.G., Pereira, L.S., Smith, M., Raes, D., Wright, J.L., 2005. FAO-56 Dual Crop Coefficient Method for Estimating Evaporation from Soil and Application Extensions. J. Irrig. Drain. Eng. 131, 2–13. doi:10.1061/(ASCE)0733-9437(2005)131:1(2)

Bugbee, B., 1992. Steady-state canopy gas exchange: system design and operation. HortScience 27, 770–776.

Candelas, F.A., García, G.J., Puente, S., Pomares, J., Jara, C.A., Pérez, J., Mira, D., Torres, F., 2015. Experiences on using Arduino for laboratory experiments of Automatic Control and Robotics. IFAC-PapersOnLine 48, 105–110. doi:10.1016/j.ifacol.2015.11.221

Cope, K.R., Snowden, M.C., Bugbee, B., 2014. Photobiological interactions of blue light and photosynthetic photon flux: Effects of monochromatic and broad-spectrum light sources. Photochem. Photobiol. 90, 574–584. doi:10.1111/php.12233

Cowan, I.R., Troughton, J.H., 1971. The relative role of stomata in transpiration and assimilation. Planta 97, 325–336. doi:10.1007/BF00390212

Garcia, R.L., Norman, J.M., McDermitt, D.K., 1990. Measurements of canopy gas exchange using an open chamber system. Remote Sens. Rev. 5, 141–162. doi:10.1080/02757259009532126

Jarvis, P.G., 1985. Coupling of Transpiration to the Atmosphere in Horticultural Crops: The Omega Factor. Acta Hort 171, 187–205.

Long, S.P., Bernacchi, C.J., 2003. Gas exchange measurements, what can they tell us about the underlying limitations to photosynthesis? Procedures and sources of error. J. Exp. Bot. 54, 2393–401. doi:10.1093/jxb/erg262

Medlyn, B.E., Duursma, R.A., Eamus, D., Ellsworth, D.S., Prentice, I.C., Barton, C.V.M., Crous, K.Y., De Angelis, P., Freeman, M., Wingate, L., 2012. Reconciling the optimal and empirical approaches to modelling stomatal conductance (vol 17, pg 2134, 2011). Glob. Chang. Biol. 18, 3476. doi:10.1111/j.1365-2486.2012.02790.x

Medlyn, B.E., Duursma, R.A., Eamus, D., Ellsworth, D.S., Prentice, I.C., Barton, C.V.M., Crous, K.Y., De Angelis, P., Freeman, M., Wingate, L., 2011. Reconciling the optimal and empirical approaches to modelling stomatal conductance. Glob. Chang. Biol. 17, 2134–2144. doi:10.1111/j.1365-2486.2010.02375.x

Muller, J., Eschenroder, a, Diepenbrock, W., 2009. Through-flow chamber CO_2/H_2O canopy gas exchange system—Construction, microclimate, errors, and measurements in a barley (Hordeum vulgare L.) field. Agric. For. Meteorol. 149, 214–229. doi:10.1016/j.agrformet.2008.08.007

NXP Semiconductors, 2012. I2C-bus specification and user manual. Rev. 4.

Penman, H.L., 1948. Natural Evaporation from Open Water, Bare Soil and Grass. Proc. R. Soc. A Math. Phys. Eng. Sci. 193, 120–145. doi:10.1098/rspa.1948.0037

Sobota, J., Pǐsl, R., Balda, P., Schlegel, M., 2013. Raspberry pi and arduino boards in control education. IFAC Proc. Vol. 10, 7–12. doi:10.3182/20130828-3-UK-2039.00024

Thomas, M.D., Hill, G., 1937. The Continuous Measurement of Photosynthesis, Respiration, and Transpiration of Alfalfa and Wheat Growing under Field Conditions. Plant Physiol. 12, 285–307.

van Iersel, M.W., Bugbee, B., 2000. A multiple chamber, semicontinuous, crop carbon dioxide exchange system: design, calibration, and data interpretation. J. Am. Soc. Hortic. Sci. 125, 86–92.

von Caemmerer, S., Farquhar, G.D., 1981. Some relationships between the biochemistry of photosynthesis and the gas exchange of leaves. Planta 153, 376–387. doi:10.1007/BF00384257

Wünsche, J.N., Palmer, J.W., 1997. Portable through-flow cuvette system for measuring whole-canopy gas exchange of apple trees in the field. HortScience 32, 653–658.

4. Growth and Photosynthesis Responses of a Super Dwarf Rice Genotype to Shade and Nitrogen Supply

Marc Schmierer[1*], Oliver Knopf[2], Folkard Asch[1]

[1]Institute of Agricultural Sciences in the Tropics, University of Hohenheim, 70599 Stuttgart, Germany

[2]Institute for Bio- and Geosciences, IBG-2: Plant Sciences, Forschungszentrum Jülich GmbH, 52428 Jülich, Germany

[*]Corresponding author at: Institute of Agricultural Sciences in the Tropics, University of Hohenheim, 70599 Stuttgart

Abstract

Specific aspects of plant cultivation require tests under fully controlled environmental conditions such as those provided by a climate chamber, which generally is space limited. In addition, such tests are sometimes performed with restricted energy supply, as found in in orbit-based space laboratories, and as a result are in low-light conditions. For these growing conditions, super dwarf plants have been developed as model crops. For example, a gibberellin (GA) deficient super dwarf rice genotype was proposed as a model crop for space flight plant experiments. We tested this genotype in a climate chamber experiment under different illumination levels and different levels of nitrogen supply to assess its suitability as a test plant under scenarios with limited resource availability. A 25 % reduction in illumination lead to a 75 % reduction in yield, mainly due to a 60 % reduction in formed tillers and 20 % reduction in kernel weight, and an 80 % reduction in illumination caused total yield loss. Whereas leaf area under reduced illumination was significantly lower, only marginal changes in the dimensions of single leaves were observed. Photosynthesis at growing light conditions was not different between control plants and plants under 75 % illumination. This was explained by a higher photochemical efficiency under lower light conditions and a reduced mesophyll resistance. Therefore, we conclude that this genotype is well- suited for plant experiments under space and light-limited conditions since it keeps its small stature and does not show shade avoidance mechanisms, such as leaf elongation, that would complicate experiments under low-light conditions. Nitrogen concentrations of 2.8 and 1.4 mmol L^{-1} lead to no differences in plant growth. We conclude that a nitrogen concentration of 1.4 mmol L^{-1} is sufficient for this genotype under the light intensities that were applied here.

4.1. Background

In the life sciences, 'model' organisms are used to represent kingdoms, phylla, classes, or families, and are often chosen for their ease of handling, non- pathogenicity, or the size of their genome. They play

an important role in understanding basic biological concepts and many major breakthroughs in biology have been driven by research on only a few representative species, such as *Escherichia coli or Arabidopsis thaliana* (Russo, 2003; Van Norman & Benfey, 2009). However, in crop science, scientists require check varieties for each crop to show generalizable responses to biotic and abiotic factors. In rice science, the variety IR64, an economically successful variety developed in 1985 by the International Rice Research Institute (IRRI), has been used as a check variety in a large number of experiments globally (Mackill & Khush, 2018). By including IR64 in their experiments, researchers are allowing their data to be checked for plausibility and, in the case of new varieties, compared before being introduced to the market.

Recent technological innovations have increased the focus on cultivating crops in fully controlled environments (Bugbee, 1992; Germer *et al.*, 2011; Pinstrup-Andersen, 2018). Such systems can be of interest for plant cultivation tests in off-the-shelf climate chambers, the recently promoted vertical farms, or even for space-based experiments on plants, such as those already being conducted on the International Space Station. A major constraint for all of these systems is a limited growing area and energy supply. Therefore, experiments either consist of only a few plants, or plants that were not grown through their full growth cycle (see Zabel et al. 2016 for review). In this context, Bugbee (1999) suggested identifying or to breeding new genotypes particularly suited for spaceflight experiments, such as plants with an extremely small stature, known as 'super dwarfs'. These super dwarf crops have potential for cultivation in space-limited systems, as they allow for a larger number of plants to be included in one experiment. Scientifically, this would allow for more treatment factors and an increased statistical power from the increase in the number of replicates. Another useful application would be single-plant cuvettes for measuring gas exchange, an area which has already yielded significant insight into crop physiology (e.g. Livingston et al. 1994; Kölling et al. 2015; Sun et al. 2016).

Following the idea of Bugbee (1999), Frantz et al. (2004) identified an extremely small growing rice genotype (line N71 from the Konoshita Collection (Kinoshita & Shinbashi, 1982)) with a short development cycle and a high harvest index, and, in contrast to formerly identified super dwarf rice genotypes, produces a full seed set. The extremely short stature of this genotype is caused by a dysfunction in the synthesis of gibberellin (GA), a plant hormone playing a key role in the generative and vegetative development of plants. The identified genotype ('Super Dwarf Rice') grows to a maximum height of around 0.2 m, rendering it a promising candidate as a model crop for rice-based studies conducted in fully-controlled environments.

Frantz et al. (2004) conducted intensive tests on Super Dwarf Rice, including studies on photoperiod, light intensity, nitrogen supply, and temperature. They reported that the genotype exhibited the highest yield efficiency (g mol photons^{-1} PAR) over a 14 h photoperiod. The harvest index was highest under 900 μmol photons m^2 s^{-1} PAR, but had a tendency to decrease when higher and lower light intensities

were included in the analysis. However, according to Frantz et al. (2004) the largest source of variance in this experiment was phenology (i.e. days to panicle emergence), which was affected by nitrogen concentration, photoperiod, and temperature. The authors concluded that Super Dwarf Rice is well suited as a model crop and that it has several benefits over *A. thaliana,* especially as its larger grain size makes it better suited for studies on yield components.

To our knowledge, no research on Super Dwarf Rice has been published since its introduction by Frantz et al. (2004) and there is a lack of data at the plant level of the response of Super Dwarf Rice to limiting environmental conditions, such as light and nitrogen supply and their effect on leaf anatomical structures and photosynthesis. Consequently, it remains unclear whether research on Super Dwarf Rice is transferable to other rice genotypes, especially due to the absent synthesis of GA. GA is a key hormone promoting cell division and elongation, GA-deficient plants usually show stunted growth and short leaves that can also be wider and thicker than in plants with normal GA synthesis, which was observed in maize (*Zea mays*) (De Souza & MacAdam, 2001) and rice (Matsukura *et al.*, 1998). Leaves of GA-deficient plants often are darker in color, probably due to an accumulation process of pigments in response to reduced leaf area (Thomas S.G., 2004).

Pigments, mainly chlorophylls and carotenoids, are the key molecules for light harvesting and funneling of excitation energy during photosynthesis. Adjusting their concentrations is one of the first acclimation processes in leaves after changes in the light environment. Weak shading, for example, was shown to increase chlorophyll content in winter wheat and rice, while stronger shade caused a reduction in pigment content (Li *et al.*, 2010a; Wang *et al.*, 2015). Increasing pigment concentration per unit leaf area allows plants to harvest light energy more efficiently. This is not only due to higher light absorption on a leaf level, but also due to more efficient light harvesting by the antenna complexes. Excitation energy is more efficiently funneled to the reaction centers and then onward to the electron transport chain, reflected by lower values of light and dark adapted PSII fluorescence (Wang *et al.*, 2015). Typically, shading increases leaf thickness, shown for rice and other species (Terashima *et al.*, 2006; Martins *et al.*, 2014; Wang *et al.*, 2015), but contrary observations were found in winter wheat (Li *et al.*, 2010a).

Adaptions of leaf pigments, leaf morphology, PSII fluorescence, and their overall impact on photosynthesis have not been investigated in Super Dwarf Rice. However, rice is one of the most important food crops in the world, and a large number of studies have been published on the relationship between photosynthesis and yield formation. To determine whether Super Dwarf Rice is suitable as a model crop for physiological studies on rice in controlled environments, more knowledge is needed.

The aim of this study is to advance the concept of Super Dwarf Rice as a model crop for controlled environments. Controlled environments are often characterized by low-light conditions. This is attributed to the fact that illuminants emit a high thermal load making it more complicated to maintain

a stable temperature and humidity. Further, energy supply can be a critical factor. For example, in all plant cultivation experiments conducted in orbit based research facilities, light intensities provided inside the growing modules range from very low to medium (50 to 720 µmol m^{-2} s^{-1}, see the review of Zabel et al., (2016). For field crops adapted to environmental conditions in the tropics and subtropics, such as rice, these light intensities are uncommonly low. Hence, the focus of this study is on growth and photosynthesis responses of Super Dwarf Rice to different illumination regimes. Also, as light-mediated responses often interact with nitrogen supply, varying nitrogen concentrations in the nutrient solution and their effects on photosynthesis, yield components, and finally yield were investigated. Flag leaf photosynthesis was measured at three phenological stages to see how Super Dwarf Rice adapts to low- light conditions. The measurements were combined with destructive sampling to assess biomass and leaf morphological data. Additionally, we performed a yield component analysis at the end of the experiment.

4.2.   Material and Methods

Plant cultivation, treatments and sampling

Super Dwarf Rice plants from line N71 from the Konoshita Collection (seeds provided by Dale Bumpers National Rice Research Center, AR, USA) were grown in a climate chamber (Percival E-75L1, CLF PlantClimatics GmbH, Wertingen) at the University of Hohenheim, Germany, in a hydroponic system using an adapted Yoshida nutrient solution (Yoshida *et al.*, 1971). The macronutrient element composition (mM) was: 2.8 N as NH_4NO_3, 0.32 P as $NaH_2PO_4*2H_2O$, 1.02 K as K_2SO_4, 1.00 Ca as $CaCl_2$, and 1.65 Mg as $MgSO_4*7H_2O$. The micronutrient element composition (µM) was: 9.10 Mn as $MnSO_4*H_2O$, 0.05 Mo as $(NH_4)_6*Mo_7O_{24}*4H_2O$, 18.50 B as H_3BO_3, 0.15 Zn as $ZnSO_4*7H_2O$, 0.16 Cu as $CuSO_4*5H_2O$ and 35.82 Fe as FeNa - EDTA. Photoperiod was set to 14h as suggested by Bugbee (1999), and temperature to 30 °C and 28 °C during light and dark periods, respectively. Relative Humidity (rH) inside the growth chamber was set to 70 %.

To provide anaerobic conditions during germination as proposed by Frantz and Bugbee (2002), seeds were transferred into a polyethylene bottle and covered with approximately 15 cm of tap water. Germination took place in darkness at 30° C. After germination, about 200 seedlings were transferred in plastic boxes (20 cm x 20 cm x 5.5 cm) with moist tissue paper. Light was supplied 8 days after germination when seedlings reached a height of 5 cm. Sixteen days after germination, seedlings were transferred into 3 hydroponic systems consisting of 60 joint 3.5 cm PVC-pipes that were placed into a 10 L plastic container (Georg Utz AG, Bremgarten, Switzerland) filled with nutrient solution. Thirty-six mm diameter ceapren plugs (Greiner Bio-One GmbH, Frickenhausen, Germany) were used to fix the seedlings into the PCV-pipes. The position of plants was changed randomly every 2nd day to prevent border effects. After onset of tillering, the main tiller of a randomly selected plants was cut open with a razor blade and checked for panicle formation with an optical microscope (Stemi 2000-C, Carl Zeiss

AG, Oberkochen, Germany). When the onset of panicle formation 52 days after germination was observed, 54 homogenous plants were transferred into 18 1.1 L pots, resulting in 3 plants per pot. The remaining plants were transferred into a 2nd climate chamber and kept as dummy plants for replacing plants used for destructive analyses during the experiment. Different illumination levels were established by 15 cm diameter PVC-U pipes with 50 cm height that were placed bottom-open over the pots. Pipes and pots were standing on a metal grate fixed at half-height inside the climate chamber. The inside of the pipes was covered with a highly reflecting light-scattering foil (Diamond ECO, Easy Grow Ltd., Grimsby, UK). Six pots were placed under tubes that were covered with a wire mesh covering the upper opening (mesh size 0.63/0.16 mm) resulting in a light intensity of 553 $\mu mol * m^{-2} * s^{-1}$. Six more pots were covered with a plastic mesh resulting in a light intensity of 157 $\mu mol * m^{-2} * s^{-1}$. Six pots were not covered at all, receiving a light intensity of about 745 $\mu mol * m^{-2} * s^{-1}$. Thus, the illumination levels were 20 % and 75 % of the control light intensity. The light intensities were measured with a SP2 Lite photometer (Kipp & Zonen, NL-2628 XH Delft) and refer to half plant-height with respect to fully-grown plants. Three pots in each light treatment group received 50% nitrogen concentration in the nutrient solution. Sampling took place at the following phenological stages: beginning of panicle emergence, beginning of flowering, ripening/onset of senescence. The phenological stages were determined when 25 % of the panicle bearing tillers reached the respective stage. Gas exchange measurements were always performed on flag leaves of tillers representative for the present phenological stage. Additionally, six randomly selected plants were sampled at the time treatments started. The plants harvested were replaced by a same-sized dummy-plant from the 2nd climate chamber to prevent biases in light interception and nutrient availability between growth phases. The size of the dummy-plants was simply altered by different N-concentration and stocking densities inside the 2nd climate chambers.

Gas exchange and chlorophyll fluorescence measurements

Gas exchange and chlorophyll fluorescence of fully expanded flag leaves were measured simultaneously with a GFS-3000/3055-F (Heinz Walz GmbH, Effeltrich, Germany). Plants were dark-adapted for a period of 60 minutes prior to the measurement. Minimal and maximal fluorescence (F_0, F_m) in the dark-adapted state were measured at a modulated light intensity of 1.2 $\mu mol * m^{-2} * s^{-1}$ and a saturating light pulse (SLP) of about 4500 $\mu mol * m^{-2} * s^{-1}$ light intensity for 0.8 s. Subsequently, actinic light of an intensity of 1500 $\mu mol * m^{-2} * s^{-1}$ was imposed until photosynthesis, stomatal conductance, and transient chlorophyll fluorescence (F_s) reached steady state. Subsequently, the light intensity was increased to 2000 $\mu mol * m^{-2} * s^{-1}$ and gas exchange and minimal and maximal fluorescence in the light-adapted state (F_0', F_m') of light saturated photosynthesis and chlorophyll fluorescence were measured. After this, a light response curve for PPFD values of 1750, 1500, 1250, 1000, 750, 500, 300, 150, 50 and 0 $\mu mol * m^{-2} * s^{-1}$ was recorded. For measurements of F_0', the actinic light was switched off directly after the SLP, and a far red light of 17 $\mu mol * m^{-2} * s^{-1}$ light intensity was supplied for 2

seconds followed by measurement of F_m' at a modulated light intensity of 1.2 µmol * m^{-2} * s^{-1}. F_s' was measured prior to the SLP together with gas exchange.

After the light response measurements, CO_2-response curves of gas exchange and chlorophyll fluorescence were recorded for CO_2-concentrations of 1200, 1000, 800, 600, 400, 300, 200, 100 and 50 µmol * mol^{-1}, respectively, following the same protocol as given above. For all measurements, steady state of photosynthesis and F_s was reached in 10 to 20 minutes. Temperature inside the cuvette was 30° C and relative humidity (rH) ranged between 50 and 60 %, depending on the stomatal conductance of the sample. Light response curves were fitted to an irradiance response model given by Ye (2007). Maximum gross photosynthesis ($P_{(g)max}$, µmol m^{-2} s^{-1}), compensation irradiance (I_{comp}, µmol m^{-2} s^{-1}), the quantum yield of photosynthesis at zero irradiance $f_{I(0)}$ (mmol mol^{-1}), and dark respiration rate (R_{Dark}) were calculated accordantly.

For the CO_2- and light-response curves, the values for stomatal conductance for water vapor and CO_2 (g_s, g_{sc}) and intercellular CO_2 concentrations were calculated according to equations B14 and B18 from von Caemmerer and Farquhar (1981).

Maximum and actual quantum yield of PSII photochemistry in the dark and light adapted state respectively ($F_v/F_m = (F_m - F_0)/ F_m$) and $\phi_{PSII} = (F_m' - F_s)/ F_m'$), the quantum yield of non-regulated non-photochemical energy loss in PSII ($\phi_{NO} = F_s/F_m$), and the quantum yield of regulated non-photochemical energy loss in PSII ($\phi_{NPQ} = F_s/ F_m' - F_s/ F_m$) were derived from the fluorescence measurements according to Genty et al. (1989) and Hendrickson et al. (2004)

Mesophyll conductance to CO_2 (g_m), chloroplastic CO_2-concentations (C_c), the product of leaf absorption and ratio of photons absorbed by PSII τ, maximum carboxylation capacity ($V_{c(max)}$), maximum electron transport capacity (J_{max}) and triose phosphate release rate (TPU) were calculated from the A-C_i measurements by using the curve-fitting approach proposed by Moualeu-Ngangue et al. (2017). In brief, the equations 6 and 3 given by Moualeu-Ngangue et al. (2017) based on Harley et al. (1992):

$$g_m = \frac{A(\tau PPFD\ \phi PSII - 4(A+R_d))}{(\tau PPFD\phi PSII(C_i - \Gamma^*) - 4(C_i - 2\Gamma^*)(A+R_d)}$$ Equation 1

$$C_c = C_i - \frac{A}{g_m}$$ Equation 2

and von Caemmerer & Farquhar (1981):

$$A_c = \frac{V_{cmax}(C_c - \Gamma^*)}{C_c + K_c(1 + O/K_O)} - R_d$$ Equation 3

$$A_j = \frac{J_{high}\ (C_c - \Gamma^*)}{4C_c + 8\Gamma^*} - R_d$$ Equation 4

$$A_P = 3TPU - R_d \qquad \text{Equation 5}$$

with initial estimations for τ, V_{cmax}, J_{high}, TPU and the measured values of A, PPFD, ϕ_{PSII}, C_i and R_{Dark} as a proxy for R_d (Farquhar & Busch, 2017) were solved successively. The values for Γ^* (CO_2 photocompensation point in the absence of respiration), K_c and K_O (Michaelis–Menten constants for CO_2 and O_2) were taken from Perdomo et al. (2016). Subsequently, the actual assimilation rates were calculated as the minimum values of equation 3 to 5 and the sum of squares were calculated from the differences between the estimated values and the measured values of A. An iterative optimization algorithm successively adapted the values of τ, V_{cmax} and J_{high} to minimize the sum of squared errors.

With the value of τ available for every sample leaf, mesophyll conductance at light saturated photosynthesis was calculated by equation 1. Hence, the functional components of relative photosynthetic limitations can be attributed to stomatal (l_s), mesophyll (l_m), and biochemical (l_b) limitations using the approach given by Grassi and Magnani (2005) (summarized as equation 7 in the original publication):

$$l_s = \frac{\frac{g_{tot}}{g_{sc}} \partial A / \partial C_c}{g_{tot} + \partial A / \partial C_c} \qquad \text{Equation 6}$$

$$l_m = \frac{\frac{g_{tot}}{g_{mc}} \partial A / \partial C_c}{g_{tot} + \partial A / \partial C_c} \qquad \text{Equation 7}$$

$$l_b = \frac{g_{tot}}{g_{tot} + \partial A / \partial C_c} \qquad \text{Equation 8}$$

where g_{tot} is the total diffusive conductance between the leaf surface and the chloroplast stroma and $\partial A / \partial C_c$ is the first partial derivative of Equation 3 with respect to C_c (see equation 3 in Flexas et al. (2012) for reference).

The actual contributions of the limiting components during light saturated photosynthesis (A_{sat}) due to stomatal and mesophyll conductance (Sl, Ml) and biochemical, or more precisely, limitations due to decreased maximum carboxylation rate (Bl) were derived by defining reference values from plants that showed the highest values in light-saturated photosynthesis. In this case, these were plants illuminated with 75 % of control light intensity and high nitrogen concentration at beginning of panicle emergence.

$$Sl = l_s * \left(\frac{G_{sc}^{ref} - G_{sc}}{G_{sc}}\right) \qquad \text{Equation 9}$$

$$Ml = l_m * \left(\frac{G_{mc}^{ref} - G_{mc}}{G_{mc}}\right) \qquad \text{Equation 10}$$

$$Bl = l_b * \left(\frac{V_{cmax}^{ref} - V_{cmax}}{V_{cmax}}\right) \qquad \text{Equation 11}$$

Fitting of light curves and A-C$_i$ curves was done with the Lmfit module for python (V.0.9.6, Newville et al., 2014) with Nelder-Mead as fitting method.

Leaf pigment analysis

The area of the flag leaf used for gas exchange measurements was measured with a Ll-3000C leaf area meter (Ll-Cor Inc., Lincoln, USA). Leaf chlorophyll and carotenoid contents were determined with a Beckman DU-640 UV–VIS spectrophotometer (Beckman Instruments Inc., Fullerton, USA) following 24 h dimethylsulfoxid (DMSO) extraction at room temperature as described in Sumanta et al. (2014). Additionally, the area of flag leaves was measured and specific leaf area (SLA) was calculated as the ratio between area and mass.

Biomass and yield component analysis

After the gas exchange measurements, plants were separated into stems, leaves, and roots and dry weights were determined after drying at 70 °C to constant weight. Tillers were counted, number of productive tillers determined, and, if generative material was present, weight and number of filled and unfilled spikelets determined. Additionally, leaf area of the entire plants was measured. Specific leaf area (SLA, leaf weight by leaf area) was calculated and leaf area ratio (LAR, leaf area by total plant biomass) calculated.

Relative reductions of yield components (RR) for each treatment group compared to control (Full N and light) were calculated as:

RR = 1 – (yield component / yield component of control).

Further, the dynamics of yield formation was analyzed by calculating the contribution of the specific yield components to total yield loss compared to control (cRR) by:

cRR= RR / sum of RR.

Statistical analysis

Statistical analysis was performed using a 2-way analysis of variances with the Statsmodels module (0.8.6) (Seabold & Perktold, 2010) for Python. Treatments means were compared according to Tukey's HSD test at a 5 % level. Data for yield components, leaf, and photosynthetic traits were analyzed separately for every phenological stage. For statistical analysis of the photosynthetic limitations analysis, a mixed model analysis was performed with the lmerTest package Version 3.1-0 (Kuznetsova *et al.*, 2017) in R (Version 3.5.2 , https:// cran.r-project.org), followed by a post-hoc analysis using the emmeans package Version1.3.3 (Searle *et al.*, 1980) to detect significant deviations for each of the limiting components during each growing phase from its respective reference value.

4.3. Results

Yield components

Yield components as well as their relative changes compared to the control treatment (full nitrogen, full illumination) and the contribution of each yield component to yield loss compared to control are shown in Table 7. Light intensity had a significant effect (P<0.01) on all yield components. However, the only significant differences between control and 75 % illumination were found in tiller number, where reduced illumination resulted in a 57 % reduction under high and low N-supply. Accordingly, all yield components of plants under strongly reduced illumination were significantly affected by light intensity. Independent of N-supply, tiller number was reduced by 72 % and 86 %, percentage of productive tillers was reduced by 95 % and 92 %, 90 %, and 72 % less kernels per panicles were produced. Spikelet fertility decreased by 91 % and 100 %, and average kernel weight was reduced by 77 % and 100 %. No significant differences of N-supply and no significant interactions between N-supply and light intensity were found. However, plants under full light and reduced N-supply produced 25 % more tillers and 7 % more kernels per panicle than control plants. This was compensated by losses in the ratio of productive tillers (18 %), spikelet fertility (5 %) and average kernel weight (4 %), resulting in a total yield loss of about 1 %, where plants under light shade produced 74 % and 80 % less grain yield under high and low N-supply respectively. Furthermore, no plants under 20 % illumination produced any yield.

The analysis of yield component dynamics revealed that the total number of tillers was the main factor causing yield reduction for plants grown under 75 % light intensity and high and low N-supply (33 % and 29 % contribution to losses in grain yield), followed by average kernel weight (15 % and 13 % contribution respectively). The contribution of other yield components was less than 10 % for both nitrogen treatments. For plants grown under 20 % illumination, the contribution of the different yield components to yield loss was relatively similar in the range of 13 % to 18 %. For plants grown without shading and reduced N-supply, the higher number of tillers and the higher number of kernels per panicle accounted for 42 % and 12 % of the dynamics in yield formation, with number of productive tillers accounting for 30 %.

Leaf traits and chlorophyll content

Table 8 shows the effects of light intensity and N-supply on leaf traits and chlorophyll levels. In all phenological phases, light intensity significantly affected leaf area (P<0.001), whole plant LAR (P<0.001 during heading and flowering, P<0.05 during ripening), average leaf length (P<0.01 during heading and flowering, P>0.05 during ripening), SLA of flag leaves (P<0.001 during heading, P<0.05 during flowering, P<0.01 during ripening) and chlorophyll *a* content (P<0.05 during heading, P<0.01 during flowering, P<0.001 during ripening). Generally, a lower light intensity lead to smaller leaf area accompanied by a higher leaf area ratio. Further, SLA and leaf area of flag leaves tended to increase

when light intensity increased. For chlorophyll *a* content, there was a general tendency to decrease with decreasing light intensity.

Light intensity also had significant influence on whole-plant SLA (P<0.01 during heading, P<0.05 during flowering). During heading, lower light intensity generally increased whole plant SLA, whereas a consistent increase of this parameter during flowering was only measured under high-N supply. Under low-N supply, 75 % light intensity lead to an increase in whole plant SLA, but a decrease was observed when illumination was reduced to 20 %. Further, light intensity had a significant effect on average leaf size (P<0.05) during ripening and the Chlorophyll *a/b* ratio during flowering (P<0.05), though post-hoc analysis did not show any differences between the treatment groups. Additionally, a higher light intensity positively affected chlorophyll *b* content during flowering and ripening (P<0.01 and P<0.001 respectively). The only significant effects of N-supply were found during the ripening phase for chlorophyll *a* content and average leaf length and size (P<0.01, P<0.05 and P<0.05 respectively).

Illumination and N-supply significantly affected LAR during flowering (P<0.01), mean leaf length during heading (P<0.05), and chlorophyll a content during ripening (P<0.001). Reduced light intensity consistently decreased LAR in low-N plants, whereas LAR of plants under high N-supply was smallest for plants under 75 % light intensity. During heading, illumination affected only mean leaf length of plants under normal N supply. Reduced light intensity under low N-supply caused a significant increase in chlorophyll *a* content compared to normal N-supply.

Gas exchange

Values for $P_{g(max)}$, I_{comp} and $f_{I(0)}$ extracted from the light response curves and values for $V_{c(max)}$ and J_{max} extracted from A/Cc measurements are shown in Table 9. Light response curves for all treatments in all phenological stages are shown in Figure 7:

Generally, maximum photosynthesis rates measured for plants under 75 % illumination were higher than for plants under control or 20 % illumination, whereas with 20 % illumination, plants showed the lowest photosynthesis rates. Photosynthesis rates generally decreased towards the end of the generative phase and this decrease was greatest for plants under 20 % illumination. N-supply significantly increased $P_{g(max)}$ during ripening (P<0.05). At 20 % illumination, plants under low N-supply were considerably lower than the values of plants under 75 % illumination under and high N-supply levels and also significantly lower than values of control plants under full N-supply. Light intensity significantly (P<0.01) affected $P_{g(max)}$ during heading and ripening and I_{comp} during heading (P<0.001) were values for 20 % illumination plants were more than 60 % lower compared to control plants. Light intensity furthermore significantly (P<0.01) increased $f_{I(0)}$ during flowering stage for control plants under low N-supply compared to plants receiving 75 % illumination under high N-supply. Assimilation values measured under the respective growing light intensities for fully illuminated plants under high

and low N-supply were 12. 8 and 9.8 µmol s^{-1} m^{-2} at heading, 9.8 and 8.6 µmol s^{-1} m^{-2} at flowering and 10.4 and 8.6 µmol s^{-1} m^{-2} during ripening. For 75 % illuminated plants the values were 11.1 and 9.6 µmol s^{-1} m^{-2} at heading, 10.5 and 9.8 µmol s^{-1} m^{-2} at flowering and 10.3 and 10.0 µmol s^{-1} m^{-2} during ripening. For plants under 20 % illumination the values were 3.5 and 3.2 µmol s^{-1} m^{-2} at heading, 2.9 and 3.0 µmol s^{-1} m^{-2} at flowering and 3.5 and 2.6 µmol s^{-1} m^{-2} during ripening. No statistical differences were found between fully and 75 % illuminated plants and between high and low N-supply during the whole experiment (P<0.05). However, plants under 20 % illumination always had significant lower Assimilation values measured under the growing light intensities. Results are illustrated in figure 3.

During ripening, light intensity significantly affected J_{max} (P<0.05) with plants receiving 75 % illumination showing the highest values. Neither light intensity nor nitrogen supply affected J_{max} or $V_{c(max)}$ during the earlier development phases.

Fv/Fm was not significantly affected by any treatment or phenological stage. Values persisted close to 0.8 or higher, giving no indication of damage to photosystem II.

Fluorescence analysis

Light response curves for ϕ_{PSII}, ϕ_{NO} and ϕ_{NPQ} are shown in Figure 9. ϕ_{PSII} linearly decreased when PPFD increased within 1000 µmol s^{-1} m^{-2} while ϕ_{NPQ} increased in the same manner, accompanied by a much smaller increase of ϕ_{NO}. Generally, under high N-supply, leaves of plants under control illumination showed higher values of ϕ_{PSII}, especially under irradiances < 1000 µmol s^{-1} m^{-2}. This difference was less pronounced under low N-supply, whereas ϕ_{NPQ} of control plants tended to be highest. Throughout the entire reproductive phase, reduced light intensity increased ϕ_{NO}.

Table 10 shows mean values for $\phi_{PSII,}$ ϕ_{NPQ} and ϕ_{NO} extracted at the respective growing irradiances of all treatment groups. Under growing irradiance, ϕ_{PSII} was always highest for plants receiving 20 % illumination and decreased with increased light intensity, whereas the opposite was the case for ϕ_{NPQ}. Plants grown under full illumination consistently showed lower values for ϕ_{NO} under their growing irradiance compared to plants under 75 % and 20 % illumination measured at their respective growing irradiances.

Photosynthetic limitation analysis

Figure 10 shows the contributions of the stomatal (SL), mesophyll (ML), and biochemical limitations (BL) to the relative reduction in light saturated assimilation rate (A_{sat}) throughout the reproductive phase. In general, A_{sat} decreased between heading and flowering with ML contributing most to the decrease. Further, a decrease in A_{sat} was measured between flowering and ripening for plants under low N-supply and full and 20 % illumination, respectively. Here, the change was due to an increased BL in fully illuminated plants and an increased BL and ML in plants receiving 20 % illumination. Accordingly, the strongest reduction in A_{sat} was recorded for plants under 20 % illumination and low

N-supply during ripening (6.4 μmol m^{-2} s^{-1} compared to the reference value of 18.5 μmol m^{-2} s^{-1} measured for plants receiving 75 % illumination and high N-supply during heading). However, A_{sat} values for high-N plants increased after flowering due to a lower ML in all illumination treatments and that was not offset by a simultaneous, though smaller, increase in SL.

A mixed model analysis was carried out to identify significant differences for each of the limiting components during the growing phases from its corresponding reference value at the beginning of the reproductive phase. ML was significantly affected by N-supply (χ^2 (1)=10.1, p<0.01), light intensity(χ^2 (2)=21.86, p<0.001), and development stage (χ^2 (2)=6.34, p<0.05). SL was neither affected by N-supply (χ^2 (1)=1.36, p<0.24) nor light intensity (χ^2 (2)=3.8462, p<0.15), but by development stage (χ^2 (5)=18.721, p<0.01). For BL, the null model was not significantly different from the full model (χ^2 (5) =1.7, p=0.9). Under high N-supply, higher light intensity significantly decreased ML at all development stages. Under low N-supply, ML was always higher for control plants and for plants receiving 20 % illumination as well as during flowering for plants receiving 75 % illumination. For both N treatments, SL was significantly increased during ripening for all light intensities.

No correlation between mesophyll conductance and SLA of flag leaves were found. Pooled over both N-levels, average SLA of fully illuminated plants was 113 cm g^{-1} and g_m was 125 mmol m^{-2} s^{-1} . The values for 75 % illuminated plants were 135 cm g^{-1} and 197 mmol m^{-2} s^{-1} and 125 cm g^{-1} and 80 mmol m^{-2} s^{-1} for plants under 20 % illumination respectively. The values are also illustrated in figure 6.

Table 7: Yield Components, relative decrease and contribution of specific yield components to grain yield loss of Super Dwarf Rice plants (ID-18h) grown under 3 levels of light intensity and 2 levels of Nitrogen supply. Different letters indicate significant differences at P < 0.05 according to Tukey's HSD. * P < 0.05, ** P < 0.01, *** P < 0.001.

Treatments		Nr. Of Tillers	Prod. Tillers (%)	Kernels per Panicle	Spikelet Filling (%)	Average Kernel Weight (mg)	Grain Yield (g)
Nitrogen	Illumination						
2.8 mmol N	Full light	24 ±0.82 (a)	0.66 ±0.04 (a)	13.2 ±0.11 (a)	0.91 ±0.023 (a)	21 ±0.32 (a)	4.002 ±0.323 (a)
	75 % illumination	10.3 ±1.09 (b)	0.64 ±0.11 (a)	11.6 ±1.27 (ba)	0.87 ±0.001 (a)	16.4 ±0.42 (a)	1.051 ±0.155 (b)
	20 % illumination	6.7 ±1.91 (b)	0.03 ±0.02 (b)	1.3 ±1.09 (c)	0.08 ±0.068 (b)	4.8 ±3.89 (b)	0.005 ±0.004 (c)
1.4 mmol N	Full light	30 ±1.25 (a)	0.54 ±0.03 (a)	14.2 ±0.92 (a)	0.87 ±0.021 (a)	20.3 ±0.14 (a)	3.98 ±0.234 (a)
	75 % illumination	10.3 ±2.13 (b)	0.56 ±0.07 (a)	12.6 ±1.67 (ba)	0.78 ±0.04 (a)	15.8 ±0.63 (a)	0.799 ±0.073 (cb)
	20 % illumination	3.3 ±1.19 (b)	0.06 ±0.05 (b)	3.7 ±2.99 (cb)	0 ±0 (b)	0 ±0 (b)	0 ±0 (c)
F_{value}	F_L	81.28***	38.91***	19.03***	248.78***	45.71***	185.14***
	F_N	0.37	0.95	0.79	4.4	1.6	0.27
	$F_{L:N}$	3.45	0.53	0.08	0.17	0.7	0.2
Relative decrease compared to control (Full N, Full Light)							
2.8 mmol N	Full light	-	-	-	-	-	-
	75 % illumination	0.57	0.03	0.13	0.04	0.22	0.74
	20 % illumination	0.72	0.95	0.9	0.91	0.77	1
1.4 mmol N	Full light	-0.25	0.18	-0.07	0.05	0.04	0.01
	75 % illumination	0.57	0.15	0.05	0.14	0.25	0.8
	20 % illumination	0.86	0.92	0.72	1	1	1
Contribution to relative yield loss							
2.8 mmol N	Full light	-	-	-	-	-	
	75 % illumination	0.58	0.03	0.13	0.04	0.22	
	20 % illumination	0.17	0.22	0.21	0.21	0.18	
1.4 mmol N	Full light	-0.42	0.31	-0.12	0.08	0.06	
	75 % illumination	0.49	0.13	0.04	0.12	0.21	
	20 % illumination	0.19	0.2	0.16	0.22	0.22	

Table 8: Leaf traits and chlorophyll content of Super Dwarf Rice plants (ID-18h) grown under 3 levels of light intensity and 2 levels of Nitrogen supply. Different letters indicate significant differences at $P < 0.05$ according to Tukey's HSD. * $P < 0.05$, ** $P < 0.01$, *** $P < 0.001$.

Development Stage	Treatments		Leaf Area (cm²)	SLA (whole-plant) (m² kg⁻¹)	Leaf Area Ratio (m² kg⁻¹)	Avg. Leaf Length (cm)	Avg. Leaf Width (cm)	Avg. Leaf Size (cm²)	Flag Leaf Area (cm²)	Flag Leaf SLA (m² kg⁻¹)	Chlorophyll a (µg cm⁻²)	Chlorophyll b (µg cm⁻²)	Chlorophyll a/b
Heading	2.8 mmol N	Full light	340 ±30 (a)	276 ±7 (b)	9 ±0.2 (b)	7.62 ±0.71 (b)	0.52 ±0.01 (a)	3.9 ±0.28 (a)	8.8 ±0.29 (a)	110 ±1 (cb)	43.6 ±1.8 (a)	17.1 ±2.3 (a)	2.6 ±0.23 (a)
		75 % illumination	219 ±30 (cb)	308 ±9 (ba)	11.3 ±0.6 (ba)	8.04 ±0.32 (b)	0.54 ±0.04 (a)	4.4 ±0.49 (a)	11 ±1.45 (a)	127 ±4 (ba)	42.5 ±1.2 (a)	18.8 ±1.6 (a)	2.3 ±0.15 (a)
		20 % illumination	138 ±18 (c)	361 ±26 (a)	12.6 ±0.4 (a)	10.2 ±0.16 (a)	0.49 ±0.01 (a)	5 ±0.19 (a)	9 ±1.15 (a)	109 ±3 (c)	37.9 ±2.5 (a)	13.3 ±1.1 (a)	2.9 ±0.08 (a)
	1.4 mmol N	Full light	338 ±5 (ba)	267 ±9 (b)	8.6 ±0.8 (b)	7.72 ±0.1 (b)	0.53 ±0.01 (a)	4.1 ±0.09 (a)	8.7 ±0.4 (a)	108 ±2 (c)	41.7 ±1.4 (a)	14.5 ±1.7 (a)	2.9 ±0.23 (a)
		75 % illumination	218 ±17 (c)	295 ±3 (ba)	11 ±0.5 (ba)	8.42 ±0.14 (ba)	0.55 ±0.02 (a)	4.7 ±0.25 (a)	9.7 ±0.14 (a)	130 ±4 (a)	39.2 ±1 (a)	15.8 ±1 (a)	2.5 ±0.13 (a)
		20 % illumination	132 ±9 (c)	330 ±13 (ba)	13.1 ±0.6 (a)	8.28 ±0.19 (ba)	0.5 ±0.01 (a)	4.2 ±0.02 (a)	10.9 ±0.63 (a)	125 ±2 (cba)	33.2 ±2.3 (a)	11.3 ±0.9 (a)	2.9 ±0.04 (a)
F_{value}	F_s		33.48***	10.52**	19.52***	7.32**	1.91	1.88	1.31	14.77***	5.66*	3.82	3.77
	F_N		0.03	1.78	0.01	1.99	0.33	0.26	0.04	3.34	3.32	2.73	1.51
	$F_{N:s}$		0.005	0.26	0.31	4.53*	0.01	1.75	1.3	3.52	0.21	0.04	0.16
Flowering	2.8 mmol N	Full light	395 ±29 (a)	275 ±6 (b)	5.7 ±0.1 (cb)	7.6 ±0.3 (a)	0.59 ±0.02 (a)	4.5 ±0.31 (a)	8.8 ±0.57 (a)	119 ±2 (a)	44.2 ±1.1 (ba)	17.7 ±1.6 (a)	2.5 ±0.16 (a)
		75 % illumination	143 ±28 (cb)	259 ±6 (b)	5 ±0.8 (c)	9.08 ±0.09 (a)	0.59 ±0.02 (a)	5.3 ±0.2 (a)	10.6 ±0.53 (a)	128 ±8 (a)	44.9 ±4.4 (ba)	13.2 ±2.6 (a)	2.7 ±0.17 (a)
		20 % illumination	117 ±21 (c)	345 ±4 (a)	10.2 ±0.3 (a)	8.69 ±0.49 (a)	0.53 ±0.03 (a)	4.6 ±0.5 (a)	9.7 ±0.86 (a)	134 ±4 (a)	27.1 ±2 (b)	8.3 ±1.1 (a)	3.4 ±0.27 (a)
	1.4 mmol N	Full light	277 ±13 (ba)	260 ±0 (b)	5.2 ±0.3 (c)	7.56 ±0.16 (a)	0.61 ±0.01 (a)	4.6 ±0.11 (a)	8.4 ±0.59 (a)	108 ±2 (a)	45.1 ±3.9 (a)	18.5 ±2.7 (a)	2.5 ±0.22 (a)
		75 % illumination	140 ±21 (c)	311 ±19 (ba)	6.6 ±0.3 (cb)	8.69 ±0.14 (a)	0.56 ±0.04 (a)	4.9 ±0.38 (a)	11.5 ±1.05 (a)	137 ±9 (a)	42.2 ±3.4 (ba)	10.1 ±1.5 (a)	3.2 ±0.16 (a)
		20 % illumination	100 ±24 (c)	276 ±14 (b)	7.8 ±0.4 (ba)	8.54 ±0.38 (a)	0.53 ±0.02 (a)	4.5 ±0.04 (a)	8.9 ±0.85 (a)	132 ±4 (a)	41.1 ±2.4 (ba)	10.6 ±1 (a)	2.9 ±0.06 (a)
F_{value}	F_s		37.76***	5.62*	27.13***	7.15**	2.37	1.42	3.46	5.3*	8.96**	7.62**	4.11*
	F_N		3.99	1.04	1.14	0.43	0	0.26	0.01	0.05	0.06	0	0.02
	$F_{N:s}$		2.45	10.99**	7.47**	0.11	0.21	0.25	0.44	1.04	0.39	0.72	2.12
Ripening	2.8 mmol N	Full light	202 ±6 (a)	246 ±16 (a)	2.4 ±0.2 (ba)	6.77 ±0.21 (ba)	0.59 ±0 (a)	4 ±0.12 (a)	9.9 ±0.6 (a)	116 ±1 (b)	43.5 ±0.9 (a)	16.2 ±0.4 (a)	2.7 ±0.02 (a)
		75 % illumination	53 ±5 (b)	199 ±17 (a)	1.8 ±0.2 (b)	6.36 ±0.56 (ba)	0.6 ±0.03 (a)	3.8 ±0.19 (a)	3.1 ±0.35 (ba)	144 ±4 (a)	36.6 ±0.3 (c)	12.9 ±0.6 (a)	2.9 ±0.16 (a)
		20 % illumination	73 ±17 (b)	358 ±60 (a)	5.7 ±0.8 (a)	8.83 ±0.43 (a)	0.58 ±0.02 (a)	5.1 ±0.32 (a)	10.2 ±0.58 (a)	134 ±4 (ba)	29.6 ±0.9 (d)	9 ±0.5 (b)	3.3 ±0.12 (a)
	1.4 mmol N	Full light	215 ±22 (a)	235 ±6 (a)	2.3 ±0.2 (ba)	5.81 ±0.07 (ba)	0.56 ±0.01 (a)	3.3 ±0.11 (a)	3.7 ±0.55 (ba)	118 ±5 (b)	41.2 ±0.6 (ba)	15.3 ±0.4 (a)	2.7 ±0.03 (a)
		75 % illumination	64 ±5 (b)	243 ±10 (a)	2.2 ±0.2 (b)	5.31 ±0.22 (b)	0.5 ±0.04 (a)	2.7 ±0.32 (a)	3.2 ±0.38 (ba)	140 ±7 (ba)	37.6 ±0.8 (cb)	13.8 ±0.7 (a)	2.7 ±0.13 (a)
		20 % illumination	44 ±15 (b)	211 ±57 (a)	3.1 ±1.1 (ba)	7.1 ±1.03 (ba)	0.57 ±0.04 (a)	4.1 ±0.89 (a)	6.9 ±0.1 (b)	121 ±3 (ba)	20.6 ±0.9 (e)	7.8 ±1.1 (b)	2.7 ±0.32 (a)
F_{value}	F_s		56.52***	0.36	6.45*	6.09*	0.35	3.89*	1.004	10.36**	182.61***	43.53***	1.44
	F_N		0.01	0.29	1.74	5.66*	3.04	4.89*	5.79*	1.35	21.07***	0.38	1.76
	$F_{N:s}$		1.04	1.39	2.49	0.22	1.13	0.06	7.65**	1.003	15.16***	1.001	1.02

Table 9 Photosynthetic parameters extracted from light response and A/Ci curves of Super Dwarf Rice plants (ID-18h) grown under 3 levels of light intensity and 2 levels of Nitrogen supply. Different letters indicate significant differences at P < 0.05 according to Tukey's HSD. * P < 0.05, ** P < 0.01, *** P < 0.001.

Development Stage		Treatments	F_v/F_m	$P_{g(max)}$ $\mu mol\ s^{-1}\ m^{-2}$	I_{comp} $\mu mol\ s^{-1}\ m^{-2}$	$f_{(I0)}$ $mmol\ mol^{-1}$	J_{max} $\mu mol\ s^{-1}\ m^{-2}$	$V_{c(max)}$ $\mu mol\ s^{-1}\ m^{-2}$
Heading	2.8 mmol N	Full light	0.82 ±0.006 (a)	19.1 ±0.7 (ba)	33.6 ±2.6 (a)	31.777 ±1.2 (a)	180 ±21 (a)	138 ±16 (a)
		75 % illumination	0.82 ±0.002 (a)	19.8 ±2 (a)	24.1 ±3.3 (cba)	32.789 ±3.2 (a)	178 ±18 (a)	142 ±11 (a)
		20 % illumination	0.82 ±0.006 (a)	14 ±0.4 (ba)	12.4 ±3.3 (cb)	30.54 ±0.8 (a)	135 ±10 (a)	111 ±13 (a)
	1.4 mmol N	Full light	0.83 ±0.004 (a)	15.2 ±1.2 (ba)	23 ±1.7 (cba)	26.337 ±3.8 (a)	152 ±2 (a)	131 ±12 (a)
		75 % illumination	0.83 ±0.005 (a)	18.1 ±0.7 (ba)	28.4 ±4.4 (ba)	29.187 ±1.4 (a)	156 ±5 (a)	131 ±8 (a)
		20 % illumination	0.81 ±0.002 (a)	12.6 ±1 (b)	9 ±2.2 (c)	28.445 ±3.6 (a)	145 ±5 (a)	124 ±5 (a)
F_{value}		F_s	2.91	8.79 **	13.12 ***	0.2	2.04	1.11
		F_N	0.07	4.31	1.11	1.97	1.07	0.02
		$F_{N:s}$	1.05	0.49	1.96	0.13	0.88	0.45
Flowering	2.8 mmol N	Full light	0.81 ±0.001 (a)	14.1 ±0.7 (a)	32.1 ±1.2 (a)	25.8 ±1.5 (ba)	141 ±15 (a)	124 ±22 (a)
		75 % illumination	0.79 ±0.004 (a)	14.8 ±0.5 (a)	18 ±3.7 (a)	42 ±5.3 (a)	133 ±8 (a)	124 ±10 (a)
		20 % illumination	0.81 ±0.006 (a)	13 ±2.1 (a)	30.6 ±4.5 (a)	29.3 ±2.5 (ba)	170 ±32 (a)	128 ±12 (a)
	1.4 mmol N	Full light	0.81 ±0.005 (a)	11.7 ±1.5 (a)	26.9 ±4.5 (a)	23.8 ±3.6 (b)	152 ±4 (a)	127 ±5 (a)
		75 % illumination	0.8 ±0.002 (a)	14.3 ±1.2 (a)	18.2 ±3.5 (a)	34.5 ±1.4 (ba)	168 ±19 (a)	161 ±43 (a)
		20 % illumination	0.8 ±0.009 (a)	9.6 ±1.6 (a)	19.3 ±2.9 (a)	32.4 ±0.7 (ba)	126 ±24 (a)	110 ±20 (a)
F_{value}		F_s	1.6	1.8	3.4	7 **	0	0.4
		F_N	0	2.3	2.3	0.6	0	0.1
		$F_{N:s}$	1.5	0.4	0.9	1.1	1.4	0.5
Ripening	2.8 mmol N	Full light	0.81 ±0.006 (a)	16.7 ±1.8 (a)	26.5 ±4.1 (a)	28.8 ±0.6 (a)	153 ±5 (a)	122 ±6 (a)
		75 % illumination	0.81 ±0.002 (a)	16.6 ±0.7 (a)	28 ±6.6 (a)	36.4 ±3.6 (a)	170 ±19 (a)	107 ±5 (a)
		20 % illumination	0.81 ±0.002 (a)	11.4 ±1.2 (ba)	10.1 ±2.8 (a)	34 ±1.7 (a)	121 ±7 (a)	136 ±30 (a)
	1.4 mmol N	Full light	0.79 ±0.006 (a)	11.6 ±1.5 (ba)	35.6 ±6.9 (a)	28.2 ±3.2 (a)	124 ±16 (a)	99 ±14 (a)
		75 % illumination	0.81 ±0.006 (a)	15.8 ±1.4 (a)	18.6 ±2.8 (a)	32.4 ±1.3 (a)	176 ±14 (a)	136 ±8 (a)
		20 % illumination	0.8 ±0.001 (a)	7.2 ±0.6 (b)	20.4 ±2.5 (a)	31.5 ±3.9 (a)	114 ±8 (a)	109 ±7 (a)
F_{value}		F_s	2.6	10.3 **	3.9	1.8	6.6 *	0.3
		F_N	3.8	6.8 *	0.5	0.8	0.6	0.3
		$F_{N:s}$	1.5	1.1	1.9	0.1	0.6	1.5

Table 10: Actual quantum yield of PSII photochemistry the light adapted state Y(PSII), the quantum yield of non-regulated non-photochemical energy loss in PSII Y(NO) and the quantum yield of regulated non-photochemical energy loss in PSII Y(NPQ) of Super Dwarf Rice plants (ID-18h) grown under 3 levels of light intensity and 2 levels of Nitrogen supply measured under the growing light conditions (754 µmol m^{-2} s^{-1} for full light, 553 µmol m^{-2} s^{-1} for 75 % illumination and 157 µmol m^{-2} s^{-1} for 20 % illumination)

Development Stage	Treatments		Y(PSII)	Y(NPQ)	Y(NO)
Heading	2.8 mmol N	Full light	0.44 ±0 (ba)	0.36 ±0 (ba)	0.2 ±0.004 (a)
		75 % illumination	0.46 ±0.03 (ba)	0.31 ±0.02 (ba)	0.23 ±0.014 (a)
		20 % illumination	0.54 ±0.03 (a)	0.24 ±0.02 (b)	0.22 ±0.005 (a)
	1.4 mmol N	Full light	0.36 ±0.04 (b)	0.46 ±0.05 (a)	0.19 ±0.008 (a)
		75 % illumination	0.4 ±0.04 (ba)	0.39 ±0.04 (ba)	0.21 ±0.002 (a)
		20 % illumination	0.51 ±0.02 (ba)	0.28 ±0.03 (b)	0.21 ±0.008 (a)
F_{value}	F_s		6.29*	8.22**	5.37*
	F_N		3.92	5.82*	3.23
	$F_{N:s}$		0.3	0.32	0.2
Flowering	2.8 mmol N	Full light	0.3 ±0.04 (c)	0.49 ±0.04 (a)	0.21 ±0.003 (b)
		75 % illumination	0.42 ±0.01 (cb)	0.35 ±0.01 (cb)	0.23 ±0.003 (ba)
		20 % illumination	0.53 ±0.03 (ba)	0.26 ±0.03 (dc)	0.21 ±0.004 (ba)
	1.4 mmol N	Full light	0.35 ±0.02 (c)	0.45 ±0.02 (ba)	0.2 ±0.009 (b)
		75 % illumination	0.4 ±0.01 (c)	0.35 ±0.01 (cb)	0.25 ±0.01 (a)
		20 % illumination	0.58 ±0.01 (a)	0.17 ±0 (d)	0.25 ±0.007 (a)
F_{value}	F_s		39.29***	47.35***	11.34**
	F_N		1.43	3.64	5.77*
	$F_{N:s}$		0.93	1.03	3.57
Ripening	2.8 mmol N	Full light	0.35 ±0.01 (b)	0.45 ±0.01 (a)	0.2 ±0.003 (a)
		75 % illumination	0.4 ±0 (b)	0.4 ±0.01 (a)	0.21 ±0.013 (a)
		20 % illumination	0.52 ±0.02 (a)	0.26 ±0.03 (cb)	0.22 ±0.007 (a)
	1.4 mmol N	Full light	0.31 ±0.02 (b)	0.48 ±0.02 (a)	0.21 ±0.008 (a)
		75 % illumination	0.4 ±0.02 (b)	0.38 ±0.02 (ba)	0.22 ±0.006 (a)
		20 % illumination	0.53 ±0.03 (a)	0.22 ±0.03 (c)	0.24 ±0.009 (a)
F_{value}	F_s		39.9***	34.11***	2.96
	F_N		0.14	0.16	3.43
	$F_{N:s}$		0.73	0.84	0.34

4.4. Discussion

Adjustments of Leaf Morphology and Yield Reduction

For most higher plants, leaves are the major organs for photosynthesis and assimilate production. Plants have a remarkable ability to adapt their morphology and biochemistry in response to the prevailing environmental conditions (Terashima *et al.*, 2006; Samuolienė *et al.*, 2012; Gong *et al.*, 2015). Adaptations to reduced light intensities are generally categorized into shade avoidance or shade tolerance mechanisms (Gommers *et al.*, 2013). Whereas shade avoidance strategies include elongation of stems and petioles as well as reduced branching, shade tolerance often results in a higher SLA and reduced chlorophyll a/b ratios as well as an increase in total leaf area and a higher leaf area ratio (LAR) (Trapani *et al.*, 1992). For Super Dwarf Rice to be used as a model crop in controlled environments that have limitations in space and energy, tolerance to low light conditions is required, rather than avoidance.

In our study, reduced light intensity significantly reduced leaf area via a strong reduction in tiller number, but increased the leaf area per total dry mass (LAR). There were only minor effects of light intensity on SLA and leaf length on a whole plant level and there were no significant effects on the size of older leaves or flag leaves. Based on the results on morphological adaptations, Super Dwarf Rice N71 exhibits pronounced shade tolerance strategies. The observed reduction in tillering leads to less self-shading, while the increase in LAR and SLA effectively increases total light capture. These features suggest Super Dwarf Rice is a suitable candidate for the growth in small-scale, low-light intensity environments.

The reduced grain yield observed in this study are consistent with previous studies on rice and other species (Cantagallo *et al.*, 2004; Mu *et al.*, 2010; Wang *et al.*, 2015). When illumination was reduced to 75 %, the reduction in tiller number was the main limitation for grain yield formation (57 % for high and low N-supply), followed by average kernel weight (22 % under high N-supply and 25 % under low N-supply), whereas 20 % illumination significantly reduced all yield components between 72 % and 100 % as compared to the fully illuminated control. Due to inhibited GA synthesis and the resulting lack in apical dominance (Frantz *et al.*, 2004), N71 tillers excessively. In our study, in plants growing under reduced light intensities, formation of new tillers was strongly reduced until heading, whereas tiller formation for fully illuminated plants increased during the same period (19 and 21.7 for fully illuminated plants under low and high N respectively compared to 11.3 and 11.7 tillers for 75 % illuminated plants and 7.3 and 7.5 for 20 % illuminated plants at heading, Figure 6). Frantz et al. (2004) found a positive relationship in N71 between light intensity and fertile heads per m^2 and grain yield, but did not specify whether this was caused by an increase in the total number of tillers or in the rate of productive tillers. It was also reported that the number of tillers per plant decreased with increasing planting density and that the higher number of plants mitigated this effect. Reduction in tiller number is partly an effect of inter-canopy shading (Casal *et al.*, 1986), as a result we conclude that the positive

relationship between grain yield and light intensity reported in their study was caused by a change in the numbers of tillers, as was the case in our experiment.

In a similar study conducted on field-grown rice over 3 growing seasons, Wang et al. (2015) reported that 47 % reduction in light intensity caused significant reductions of all yield components, except number of spikelets per panicle and spikelets per m^2 and showed that a decrease in grain filling and thousand grain weight had the largest effects on grain yield. However, strong genetic and environmental effects were identified, which agrees with results reported earlier on rice and wheat (Takai *et al.*, 2006; Li *et al.*, 2010a; Yoshinaga *et al.*, 2013; Stuerz *et al.*, 2014). In our study, we found significant effects of light intensity on filled grains per panicle due to the strong reduction of spikelets per panicle under minimal illumination, but no significant difference was found between spikelets per panicle in control plants and 75 % illuminated plants. In our study, three plants were grown in one tube, resulting in self-shading conditions comparable to a canopy. Lower light levels decreased tiller number accompanied by a smaller reduction in the ratio of productive tillers and in the number of filled spikelets per panicle. Therefore, it can be assumed that N71 would form a smaller number of spikelets per m^2 when grown in a canopy scenario under sub-optimal light conditions. In summary, reducing tillering seems to be the dominant reaction of N71 to sub-optimal light supply. This can be beneficial in studies where high light supply is not applicable e.g. due to technical limitations because the reduced self-shading comes along with a more homogenous light environment in the canopy and a higher light intensity at meristems like leaves and meristems could the observed reduction in kernel weight could result in decreased germination rates. Due to protocol reasons we did not carry out a germination test on the harvested seeds and propose this to be investigated in further studies.

Parallel with the onset of the light intensity treatments, nitrogen concentration in the nutrient solution was reduced to 1.4 mmol L^{-1} for half of the plants (Yoshida *et al.*, 1971). Since there was no further increase in yield when nitrogen concentration was doubled, we assume that for yield formation, a nitrogen concentration of 1.4 mmolL^{-1} is sufficient for N71 under the given conditions. Accordingly, further research on light/nitrogen interactions incorporating this genotype should be carried out under lower N concentrations than used in this study.

Photosynthesis rates under decreased illumination and changes in chlorophyll content

Assimilation of CO_2 as part of photosynthesis involves both light dependent and light independent reactions. Plants have the ability to adjust and balance these reactions at a number of set points. In a multi-genotype study on rice, Wang et al (2015) showed that lower illumination levels in some genotypes can decrease maximum photosynthesis rates ($P_{g(max)}$), maximum electron transport (J_{max}), and maximum carboxylation rates ($V_{c(max)}$), whereas in some plants these parameters stayed constant or increased combined with increased values for the efficiency of PSII photochemistry (Fv/Fm) and reduced non-photochemical quenching (NPQ). Since latter genotypes showed more stable grain yield

under low light conditions, the authors reasoned these adaptations are an expression of shade tolerance. Similar data exist for other species (Dai *et al.*, 2009; Gong *et al.*, 2015; Song & Li, 2016). In our study, $P_{g(max)}$ was consistently highest when illumination was decreased to 75 % of the control treatment. These plants also showed a higher initial quantum yield (f_{I0}), resulting in a steeper initial slope of the light response curves (Figure 7). Accordingly, assimilation values compared from plants grown under full and 75 % light intensity were not different, even when measured under the respective growing irradiances (Figure 8).

Figure 9 shows the complementary quantum yields of chlorophyll fluorescence quenching measured during light response curves. At the same light intensities, plants grown under 75 % illumination did not transfer higher ratios of the excitation energy into photochemistry. As shown, this was the case across the entire light response curves. The only exception was measured during ripening for low-N plants, during which plants receiving 75 % illumination had higher rates of photochemical quenching than control plants. However, this was not accompanied by higher assimilation rates, as can be seen by the light-response curves. Under strong light, plants grown under the highest light intensity handled excessive light energy more efficiently, indicated by higher ratios of non-photochemical and lower rates of non-regulated-non-photochemical quenching, as the latter is considered a parameter indicating the inability of a plant to protect itself from light stress (Klughammer & Schreiber, 2008). Interestingly, the trend of the curves as well as the differences between the light treatments are in accordance with previously published measurements on, such as wheat and wintercreeper (*Euonymus fortunei*) (Zivcak *et al.*, 2013; Song & Li, 2016). Quantum yields of photochemical and non-photochemical energy conversions indicate that plants grown under reduced light intensity exhibit a higher photochemical efficiency of PSII (Table 10). This partly explains why assimilation rates measured under the growing light intensities were not different between control plants and plants under 75 % illumination.

In contrast, we found that reduced light intensity resulted in a decrease of the concentrations of both pigments as well as increased chlorophyll a/b ratios. Studies on rice and other species (Dai *et al.*, 2009; Mu *et al.*, 2010; Wang *et al.*, 2015) found significant increases of chlorophyll a and b contents and a decreasing chlorophyll a/b ratio under reduced light intensity. This is usually interpreted as an adaptation process to improve light harvesting and funneling. To this moment, we have no explanation for this observation in N71. However, interactions between GA content in leaves and chlorophyll concentrations have been demonstrated in several studies (Szalai, 1968; Li *et al.*, 2010b) and it is possible it was linked with GA deficiency in our study. It should be further investigated in future research.

The actual photosynthesis rate under light saturating conditions is limited by the concentration of CO_2 at the site of carboxylation and the biochemical capacity of enzymatic apparatus of the Calvin Cycle, in this case represented by the parameter $V_{c(max)}$. The CO_2 concentration is a result of the strength of

photosynthesis itself, the CO_2 concentration of the ambient air, and the conductance of stomatal and mesophyll components between the ambient air and the inside of the chloroplast. In our study, stomatal and mesophyll limitations of plants under 75 % illumination were always smaller compared to control plants and plants receiving 20 % illumination. In all treatments, mesophyll conductance was the dominant contributor to reductions in photosynthesis. No clear pattern emerged for the contribution of the biochemical limitations between the treatments and over time. The results from this study regarding Super Dwarf Rice support earlier results by Martins et al. (2014) on shade-tolerant coffee leaves but are in contrast with results published on non-shade tolerant trees species and sugar beet (Grassi & Magnani, 2005; Grassi *et al.*, 2009; Sagardoy *et al.*, 2010) where biochemical and stomatal limitations dominated.

In many of the earlier experiments, confounding abiotic stresses such as heat, high VPD, drought, or zinc toxicity increased stomatal resistance and the g_m/g_s ratio and thus do not allow evaluating the effect of light intensity alone or in interaction with mechanisms conferring low light intensity tolerance. In this study, plants were grown without additional stresses in a commonly used nutrient solution under controlled environmental conditions where stomatal limitations are low simply because of non-limited water supply. In studies on Walnut (*Juglans regia*) and several *Acer* species, Piel et al. (2002) and Hanba et al. (2002) found a positive relation between light and mesophyll conductance, but these results were confounded by several environmental and physiological factors, especially a higher leaf thickness resulting in a higher mesophyll surface area exposed to intercellular air spaces. In Super Dwarf Rice, no correlation between mesophyll conductance and leaf thickness was found (Figure 11). In summary, photosynthesis of N71 under low light intensities is characterized by shade-tolerance mechanisms.

Several studies on low-N supply have linked reduced photosynthesis rates to a decrease in mesophyll conductance (Caemmerer & Evans, 1991; Warren, 2004). In this study, reducing the nitrogen concentration in the nutrient solution by 50 % neither lead to marked reductions in photosynthesis rates nor differences in the ratio of the different limiting components between the two treatments. There was no clear contribution of different N-supply levels to changes in PSII chlorophyll fluorescence patterns as was formerly demonstrated (Verhoeven *et al.*, 1997; Cheng, 2003). However, we assume that the tested N-levels were not sufficiently low enough to induce any changes in PSII efficiency (Shrestha *et al.*, 2012).

4.5. Conclusion

As proposed prior in the literature, Super Dwarf Rice seems to be a promising model crop, especially when the experimental situation is restricted in space or other resources. Its small size allows researchers to include more plants in the experiment and its small height offers the possibility to use it in specially designed, space-saving system such as multi-level racks, used in space flight experiments and many indoor research facilities that rely on experiments under controlled environmental conditions. Especially in plant growth chambers on research facilities in space, such as the International Space

Station, plant production units operate with medium to very low illumination intensities. In this study, we have demonstrated that Super Dwarf Rice only undergoes marginal morphological and anatomical changes when grown under low light conditions. The strongest morphological constraint under low illumination was a strong reduction in tiller number, but even under light intensities as low as 150 µmol m^{-2} s^{-1}, tillering still takes place, allowing researchers to examine carbon allocation or pooling during plant development. The fact that leaf elongation is strongly suppressed could ease the growth of this genotype in low-light, low-height growing racks. In summary, this rice genotype seems to be a promising candidate for experiments on one of the world's most important crops in microgravity. However, when N71 is grown for food production, light levels should be high since strong reductions in yield can occur under low light conditions. When grown in Yoshida nutrient solution, a nitrogen concentration of 1.44 mmol was shown to be sufficient, and doubling it to 2.8 mmol during tillering, as usually proposed, is not necessary as indicated by the lack of changes in yield, morphology or photosynthesis in our study. Photosynthesis of N71 was also remarkably stable under reduced illumination. This was mostly due to a higher mesophyll conductance under reduced light. This has not been observed in previous studies, and further research is needed to determine if this is a unique feature of N71.

4.6. References

Bugbee B. 1992. Determining the potential productivity of food crops in controlled environments. *Adv Space Res*, **12**(5): 85–95.

Bugbee B. 1999. Engineering plants for spaceflight environments. *Gravitational Sp Biol Bull*, **12**(2): 67–74.

Caemmerer S, Evans J. 1991. Determination of the Average Partial Pressure of CO_2 in Chloroplasts From Leaves of Several C3 Plants. *Funct Plant Biol*, **18**(3): 287.

von Caemmerer S, Farquhar G D. 1981. Some relationships between the biochemistry of photosynthesis and the gas exchange of leaves. *Planta*, **153**(4): 376–387.

Cantagallo J E, Medan D, Hall A J. 2004. Grain number in sunflower as affected by shading during floret growth, anthesis and grain setting. *Field Crops Res*, **85**(2–3): 191–202.

Casal J J, Sanchez R a., Deregibus V a. 1986. The effect of plant density on tillering: The involvement of R/FR ratio and the proportion of radiation intercepted per plant. *Environ Exp Bot*, **26**(4): 365–371.

Cheng L. 2003. Xanthophyll cycle pool size and composition in relation to the nitrogen content of apple leaves. *J Exp Bot*, **54**(381): 385–393.

Dai Y, Shen Z, Liu Y, Wang L, Hannaway D, Lu H. 2009. Effects of shade treatments on the photosynthetic capacity, chlorophyll fluorescence, and chlorophyll content of Tetrastigma hemsleyanum Diels et Gilg. *Environ Exp Bot*, **65**(2–3): 177–182.

Farquhar G D, Busch F A. 2017. Changes in the chloroplastic CO_2 concentration explain much of the observed Kok effect: a model. *New Phytol*, **214**(2): 570–584.

Flexas J, Barbour M M, Brendel O *et al.* 2012. Mesophyll diffusion conductance to CO_2: An unappreciated central player in photosynthesis. *Plant Sci*, **193–194**: 70–84.

Frantz J M, Bugbee B. 2002. Anaerobic conditions improve germination of a gibberellic acid deficient rice. *Crop Sci*, **42**(2): 651–654.

Frantz J M, Pinnock D, Klassen S, Bugbee B. 2004. Characterizing the Environmental Response of a Gibberellic Acid–Deficient Rice for Use as a Model Crop. *Agron J*, **96**(4): 1172–1181.

Genty B, Briantais J-M, Baker N R. 1989. The relationship between the quantum yield of photosynthetic electron transport and quenching of chlorophyll fluorescence. *Biochim Biophys Acta - Gen Subj*, **990**(1): 87–92.

Germer J, Sauerborn J, Asch F, de Boer J, Schreiber J, Weber G, Müller J. 2011. Skyfarming an ecological innovation to enhance global food security. *J für Verbraucherschutz und Leb*, **6**(2): 237–251.

Gommers C M M, Visser E J W, Onge K R S, Voesenek L A C J, Pierik R. 2013. Shade tolerance: When growing tall is not an option. *Trends Plant Sci*, **18**(2): 65–71.

Gong W Z, Jiang C D, Wu Y S, Chen H H, Liu W Y, Yang W Y. 2015. Tolerance vs. avoidance: two strategies of soybean (Glycine max) seedlings in response to shade in intercropping. *Photosynthetica*, **53**(2): 259–268.

Grassi G, Magnani F. 2005. Stomatal, mesophyll conductance and biochemical limitations to photosynthesis as affected by drought and leaf ontogeny in ash and oak trees. *Plant, Cell Environ*, **28**(7): 834–849.

Grassi G, Ripullone F, Borghetti M, Raddi S, Magnani F. 2009. Contribution of diffusional and non-diffusional limitations to midday depression of photosynthesis in arbutus unedo L. *Trees - Struct Funct*, **23**(6): 1149–1161.

Hanba Y T, Kogami H, Terashima I. 2002. The effect of growth irradiance on leaf anatomy and photosynthesis in Acer species differing in light demand. *Plant, Cell Environ*, **25**(8): 1021–1030.

Harley P C, Loreto F, Di Marco G, Sharkey T D. 1992. Theoretical Considerations when Estimating the Mesophyll Conductance to CO_2 Flux by Analysis of the Response of Photosynthesis to CO_2. *Plant Physiol*, **98**: 1429–1436.

Hendrickson L, Furbank R T, Chow W S. 2004. A simple alternative approach to assessing the fate of absorbed light energy using chlorophyll fluorescence. *Photosynth Res*, **82**(1): 73–81.

Kinoshita T, Shinbashi N. 1982. Identification of Dwarf Genes and Their Character Expression in the Isogenic Background. *Japanese J Breed*, **32**(3): 219–231.

Klughammer C, Schreiber U. 2008. Complementary PS II quantum yields calculated from simple fluorescence parameters measured by PAM fluorometry and the Saturation Pulse method. *PAM Appl notes*: 27–35.

Kölling K, George G M, Künzli R, Flütsch P, Zeeman S C. 2015. A whole-plant chamber system for parallel gas exchange measurements of Arabidopsis and other herbaceous species. *Plant Methods*, **11**(1): 48.

Kuznetsova A, Brockhoff P B, Christensen R H B. 2017. lmerTest Package: Tests in Linear Mixed Effects Models. *J Stat Softw*, **82**(13): 1–26.

Li H, Jiang D, Wollenweber B, Dai T, Cao W. 2010a. Effects of shading on morphology, physiology and grain yield of winter wheat. *Eur J Agron*, **33**(4): 267–275.

Li J R, Yu K, Wei J R, Ma Q, Wang B Q, Yu D. 2010b. Gibberellin retards chlorophyll degradation during senescence of paris polyphylla. *Biol Plant*, **54**(2): 395–399.

Livingston N J, Davies G J, Eby B M, Filek G, Fuchs E E, Pepin S, Percy R E. 1994. A whole-plant cuvette system to measure short-term responses of conifer seedlings to environmental change. *Tree Physiol*, **14**(7–9): 759–768.

Mackill D J, Khush G S. 2018. IR64: a high-quality and high-yielding mega variety. *Rice*, **11**(1).

Martins S C V, Galmés J, Cavatte P C, Pereira L F, Ventrella M C, DaMatta F M. 2014. Understanding the Low Photosynthetic Rates of Sun and Shade Coffee Leaves: Bridging the Gap on the Relative Roles of Hydraulic, Diffusive and Biochemical Constraints to Photosynthesis (GTS Beemster, Ed,). *PLoS One*, **9**(4): e95571.

Matsukura C, Itoh S I, Nemoto K, Tanimoto E, Yamaguchi J. 1998. Promotion of leaf sheath growth by gibberellic acid in a dwarf mutant of rice. *Planta*, **205**(2): 145–152.

Moualeu-Ngangue D P, Chen T W, Stützel H. 2017. A new method to estimate photosynthetic parameters through net assimilation rate−intercellular space CO_2 concentration (A−Ci) curve and chlorophyll fluorescence measurements. *New Phytol*, **213**(3): 1543–1554.

Mu H, Jiang D, Wollenweber B, Dai T, Jing Q, Cao W. 2010. Long-term low radiation decreases leaf photosynthesis, photochemical efficiency and grain yield in winter wheat. *J Agron Crop Sci*, **196**(1): 38–47.

Newville M, Ingargiola A, Stensitzki T, Allen D B. 2014. LMFIT: Non-Linear Least-Square Minimization and Curve-Fitting for Python. *Zenodo*.

Van Norman J M, Benfey P N. 2009. Arabidopsis thaliana as a model organism in systems biology. *Wiley Interdiscip Rev Syst Biol Med*, **1**(3): 372–379.

Perdomo J A, Carmo-Silva E, Hermida-Carrera C, Flexas J, Galmés J. 2016. Acclimation of Biochemical and Diffusive Components of Photosynthesis in Rice, Wheat, and Maize to Heat and Water Deficit: Implications for Modeling Photosynthesis. *Front Plant Sci*, **7**(November): 1–16.

Piel C, Frak E, Le Roux X, Genty B. 2002. Effect of local irradiance on CO_2 transfer conductance of mesophyll in walnut. *J Exp Bot*, **53**(379): 2423–30.

Pinstrup-Andersen P. 2018. Is it time to take vertical indoor farming seriously? *Glob Food Sec*,

17(September): 233–235.

Russo E. 2003. Special Report: The birth of biotechnology. *Nature*, **421**(6921): 456–457.

Sagardoy R, Vázquez S, Florez-Sarasa I D, Albacete A, Ribas-Carbó M, Flexas J, Abadía J, Morales F. 2010. Stomatal and mesophyll conductances to CO_2 are the main limitations to photosynthesis in sugar beet (Beta vulgaris) plants grown with excess zinc. *New Phytol*, **187**: 145–158.

Samuolienė G, Sirtautas R, Brazaitytė A, Duchovskis P. 2012. LED lighting and seasonality effects antioxidant properties of baby leaf lettuce. *Food Chem*, **134**(3): 1494–1499.

Seabold S, Perktold J. 2010. Statsmodels: Econometric and Statistical Modeling with Python. In: van der Walt S,, Millman J, eds. *Proceedings of the 9th Python in Science Conference*. 57–61.

Searle S R, Speed F M, Milliken G A. 1980. Population Marginal Means in the Linear Model: An Alternative to Least Squares Means. *Am Stat*, **34**(4): 216–221.

Shrestha S, Brueck H, Asch F. 2012. Chlorophyll index, photochemical reflectance index and chlorophyll fluorescence measurements of rice leaves supplied with different N levels. *J Photochem Photobiol B*, **113**: 7–13.

Song X, Li H. 2016. Effects of building shade on photosynthesis and chlorophyll fluorescence of Euonymus fortunei. *Acta Ecol Sin*, **36**(5): 350–355.

De Souza I R P, MacAdam J W. 2001. Gibberellic acid and dwarfism effects on the growth dynamics of B73 maize (Zea mays L.) leaf blades: A transient increase in apoplastic peroxidase activity precedes cessation of cell elongation. *J Exp Bot*, **52**(361): 1673–1682.

Stuerz S, Sow A, Muller B, Manneh B, Asch F. 2014. Yield components in response to thermal environment and irrigation system in lowland rice in the Sahel. *Field Crops Res*, **163**(October 2015): 47–54.

Sumanta N, Haque C I, Nishika J, Suprakash R. 2014. Spectrophotometric Analysis of Chlorophylls and Carotenoids from Commonly Grown Fern Species by Using Various Extracting Solvents. *Res J Chem Sci Res J Chem Sci*, **4**(9): 2231–606.

Sun S, Moravek A, Von Der Heyden L, Held A, Sörgel M, Kesselmeier J. 2016. Twin-cuvette measurement technique for investigation of dry deposition of O3 and PAN to plant leaves under controlled humidity conditions. *Atmos Meas Tech*, **9**(2): 599–617.

Szalai I. 1968. Gibberellinsäure und Chlorophyllgehalt des Blattes von Phaseolus vulgaris L. *Planta*, **83**(2): 161–165.

Takai T, Matsuura S, Nishio T, Ohsumi A, Shiraiwa T, Horie T. 2006. Rice yield potential is closely related to crop growth rate during late reproductive period. *Field Crops Res*, **96**(2–3): 328–335.

Terashima I, Hanba Y T, Tazoe Y, Vyas P, Yano S. 2006. Irradiance and phenotype: Comparative eco-development of sun and shade leaves in relation to photosynthetic CO_2 diffusion. *J Exp Bot*, **57**(2 SPEC. ISS.): 343–354.

Thomas S.G. S T-P. 2004. Update on gibberellin signaling. A tale of the tall and the short. *Plant Physiol*, **135**(2): 668–676.

Trapani N, Hall A J, Sadras V O, Vilella F. 1992. Ontogenetic changes in radiation use efficiency of sunflower (Helianthus annuus L.) crops. *Field Crops Res*, **29**(4): 301–316.

Verhoeven A S, Demmig-Adams B, Adams W W. 1997. Enhanced employment of the xanthophyll cycle and thermal energy dissipation in spinach exposed to high light and N stress. *Plant Physiol*, **113**(3): 817–824.

Wang L, Deng F, Ren W J. 2015. Shading tolerance in rice is related to better light harvesting and use efficiency and grain filling rate during grain filling period. *Field Crops Res*, **180**: 54–62.

Warren C R. 2004. The photosynthetic limitation posed by internal conductance to CO_2 movement is increased by nutrient supply. *J Exp Bot*, **55**(406): 2313–2321.

Ye Z-P. 2007. A new model for relationship between irradiance and the rate of photosynthesis in Oryza sativa. *Photosynthetica*, **45**(4): 637–640.

Yoshida S, Forno D A, Cock J. 1971. *Laboratory manual for physiological studies of rice*. Los Baños, Laguna, Philippines: International Rice Research Institute.

Yoshinaga S, Takai T, Arai-Sanoh Y, Ishimaru T, Kondo M. 2013. Varietal differences in sink production and grain-filling ability in recently developed high-yielding rice (Oryza sativa L.) varieties in Japan. *Field Crops Res*, **150**: 74–82.

Zabel P, Bamsey M, Schubert D, Tajmar M. 2016. Review and analysis of over 40 years of space plant growth systems. *Life Sci Sp Res*, **10**: 1–16.

Zivcak M, Brestic M, Balatova Z, Drevenakova P, Olsovska K, Kalaji H M, Yang X, Allakhverdiev S I. 2013. Photosynthetic electron transport and specific photoprotective responses in wheat leaves under drought stress. *Photosynth Res*, **117**(1–3): 529–546.
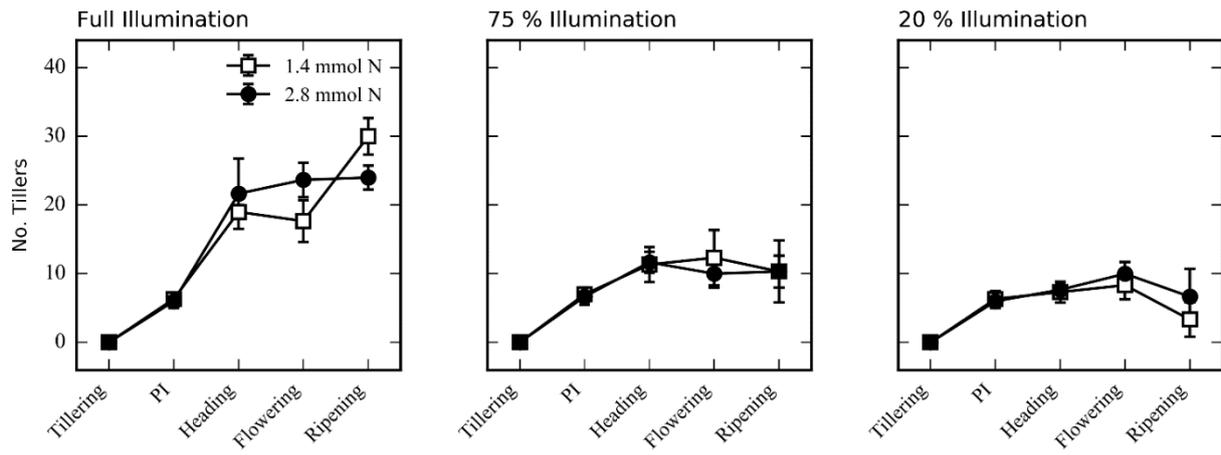
Figure 6: No. of tillers of a super dwarf rice variety grown at different light intensities and nitrogen concentrations measured at 3 different development stages.
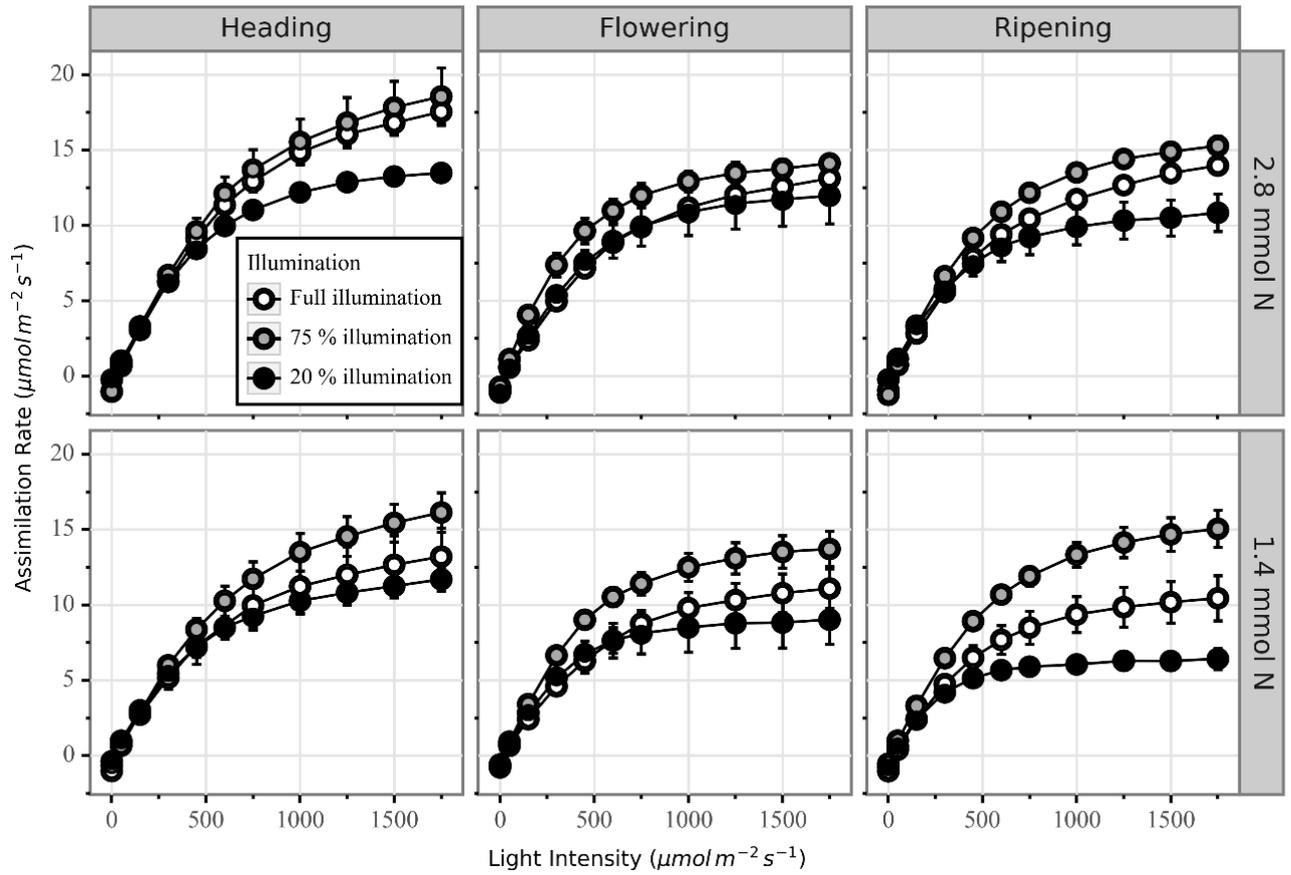
Figure 7: Light response curves of Super Dwarf Rice plants (ID-18h) grown under 3 levels of illumination and 2 levels of nitrogen supply.
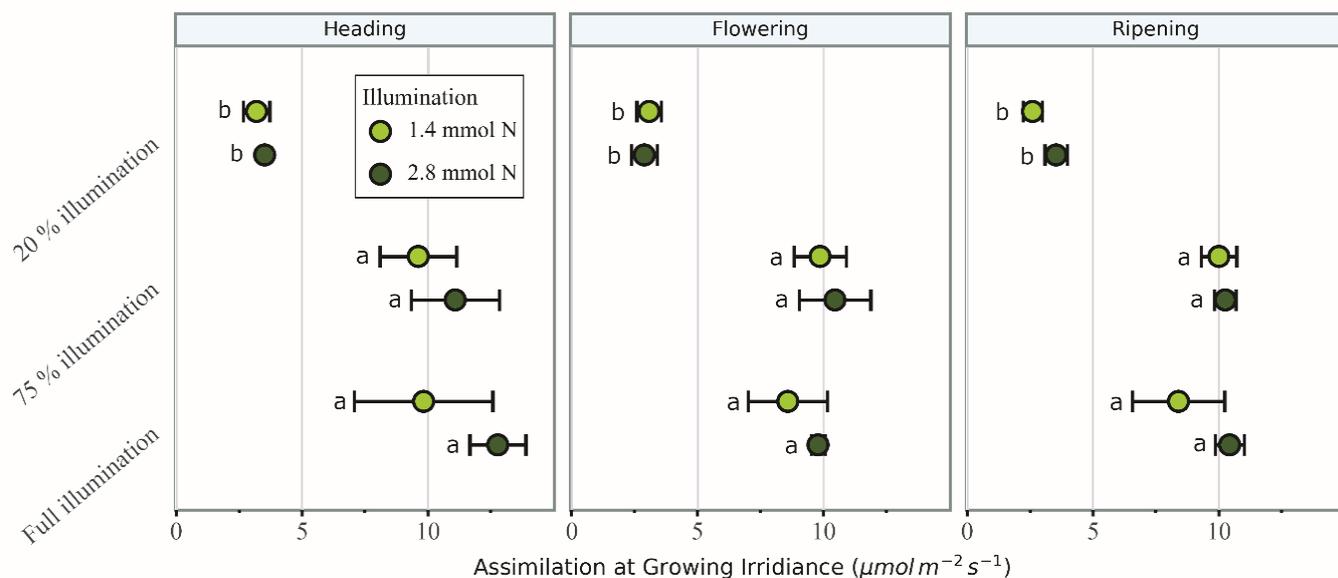
Figure 8: Assimilation values of Super Dwarf Rice grown at different light intensities and nitrogen concentrations measured under at 3 different development stages at growing irridiance. Different letters in each plot indicate significant differences at $P<0.05$ measured with by Tukeys LSD. F values were 31.2 for shading, 3.1 for nitrogen supply and 0.7 for shading:nitgrogen at heading, 59.6 for shading, 0.84 for nitrogen supply and 0.48 for shading:nitrogen at flowering, 76,8 for shading, 4.4 for nitrogen supply and 1.03 for shading:nitrogen at ripening. P values for shading were <0.001 at all development stages.
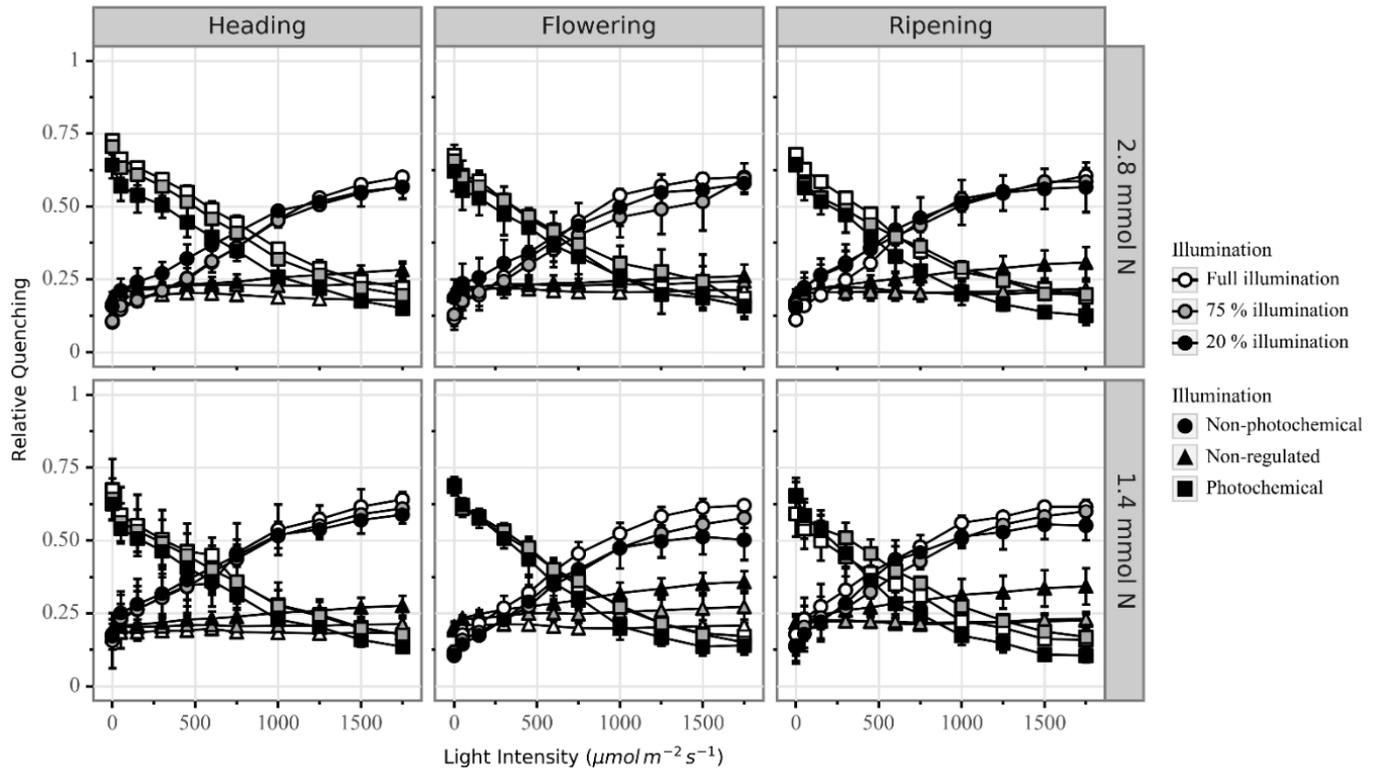
Figure 9: Irradiance response curves of Non-photochemical and photochemical fluorescence quenching and non-regulated energy loss of Super Dwarf Rice plants (ID-18h) grown under 3 levels of shading and 2 levels of Nitrogen supply.
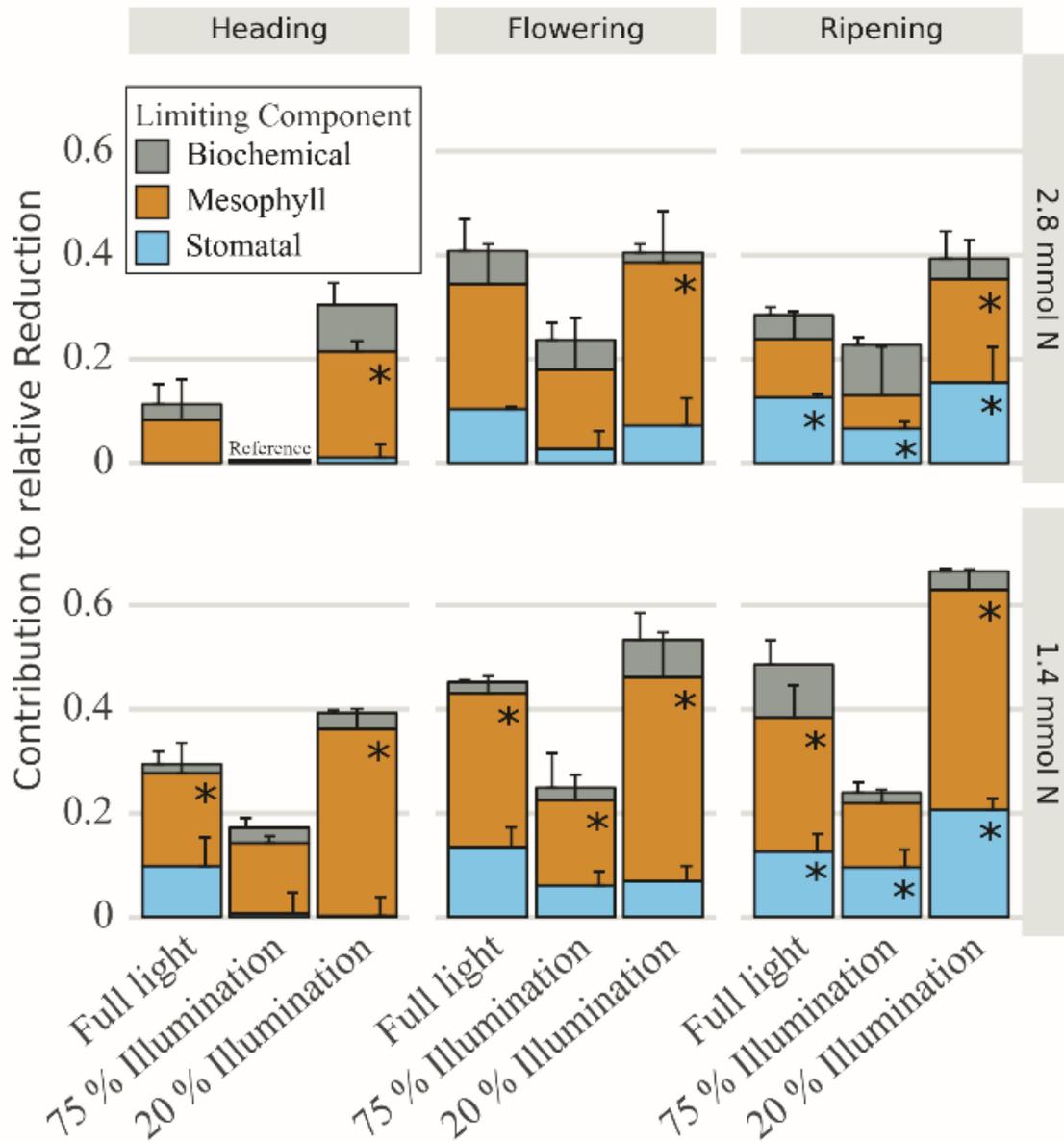
Figure 10: Relative reduction of light saturated photosynthesis rates and the contributions of different limiting components of a super dwarf rice variety grown at different light intensities and nitrogen concentrations measured at 3 different development stages at growing irradiance. Stars indicate significant differences (P≤0.05) from the reference value.
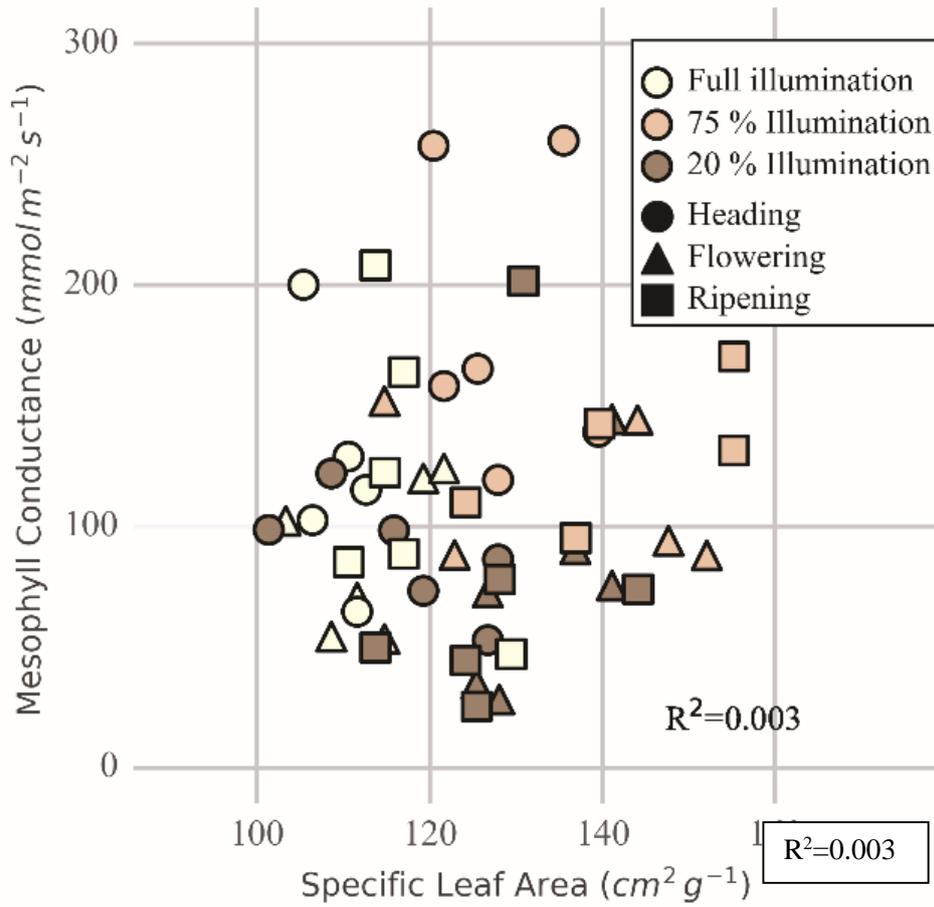
Figure 11: Mesophyll conductance plotted vs. specific leaf area of a super dwarf rice variety grown at different light intensities and nitrogen concentrations measured at 3 different development stages at growing irridiance.

5. A Python Tool for Extracting Leaf Biochemical Parameters from A-Ci curves and Photosynthesis Simulations

[*]Marc Schmierer, Folkard Asch

Institute of Agricultural Sciences in the Tropics, University of Hohenheim, 70599 Stuttgart, Germany

Submitted to *MethodsX* (MethodsX)

[*]Corresponding author at: Institute of Agricultural Sciences in the Tropics, University of Hohenheim, 70599 Stuttgart, Germany. Email address: marc.schmierer@uni-hohenheim.de (M. Schmierer)

Abstract

Plant studies often comprise simulations of photosynthesis and the gas exchange of leaves. The underlying biochemistry is usually modelled via the classic Farquhar-von Caemmerer-Berry approach, whereas mechanisms that regulate gas exchange processes, such as the adjustment of stomatal aperture, must be assessed with semi-mechanistic models that include parameters representing the intrinsic water use efficiency (WUE) of the leaf as a function of ambient concentrations of CO_2 and water vapor, plant water status, and assimilation rate. Here, we present an object-oriented software tool written in Python for simulating photosynthesis and gas exchange of leaves implementing a recently published model. Specifically, it computes actual photosynthesis and transpiration rates as well as stomatal conductance and the intercellular CO_2-concentration. We combine the gas exchange calculations with a simulation of the thermophysical properties of the ambient air including support for physical units via the Astropy package. We show an example of implementation by scaling up to canopy level and simulating a multilayer leaf model. The module also provides functions to extract parameters for stomatal behavior and leaf biochemistry from gas exchange measurements.

5.1. Method Details

Background

Plants assimilate carbon dioxide (CO_2) and release water (H_2O) vapor to the atmosphere. Since both these processes share the same path of diffusion (mainly the stoma), they are closely coupled to each other and it follows that carbon gain is always accompanied by water loss. The balance between the two competing processes has been observed to vary between plant species, depending on ecophysiological origin (Lin et al., 2015). When modelling photosynthesis, the following equation can be used to calculate stomatal conductance, g_s (mmol m^2 s^{-1}) (Medlyn et al., 2011):

$$g_s = g_0 + \left(1 + \frac{g_1}{\sqrt{D}}\right)\frac{A}{C_a} \tag{1}$$

where A is the steady state photosynthesis rate for any given environmental conditions (μmol m^2 s^{-1}), C_a is the CO_2 concentration (μmol mol^{-1}) of the ambient air, D is the vapor pressure deficit (kPa), g_0 is the residual stomatal conductance (when assimilation is zero), and g_1 is a dimensionless, empirically estimated parameter that represents the instantaneous water use efficiency of the plant. Whereas C_a and D are environmental conditions, g_0 and g_1 are estimated. A is generally calculated using the Farquhar-von Caemmerer-Berry model, which is based on both the minimum of the Rubisco-limited (A_c) and the electron transport-limited (A_j) assimilation rates:

$$A_c = \frac{V_{c(max)}(C_c - \Gamma^*)}{C_c + K_m} \tag{2}$$

$$A_j = \frac{J(C_c - \Gamma^*)}{4C_c + 8\Gamma^*} \tag{3}$$

$V_{c(max)}$ is the maximum carboxylation capacity (μmol m^2 s^{-1}), J is the light induced electron transport rate (μmol m^2 s^{-1}), K_m is the Michaelis-Menten constant for CO_2 assimilation in the presence of O_2 (μmol mol^{-1}), and Γ^* is the CO_2 compensation point in the absence of respiration (μmol mol^{-1}). C_c is the CO_2 concentration inside the chloroplast (μmol mol^{-1}) and is calculated by the equation, $C_c = C_i - A/g_m$, where C_i is the leaf internal CO_2 concentration (μmol mol^{-1}), and g_m is the leaf mesophyll conductance for CO_2 (mmol m^2 s^{-1}). In turn, C_i can be calculated by the equation $C_i = C_a - A/g_s$. J can be calculated by several approaches including a parameter for the maximum electron transport capacity (J_{max}) and curvature factors for low and high light levels (e.g. Ögren and Evans (1993); von Caemmerer and Farquhar (1981)).

In simulations, the calculation of g_s from Equation 1 is not possible since the steady state photosynthesis rate (A) of for any environmental condition is unknown at first. However, it can be solved by a combination of the above-mentioned formulas using a system of quadratic or cubic equations that must be solved simultaneously. This is known as a coupled A-g_s model. Building on this, Moualeu-Ngangue et al. (Moualeu-Ngangue et al., 2016) recently developed an approach to model time-dynamic responses of stomatal conductance to changing environmental conditions. This facilitates the calculation of transitional photosynthesis rates when ambient conditions change and the leaf readjusts. As shown by the authors, this can be of importance when estimating the effect of stomatal response time on WUE, especially during days with unstable weather conditions.

The methods described above include a couple of parameters that have to be estimated before simulating photosynthesis. This is usually done by measuring photosynthesis on leaf level and fitting the data to the formulas (1), (2) and (3). This module provides a function to extract leaf biochemical parameters form A- C_i curves using an approach that includes an estimation of g_m (Moualeu-Ngangue et al., 2017)

and another function that allows the estimation of g_0 and g_1 in equation (1) from gas exchange measurements under varying environmental conditions (VPD and CO_2-concentration).

Further, we have implemented the method of Moualeu-Ngangue et al. (Moualeu-Ngangue et al., 2016) in the Python programming language (Python Software Foundation, https://www.python.org/). We have chosen an object-oriented approach in order to facilitate scalability and to allow for inheritance. It can be integrated into crop growth models and operate at the scale of an individual canopy or an ecosystem. The ambient air is represented by a separate class that can easily be instantiated by specifying only temperature and relative humidity (rH) and automatically generates attributes of all major thermophysical properties such as vapor pressure deficit (VPD) or specific humidity (sH). Finally, we included support for physical quantities via the Astropy package (Robitaille et al., 2013) to ensure consistency among physical units. The package is available on GitHub and PyPi and can be installed via pip.

5.2. Method Description

The module includes a function for estimating leaf biochemical parameters leaf called *fitLeafBio*. Data for leaf temperature (°C), Assimilation rate (μmol m^2 s^{-1}), Irradiance (μmol m^2 s^{-1}), leaf internal CO_2-concentration (μmol mol^{-1}) and the photosynthetic yield of photosystem II (YII) from combined gas exchange and fluorescence measurements have to be provided as *numpy* arrays. Dark respiration (Rd, μmol m^2 s^{-1}) must be passed as a scalar value. Further, values for Γ^*, K_m and K_o can be passed as arguments. If not, standard values from (Moualeu-Ngangue et al., 2017) are used. For fitting the data to the model, the residual function from the *lmfit* module (Newville et al., 2014) is used and the results are available as a *minimizer result* object. The fitted parameter values can be printed by assessing its *out* attribute. Also, values for g_m and C_c can be accessed via the respective properties. An example fitting process is available in the docstring of the *fitLeafBio* class.

Similarly, the parameter values for g_0 and g_1 can be estimated by the *fit_g0_g1* class. The user must provide values for stomatal conduction (gs), assimilation rate, VPD, and leaf external CO_2-concentration as numpy arrays. Note that there should be independent variations among the data to ensure a robust fit. Again, estimated parameter values are available in the *out* property of the created class instance. An example is given again in the docstring.

Since both *fitLeafBio* and *fit_g0_g1* are ure using the *minimize* function of *lmfit* the fitting algorithm can be specified. We are using the least squares method as default, but others can be specified when calling the *fit* function. See the methods section of the *lmfit* documentation for a list of available methods. In order to support the full functionality of the minimize function, *fitLeafBio and fit_g0_g1* accept *keyword* arguments of the *minimize* function that can simply be passed when calling the *fit* function.

The method for simulating leaf photosynthesis consists out of 2 classes: *mLeaf* and *Vapour*. Before starting a simulation with an instance of *mLeaf*, we have to create an instance of *vapour* that typifies the ambient air. This is easily done with:

>>>air= vapour()

The default values for temperature are 25° C and 50 % relative humidity. The default CO_2 (here: cs) concentration is 400 µmol mol^{-1}. We can also specify the intensity of photosynthetic active radiation (PAR, µmol cm^{-2} s^{-1}), solar inclination (°) and the ratio of diffuse to direct light (unitless). Customization is done by calling the class with the respective values including the associated physical units:

>>>air=vap(temp=28*u.Celsius, rH=0.5, cs=300*u.umol/u.mol)

The *__init__* function of a *vapour* object calculates a couple of thermophysical qualities and provides them as properties. They can be assessed and modified by using their denotation. However, internally they are protected by getter and setter methods to avoid physical inconsistencies. That means that whenever one of the physical properties is changed by the user, the class ensures that the rest is recalculated given the new conditions. An example with our vapour instance:

>>>air.sH   #print specific humidity

11.725 g kg^{-1}

>>>air.sH=5*u.g/u.kg   #change specific humidity to 5 g kg^{-1}

>>>air.rH   #check relative humidity

0.214

We see that the relative humidity changed from 50 % to 21 % due to the change in specific humidity.

A *vapour* object has a defined volume that can be specified when instantiating (default 1 m^2) and thus provides values for masses of water vapor and CO_2. The operators '+' and '-' can be used to add 2 instances to each other or to subtract a defined volume from an instance. The operators '*' and '/' can be used to multiply or divide the volume of an instance. Further, 2 objects can be mixed with each other in the form of *air3=air1.mix(air2)* with the new object having the volume of *air1*. Alternatively, the argument *inplace=True* can be passed to replace *air1* with a copy of the mixed instance.

The calculations between the different types of humidity is performed by calculating the saturation water vapor pressure by a Magnus formula including an enhancement factor for air pressure followed by recalculating values for relative, absolute and specific humidity (Alduchov and Eskridge, 1996). For calculations including the slope of the saturating pressure to temperature we used the formula given in

Moualeu-Ngangue et al. (2016). For physical constants we either used values from the *Astropy* package if available or values provided in Jones (2013).

Simulations of leaf photosynthesis can be done by using the *mLeaf* class. A leaf can be instantiated by calling the class with parameters for leaf biochemistry. A list of parameters accepted by the __init__ method including their units and default values is given in

Table 11. Simulating is done by calling the *step* function by passing a *vapour* object. The *vapour* object provides all information about the atmospheric conditions that are necessary for solving the coupled model. The calculation is done in several steps as described by Moualeu-Ngangue et al. (2016). At first, the target rates for RuPB and Rubisco limited photosynthesis are calculated by solving the cubic equation given by Moualeu-Ngangue et al. (2016). This is done using the *sympy* library for symbolic mathematics (Meurer et al., 2017). The actual steady state photosynthesis rate is taken as the minimum of RuPB and Rubisco limited photosynthesis rates. In the next step, the target stomatal conductance is calculated according to equation (1) using the steady state photosynthesis rate calculated earlier. Subsequently, changes in stomatal conductance and the actual stomatal conductance are calculated according to equation (15) given by Moualeu-Ngangue et al. (2016). Changes in leaf temperature are calculated accordingly. Finally, the actual photosynthesis rate is calculated as the minimum of equations (2) and (3) by using the actual stomatal conductance for calculating C_c. Transpiration rate is calculated according to Fick's laws of diffusion. The default time step size is 1 second. When simulating large time steps, the *step* function must be called by specifying the time step size. In this case, the steady values for photosynthesis and stomatal conductance are used as actual rates. Instances of the *mLeaf* class are meant to run in a *for* loop. This offers the possibility to simulate changes in atmospheric conditions in every time step to e.g. create synthetic light or CO_2 response curves. The module additionally offers two classes for creating arrays of *vapour* and *mLeaf*. These two classes are called *vaparray* and *leafarray*. They overload the *__setitem__* and *__getitem__* operators and should be used instead of lists or *numpy* arrays.

We give a short example of creating a light response curve and storing the results in a *leafarray*:

```
>>>from ownClasses.mLeaf import leaf,leafArray

>>>from ownClasses.vapour import vap, vapArray

>>>air=vap(temp=28*u.Celsius,rH=0.4,par=0*u.umol/u.m**2/u.s,cs=400 *u.umol/u.mol)

>>>myLeaf=leaf(outAir=air,g0=0.008*u.mol/u.m**2/u.s,g1= 3.8 *u.kPa**0.5)

>>>lr=leafArray()

>>>for i in range(0,10):

>>>     a.step(air)

>>>     air.PAR+=150 * u.umol/u.m**2/u.s

>>>     lr.append(myLeaf)

>>>print(lr[1].tA)
```

The calculated gas exchange parameters are accessible as class attributes..

5.3. Example application

The source code of this package contains an example file that contains a practical application the *vapour* and *mLeaf* classes. In short, we used a crop growth model to simulate plant (Teh, 2006) to calculate growth, respiration and biomass partitioning and extended the canopy photosynthesis model by a multi-layer approach as (Anten, 1997; Cavazzoni et al., 2002). Here, we give a short summary of how the 2 classes can be used to implement such a model.

At first, we define a class called *canopy*. Among many other variables, different leaf layers are simulated, each with sunlit and shaded leaves. We can specify the number of layers when instantiating the class. In the *__init__* function, instantiate the layers by creating a *leafArray* for sunlit and shaded leaves and fill them with instances of *mLeaf*:

>>>self.sunLeafes=leafArray()

>>>[self.sunLeafes.append(leaf(g1=g1)) for i in range(0,self.layers)]

>>>self.shadeLeafes=leafArray()

>>> [self.shadeLeafes.append(leaf(g1=g1)) for i in range(0,self.layers)]

Every leaf layer will receive different light intensities and this will impose different assimilation and transpiration rates. To implement this in our model, we create arrays of *vapour* classes for each leaf layer:

>>> self.sunAir=vapArray([])

>>> [self.sunAir.append(cp.deepcopy(inAir)) for i in range(0,self.layers)]

>>> self.shadeAir=vapArray([])

>>>[self.shadeAir.append(cp.deepcopy(inAir)) for i in range(0,self.layers)]

The simulation can be run by repeatedly running the *step()* function of the *canopy* instance. Atmospheric conditions are defined by passing a *vapour* instance. Keep in mind, that a *vapour* object also provides attributes for solar inclination. Solar inclination can be obtained from the pysolar module for example (Stafford, 2018). Inside the *step()* function, light intensities for sunlit and shaded leaves are calculated in a top-down approach through all leaf layers. Next, photosynthesis and transpiration rates are calculated based on light intensity and atmospheric conditions. Finally, the resulting air humidity and CO_2 concentration inside the canopy is calculated by using the *transpire* and *assim* functions of the *vapour* class passing the total assimilation and transpiration rates of the time step:

>>>self.PostTransInAir.transpire(self.Ttot)

>>>self.PostTransInAir.assim(self.Atot)

The rest of the *step()* function calculates plant growth and development based on the calculated assimilation rates. The required air flow for keeping humidity and CO_2 values at a desired level are calculated outside the *canopy* class.

5.4. Conclusion

This package provides functions for fitting A-C_i response curves and coupled A-g_s models in one of the most popular programming language in the scientific community. Further, the possibility to simulate photosynthesis with respect to a multitude of parameters offers students, teachers and researchers the possibility to examine and understand the complex relationships inside the photosynthetic machinery of leaves as described in the current literature.

We will add more features and functionality to the package in future, but we think that it has reached a state where it can serve as a decent starting point for an exhaustive photosynthesis module in python. By making it public, we hope to invite enthusiastic python programmers to check our code for errors and to contribute new features and methods. Pull requests welcome!

Table 11: Parameter accepted by the *init* function of *mLeaf* and their units of measurement

Parameter		Unit	Default Value
$Vcmax_{25}$	maximum rate of carboxylation at 25° C	$\mu mol\ m^{-2}\ s^{-1}$	121
$Jmax_{25}$	maximum rate of electron transport at 25° C	$\mu mol\ m^{-2}\ s^{-1}$	150
$gamStar_{25}$	CO2 compensation point in absence of respiration	$\mu mol\ mol^{-1}$	40.302
K_m	Michaelis-Menten constant for CO_2 assimilation in the presence of O_2	$\mu mol\ mol^{-1}$	911
Rd_{25}	Dark respiration at 25° C	$\mu mol\ m^{-2}\ s^{-1}$	1
g_0	Residual stomatal conductance when Assimilation is zero	$\mu mol\ m^{-2}\ s^{-1}$	0.009
g_1	estimated parameter that represents the instantaneous water use efficiency of the plant	$kPa^{0.5}$	1.51
theta			0.75
k2ll			0.225
g_m	Mesophyl conductance to CO_2	$mol\ m^{-2}\ s^{-1}$	0.3
outAir	Object of class vapour	N/A	N/A

5.5. References

Alduchov, O.A., Eskridge, R.E., 1996. Improved Magnus Form Approximation of Saturation Vapor Pressure. J. Appl. Meteorol. 35, 601–609. https://doi.org/10.1175/1520-0450(1996)035<0601:IMFAOS>2.0.CO;2

Anten, N.P.R., 1997. Modelling canopy photosynthesis using parameters determined from simple non-destructive measurements. Ecol. Res. 12, 77–88. https://doi.org/10.1007/BF02523613

Cavazzoni, J., Volk, T., Tubiello, F., Monje, O., 2002. Modelling the effect of diffuse light on canopy photosynthesis in controlled environments. Acta Hortic. 593, 39–45.

Jones, H.G., 2013. Plants and microclimate: A quantitative approach to environmental plant physiology, 3rd ed. Cambridge University Press, Cambridge, UK. https://doi.org/10.1017/CBO9780511845727

Lin, Y.-S., Medlyn, B.E., Duursma, R.A., Prentice, I.C., Wang, H., Baig, S., Eamus, D., de Dios, V.R., Mitchell, P., Ellsworth, D.S., de Beeck, M.O., Wallin, G., Uddling, J., Tarvainen, L., Linderson, M.-L., Cernusak, L.A., Nippert, J.B., Ocheltree, T.W., Tissue, D.T., Martin-StPaul, N.K., Rogers, A., Warren, J.M., De Angelis, P., Hikosaka, K., Han, Q., Onoda, Y., Gimeno, T.E., Barton, C.V.M., Bennie, J., Bonal, D., Bosc, A., Low, M., Macinins-Ng, C., Rey, A., Rowland, L., Setterfield, S.A., Tausz-Posch, S., Zaragoza-Castells, J., Broadmeadow, M.S.J., Drake, J.E., Freeman, M., Ghannoum, O., Hutley, L.B., Kelly, J.W., Kikuzawa, K., Kolari, P., Koyama, K., Limousin, J.-M., Meir, P., Lola da Costa, A.C., Mikkelsen, T.N., Salinas, N., Sun, W., Wingate, L., 2015. Optimal stomatal behaviour around the world. Nat. Clim. Chang. 5, 1–6. https://doi.org/10.1038/nclimate2550

Medlyn, B.E., Duursma, R.A., Eamus, D., Ellsworth, D.S., Prentice, I.C., Barton, C.V.M., Crous, K.Y., De Angelis, P., Freeman, M., Wingate, L., 2011. Reconciling the optimal and empirical approaches to modelling stomatal conductance. Glob. Chang. Biol. 17, 2134–2144. https://doi.org/10.1111/j.1365-2486.2010.02375.x

Meurer, A., Smith, C.P., Paprocki, M., Čertík, O., Kirpichev, S.B., Rocklin, M., Kumar, Am., Ivanov, S., Moore, J.K., Singh, S., Rathnayake, T., Vig, S., Granger, B.E., Muller, R.P., Bonazzi, F., Gupta, H., Vats, S., Johansson, F., Pedregosa, F., Curry, M.J., Terrel, A.R., Roučka, Š., Saboo, A., Fernando, I., Kulal, S., Cimrman, R., Scopatz, A., 2017. SymPy: symbolic computing in Python. PeerJ Comput. Sci. 3, e103. https://doi.org/10.7717/peerj-cs.103

Moualeu-Ngangue, D.P., Chen, T.-W., Stützel, H., 2016. A Modeling Approach to Quantify the Effects of Stomatal Behavior and Mesophyll Conductance on Leaf Water Use Efficiency. Front. Plant Sci. 7, 1–15. https://doi.org/10.3389/fpls.2016.00875

Moualeu-Ngangue, D.P., Chen, T.W., Stützel, H., 2017. A new method to estimate photosynthetic parameters through net assimilation rate−intercellular space CO_2 concentration (A−Ci) curve and chlorophyll fluorescence measurements. New Phytol. 213, 1543–1554. https://doi.org/10.1111/nph.14260

Newville, M., Ingargiola, A., Stensitzki, T., Allen, D.B., 2014. LMFIT: Non-Linear Least-Square Minimization and Curve-Fitting for Python. Zenodo. https://doi.org/10.5281/ZENODO.11813

Ögren, E., Evans, J.R., 1993. Photosynthetic light-response curves. Planta 189, 182–190. https://doi.org/10.1007/BF00195075

Robitaille, T.P., Tollerud, E.J., Greenfield, P., Droettboom, M., Bray, E., Aldcroft, T., Davis, M., Ginsburg, A., Price-Whelan, A.M., Kerzendorf, W.E., Conley, A., Crighton, N., Barbary, K., Muna, D., Ferguson, H., Grollier, F., Parikh, M.M., Nair, P.H., Günther, H.M., Deil, C., Woillez, J., Conseil, S., Kramer, R., Turner, J.E.H., Singer, L., Fox, R., Weaver, B.A., Zabalza, V., Edwards, Z.I., Azalee Bostroem, K., Burke, D.J., Casey, A.R., Crawford, S.M., Dencheva, N., Ely, J., Jenness, T., Labrie, K., Lim, P.L., Pierfederici, F., Pontzen, A., Ptak, A., Refsdal, B., Servillat, M., Streicher, O., 2013. Astropy: A community Python package for astronomy. Astron. Astrophys. 558, A33. https://doi.org/10.1051/0004-6361/201322068

Stafford, B., 2018. pysolar. https://doi.org/10.5281/zenodo.1461066

Teh, C., 2006. Introduction to Mathematical Modeling of Crop Growth. How The Equations are Derived and Assembled into a Computer Model. BrownWalker Press, Boca Raton, Florida, USA.

von Caemmerer, S., Farquhar, G.D., 1981. Some relationships between the biochemistry of photosynthesis and the gas exchange of leaves. Planta 153, 376–387. https://doi.org/10.1007/BF00384257

6. General Discussion

To date, not much has been reported in the literature on the energy demand of LED lighting for indoor crop production. In our study, the estimated energy requirement for the production of 2500 g dry matter per square meter ranged between 265 and 606 kWh with the different values calculated for an optimistic and a pessimistic scenario varying in technical and physiological assumptions. The respective conversion efficiencies from electrical energy to energy assimilated into phytomass at the end of the production cycle were 2.07 % and 4.72 % and thereby lower than the theoretical maximal conversion efficiencies for C3 plants of 9.5 % given by Amthor (2010) and Zhu et al. (2008). However, considering the losses that occur during the conversion from electric energy to light (given a LED efficiency of 48 % based on our calculation derived from the datasheet of the considered LEDs), conversion efficiencies increase to 4.0 % and 9.1 %. This shows the plausibility of our approach since our values are still lower than the theoretical maximum values and well in the range of values measured for radiation use efficiency (RUE) for C3 plants in the field that range from 3.2 % (rice) to 4.5 % (sugar beet) (Amthor, 2010).

Physiological uncertainties regarding the exact quantum requirements for ATP and NAD(P)H synthesis were considered by assuming that either 3 or 4 H^+ were required for the production of 1 molecule ATP (Kobayashi' et al., 1995; Sacksteder et al., 2000). This factor increased the energy conversion efficiency by 32 %. This shows that clarification of the quanta/ATP stoichiometry is not only of scientific interest but has large practical implications for plant production scenarios.

Carbon dioxide enrichment of greenhouse air is a well-established fertilization technology used in protected vegetable gardening (Wittwer and Robb, 1964; Xin et al., 2015). It affects plant productivity by lowering relative rates of photorespiration thus increasing the rates of carbon assimilation. We assumed that the rates of photorespiration decrease from 0.28 to 0.05 by application of this management strategy. Consequently, the total energy demand for one production cycle decreased by about 38 %. Since this technology is relatively easy to implement and market ready systems are already available, we assume that CO_2 fertilization is an essential subsystem of any indoor farm. However, it should be noted that confounding effects of CO_2 enrichment on nutrient uptake and assimilation, and grain composition and quality (Erda et al., 2005; Fangmeier et al., 1999) should be considered. Further, occupational safety issues can arise during system failures because CO_2 is gas potential hazardous to humans in high concentrations. Adequate gas detectors should be used.

The ratio between emitted quanta and quanta absorbed and used for photosynthesis by the canopy is an important factor for energy requirements of indoor plant production systems. In the field, this value varies strongly during the production cycle with values between 90-95 % for dense canopies (Amthor, 2010). Moreover, further losses of light energy can occur due to so-called inactive absorption by pigments not embedded in photosynthesis. Increasing the rates for PAR absorption from 70 % to 95 %

91

decreased the energy demand for the production cycle by 24 %. Considering the technical aspects of high absorption rates is probably the most complex management strategy reviewed in this study. High absorption rates can be achieved by a couple of approaches such as highly reflective surfaces, dynamic adjustment of the orientation of the lighting systems, and dynamic planting densities. Especially at the beginning of the cropping period, energy requirements calculated per m^2 were extremely low because leaf area index and growth rates were small. Hence, increasing the number of plants per m^2 at this point followed by a readjustment in the later growing phase could be a feasible approach to increase absorption rates. Additionally, per hectare yield would increase due to a higher mean planting density over time.

It should be noted that the calculated energy requirements discussed here refer to the lighting systems only and do not include electricity needed for heating, humidification or dehumidification, possible systems for shifting plants, and automated harvesting technologies. However, as discussed by Beacham et al. (2019), it is to be expected that energy costs for lighting constitute the major component of any controlled environment farm relying on artificial illumination. This means on the other hand that lighting systems offer the largest optimization possibilities for reducing energy requirements of such farms and since the above mentioned management practices, especially high PAR absorption rates, are of theoretical nature and more information is needed about the requirements of plants concerning the light environment in controlled environments.

Extensive literature already exists about effects of spectral and directional quality of artificial light sources on plants. Brodersen et al. (2008), for example, have shown that canopy photosynthesis under high levels of diffuse light can increase even though photosynthesis on leaf level decreases at the same time. This was attributed to the effect that diffuse light penetrates deeper into the canopy thus reducing shading effects. Ample information is available in the current literature on effects of light quality on plant growth and development. Several multi-species experiments have shown that the spectral composition of the light source, particularly relative and absolute levels of blue light in the spectrum have distinct effects on morphology and photosynthesis (Cope and Bugbee, 2013; Stefański et al., 2019). However, the effects seem to be highly species specific. Dougher and Bugbee (2001), for example, found blue light to be essential for normal development of lettuce but not for soybean and wheat. This means, that any optimization strategy targeting the light supply in controlled environment farms must be adapted to the species in question. Further, since photosynthesis and plant development are directly and indirectly affected by environmental parameters such as temperature, air humidity, and CO_2-concentration (Lin et al., 2015), research tools are needed allowing manipulation of all mentioned factors simultaneously. We developed and tested an instrument capable of measuring photosynthesis and transpiration in real time under controlled environmental conditions. The objective of this work was to check if such a system could be built from readily available off-the-shelf materials. We used relatively low-cost sensors intended for home applications. The developed gas exchange measurement

system had a base area of 2.2 m^2 and a height of 1.56 m, thus allowing research on several plants simultaneously. The system included a humidification and heating system, LED-panels and sensors to measure temperature, relative humidity and CO^2-concentration and pressure. Air was passed through the system by ventilators and all the parameters were measured in 1-second intervals before and after flowing through the chamber. Values of photosynthesis and transpiration were calculated from the differences of CO_2 and water vapor concentrations before and after passing through the chamber multiplied by the flow rate. The flow rate was calculated using the standard formula of an exponential decay process applied to the rate of change in water vapour concentration after changing the humidity of the incoming air. Control of humidity and transpiration was done by a microcontroller based system connected to the humidifier and the heating/cooling systems. For cooling, peltier elements were used. Heating was done by a series of load resistors. Humidification was done by ultra-sonic nebulizers. The accuracy of the transpiration measurement by comparing calculated transpiration rates to water loss measured with a balance. The results indicate that around 90 % of the transpirational water was detected by the system. We conclude that parts of the transpirational water condensed on the surfaces thus not leaving the chamber. This circumstance should be accounted for when data acquired with the system is used for modelling purposes. Further, when checking the accuracy of the H_2O and CO_2 sensors using an industry quality infrared gas analyzer (IRGA), we found significant deviations from the values given by the IRGA and used this data for calibration of the CO_2 sensors. Further, the responses of the CO_2-sensors were linearly coupled to the H_2O concentrations (about -0.1 % ppm CO_2 / ppm H_2O). A regression analysis was performed and the coefficients were used to correct the sensor readings.

Similar systems have been reported in the past, some of them dating back to the first part of the last century (Garcia et al., 1990; Muller et al., 2009; Thomas and Hill, 1937; Wünsche and Palmer, 1997). The most sophisticated system probably has been described by van Iersel and Bugbee (2000) consisting of 10 chambers connected to an IRGA measuring CO_2 and H_2O concentrations in the chambers successively in 5-minute intervals. The accuracies of the measurements given by the authors (±2 %) were higher than in our system, but the total system costs were much higher (48 000 €, inflation-adjusted according to the calculator provided on https://westegg.com/inflation/). For our system, costs for electronics was less than 140 € and costs for humidification, heating, and cooling systems were less than 600 €. Additional costs for LED panels and casing accrue but they strongly depend on the size of the system. In our case, we spend about 1000 € for the housing and the LED panels.

We conclude that building a canopy-gas-exchange measurement system with sufficient accuracy to measure gross photosynthesis and transpiration of a plant stand is possible with off-the-shelf material that are nowadays available for relatively low costs. The electronics do not have to be completely self-assembled and developed. Instead, standard systems like *Arduino* and single board computers like the *Raspberry PI* could be used as they have been already shown to be helpful in scientific applications (Candelas et al., 2015; Sobota et al., 2013).

Further, our system is scalable and the described electronics and software can be applied in smaller systems designed for measuring single-plant gas-exchange. Such systems are an essential tool for research targeting strategies for optimizing light end environmental parameters in indoor plant production systems. The low costs would allow a higher number of experimental units and thus offer the possibility of high throughput experiments screening different combinations of environmental and light quality/direction parameters at the same time.

Extremely small plants could be used in such cuvettes to measure whole-plant gas exchange. In a climate chamber experiment, we tested a super-dwarf rice genotype (N71) for its suitability as a model crop and as a candidate for rice production in plant factories since it was outlined by Yamori and Zhang (2014) that the tallness of common rice genotype is a constraint for growing this crop in state-of-the-art multi-level racks as used in indoor vegetable production. We tested the response of N71 to different illumination and nitrogen supply levels since different data were published in the past about yield and morphological responses of rice to shade and nitrogen supply (Makino et al., 1997; Wang et al., 2015; Yamori and Zhang, 2014). In our study, a reduction in illumination led to a significant reduction in grain yield. This is consistent with previous studies on rice and other species (Cantagallo et al., 2004; Mu et al., 2010; Wang et al., 2015). A reduction in tiller number was the main limitation for grain yield formation (57 % for high and low N-supply) when illumination was reduced to 75 %, followed by average kernel weight (22 % under high N-supply and 25 % under low N-supply), whereas 20 % illumination significantly reduced all yield components between 72 % and 100 % as compared to the fully illuminated control. In contrast, Wang et al. (2015) reported that a 47 % reduction in light intensity caused significant reductions of all yield components, except number of spikelets per panicle and spikelets per m^2. The authors stated that a decrease in grain filling and thousand-grain weight had the largest effects on grain yield. However, strong genetic and environmental effects were identified, which agrees with results reported earlier on rice and wheat (H. Li et al., 2010; Stuerz et al., 2014; Takai et al., 2006; Yoshinaga et al., 2013). In summary, a reduction in tillering seems to be the dominant response of N71 to low illumination conditions. This can be beneficial in studies where high light supply is not applicable, e.g. due to technical limitations, because the reduced self-shading comes along with a more homogenous light environment in the canopy and a higher light intensity at meristems. The second highest effect on yield reduction under reduced light was a reduction in kernel weight, which could result in decreased germination rates when seeds are intended for being reused in the same facility. Since the generative material from our study was dried to equilibrium at 75° C after harvest, we were not able to carry out a germination test. We propose this to be investigated in future studies.

In our study, reduced light intensity significantly reduced leaf area via a strong reduction in tiller number, but increased the leaf area per total dry mass (LAR). Only minor effects of light intensity on SLA and leaf length were measured on whole plant level and no significant effects on the size of older leaves or flag leaves were found. Based on the results on morphological adaptations, N71 exhibits

pronounced shade tolerance strategies. The observed reduction in tillering leads to less self-shading, while the increase in LAR and SLA effectively increases total light capture. These features render Super Dwarf Rice a suitable candidate for the growth in small-scale, low-light intensity environments. Further, for Super Dwarf Rice to be used as a model crop in controlled environments, which have limitations in space and energy, tolerance to low light conditions is required because elongation of stems and leaves is unwanted since this would increase the necessary space between light panels and plants.

In our study, $P_{g(max)}$ was constantly highest when illumination was decreased to 75 % of the control treatment. These plants also showed a higher initial quantum yield (f_{I0}), resulting in a steeper initial slope of the light response curves. Accordingly, assimilation values compared from plants grown under full and 75 % light intensity were not different, even when measured under the respective growing irradiances. Quantum yields of photochemical and non-photochemical energy conversions indicate that plants grown under reduced light intensity exhibit a higher photochemical efficiency of PSII. This partly explains why assimilation rates were not different when light intensity was decreased to 75 %. The differences between the light treatments are in accordance with data previously published non-tropical plants such as wheat and wintercreeper (*Euonymus fortunei*) (Song and Li, 2016; Zivcak et al., 2013). In all treatments, mesophyll conductance was the dominant contributor to the reductions in photosynthesis. No clear pattern emerged for the contribution of the biochemical limitations between the treatments and over time. The results from this study regarding Super Dwarf Rice support earlier results by Martins et al. (2014) on shade-tolerant coffee leaves but are in contrast with results published on non-shade tolerant trees species and sugar beet (Grassi et al., 2009; Grassi and Magnani, 2005; Sagardoy et al., 2010) where biochemical and stomatal limitations dominated. However, in those studies, confounding abiotic stresses such as heat, high VPD, drought, or zinc toxicity increased stomatal resistance and hence the g_m/g_s ratio and thus do not allow evaluating the effect of light intensity alone or in interaction with mechanisms conferring low light intensity tolerance.

Studies on rice and other species (Dai et al., 2009; Mu et al., 2010; Wang et al., 2015) found significant increases of chlorophyll a and b contents and a decreasing chlorophyll a/b ratio under reduced light intensity. In contrast, reduced light intensity resulted in a decrease of the concentrations of both pigments. Moreover, reduced light intensities tended to increase the chlorophyll a/b ratio mainly caused by a stronger decay of chlorophyll a. This is in contrast to the above-mentioned studies and we do not have an explanation for this observation in N71. However, interactions between the hormone gibberellic acid (GA) content in leaves and chlorophyll concentrations have been demonstrated in several studies (J. R. Li et al., 2010; Szalai, 1968) and the possibility exists that the GA deficiency of N71 is the reason for the observed effects. This hypothesis should be addressed in further research.

Moreover, since a reduction in tiller number was the main contributor to yield loss, further experiments should investigate the possibility if the number of fertile heads per area under low light can be kept constant by adjusting planting density, thus keeping up a high per area yield under low light conditions.

We did not record any remarkable differences regarding yield, morphology, or photosynthesis between the nitrogen treatments. When grown in Yoshida or a similar nutrient solution for food production purposes, a Nitrogen concentration of 1.44 mmol seems to be sufficient. It seems not to be necessary to double it to 2.8 mmol during tillering as proposed by (Yoshida et al., 1971). In science, future studies that focus on light/nitrogen effects such as published by Makino et al. (1997) should include much lower nitrogen concentrations.

This research shows that the interactions between photosynthesis, growth, and yield formation are complex and not always easy to assess. Research tools are needed to understand and simulate photosynthesis to gain insides into these processes. We have developed a tool for simulating photosynthesis in the Python programming language. Python programs can be executed on small single-board computer that can be used to control research instruments like the above mentioned gas-exchange measuring systems or, moreover, whole plant factories thus offering the possibility to run model-based control of environmental parameters (Hou and Wang, 2013). For example, when data about the response of stomata to the environment of a plant or a plant stand is available, optimal values for temperature, humidity etc. can be acquired from the simulation to maximize photosynthesis and minimize water loss at the same time. In this work it was shown that controlled environment farming is more than just putting plants in a greenhouse. Special biological and physiological knowledge about crops is necessary and the interplay between photosynthesis, quantum requirements and energy demand must be understood in order to avoid the energy demand of such a system becoming too large. Models and tools are needed to create a controlled environment in which the plants can grow optimally and energy-efficiently. This work tries to make a contribution to this.

References

Amthor, J.S., 2010. From sunlight to phytomass: on the potential efficiency of converting solar radiation to phyto-energy. New Phytol. 188, 939–959. https://doi.org/10.1111/j.1469-8137.2010.03505.x

Beacham, A.M., Vickers, L.H., Monaghan, J.M., 2019. Vertical farming: a summary of approaches to growing skywards. J. Hortic. Sci. Biotechnol. https://doi.org/10.1080/14620316.2019.1574214

Brodersen, C.R., Vogelmann, T.C., Williams, W.E., Gorton, H.L., 2008. A new paradigm in leaf-level photosynthesis: direct and diffuse lights are not equal. Plant. Cell Environ. 31, 159–164. https://doi.org/10.1111/j.1365-3040.2007.01751.x

Candelas, F.A., García, G.J., Puente, S., Pomares, J., Jara, C.A., Pérez, J., Mira, D., Torres, F., 2015. Experiences on using Arduino for laboratory experiments of Automatic Control and Robotics. IFAC-PapersOnLine 48, 105–110. https://doi.org/10.1016/j.ifacol.2015.11.221

Cantagallo, J.E., Medan, D., Hall, A.J., 2004. Grain number in sunflower as affected by shading during floret growth, anthesis and grain setting. Field Crops Res. 85, 191–202. https://doi.org/10.1016/S0378-4290(03)00160-6

Cope, K.R., Bugbee, B., 2013. Spectral Effects of Three Types of White Light-emitting Diodes on Plant Growth and Development: Absolute versus Relative Amounts of Blue Light. HortScience 48, 504–509. https://doi.org/10.21273/HORTSCI.48.4.504

Dai, Y., Shen, Z., Liu, Y., Wang, L., Hannaway, D., Lu, H., 2009. Effects of shade treatments on the photosynthetic capacity, chlorophyll fluorescence, and chlorophyll content of Tetrastigma hemsleyanum Diels et Gilg. Environ. Exp. Bot. 65, 177–182. https://doi.org/10.1016/j.envexpbot.2008.12.008

Dougher, T.A.O., Bugbee, B., 2007. Differences in the Response of Wheat, Soybean and Lettuce to Reduced Blue Radiation¶. Photochem. Photobiol. 73, 199–207. https://doi.org/10.1562/0031-8655(2001)0730199DITROW2.0.CO2

Erda, L., Wei, X., Hui, J., Yinlong, X., Yue, L., Liping, B., Liyong, X., 2005. Climate change impacts on crop yield and quality with CO2 fertilization in China. Philos. Trans. R. Soc. B Biol. Sci. 360, 2149–2154. https://doi.org/10.1098/rstb.2005.1743

Fangmeier, A., De Temmerman, L., Mortensen, L., Kemp, K., Burke, J., Mitchell, R., Van Oijen, M., Weigel, H.J., 1999. Effects on nutrients and on grain quality in spring wheat crops grown under elevated CO_2 concentrations and stress conditions in the European, multiple-site experiment "ESPACE-wheat." Eur. J. Agron. 10, 215–229. https://doi.org/10.1016/S1161-0301(99)00012-X

Garcia, R.L., Norman, J.M., McDermitt, D.K., 1990. Measurements of canopy gas exchange using an open chamber system. Remote Sens. Rev. 5, 141–162. https://doi.org/10.1080/02757259009532126

Grassi, G., Magnani, F., 2005. Stomatal, mesophyll conductance and biochemical limitations to photosynthesis as affected by drought and leaf ontogeny in ash and oak trees. Plant, Cell Environ. 28, 834–849. https://doi.org/10.1111/j.1365-3040.2005.01333.x

Grassi, G., Ripullone, F., Borghetti, M., Raddi, S., Magnani, F., 2009. Contribution of diffusional and non-diffusional limitations to midday depression of photosynthesis in arbutus unedo L. Trees - Struct. Funct. 23, 1149–1161. https://doi.org/10.1007/s00468-009-0355-7

Hou, Z.S., Wang, Z., 2013. From model-based control to data-driven control: Survey, classification and perspective. Inf. Sci. (Ny). 235, 3–35. https://doi.org/10.1016/j.ins.2012.07.014

Kobayashi', Y., Kaiser, W., Heber, U., 1995. Bioenergetics of Carbon Assimilation in Intact Chloroplasts: Coupling of Proton to Electron Transport at the Ratio $H^+/e=3$ Is Incompatible with $H+/ATP=3$ in ATP Synthesis, Plant Cell Physioi.

Li, H., Jiang, D., Wollenweber, B., Dai, T., Cao, W., 2010. Effects of shading on morphology, physiology and grain yield of winter wheat. Eur. J. Agron. 33, 267–275. https://doi.org/10.1016/j.eja.2010.07.002

Li, J.R., Yu, K., Wei, J.R., Ma, Q., Wang, B.Q., Yu, D., 2010. Gibberellin retards chlorophyll degradation during senescence of *paris polyphylla*. Biol. Plant. 54, 395–399. https://doi.org/10.1007/s10535-010-0072-5

Lin, Y.-S., Medlyn, B.E., Duursma, R.A., Prentice, I.C., Wang, H., Baig, S., Eamus, D., de Dios, V.R., Mitchell, P., Ellsworth, D.S., de Beeck, M.O., Wallin, G., Uddling, J., Tarvainen, L., Linderson, M.-L., Cernusak, L.A., Nippert, J.B., Ocheltree, T.W., Tissue, D.T., Martin-StPaul, N.K., Rogers, A., Warren, J.M., De Angelis, P., Hikosaka, K., Han, Q., Onoda, Y., Gimeno, T.E., Barton, C.V.M., Bennie, J., Bonal, D., Bosc, A., Low, M., Macinins-Ng, C., Rey, A., Rowland, L., Setterfield, S.A., Tausz-Posch, S., Zaragoza-Castells, J., Broadmeadow, M.S.J., Drake, J.E., Freeman, M., Ghannoum, O., Hutley, L.B., Kelly, J.W., Kikuzawa, K., Kolari, P., Koyama, K., Limousin, J.-M., Meir, P., Lola da Costa, A.C., Mikkelsen, T.N., Salinas, N., Sun, W., Wingate, L., 2015. Optimal stomatal behaviour around the world. Nat. Clim. Chang. 5, 1–6. https://doi.org/10.1038/nclimate2550

Makino, A., Sato, T., Nakano, H., Mae, T., 1997. Leaf photosynthesis, plant growth and nitrogen allocation in rice under different irradiances. Planta 203, 390–398.

Martins, S.C. V, Galmés, J., Cavatte, P.C., Pereira, L.F., Ventrella, M.C., DaMatta, F.M., 2014. Understanding the Low Photosynthetic Rates of Sun and Shade Coffee Leaves: Bridging the Gap on the Relative Roles of Hydraulic, Diffusive and Biochemical Constraints to Photosynthesis. PLoS One 9, e95571. https://doi.org/10.1371/journal.pone.0095571

Mu, H., Jiang, D., Wollenweber, B., Dai, T., Jing, Q., Cao, W., 2010. Long-term low radiation decreases leaf photosynthesis, photochemical efficiency and grain yield in winter wheat. J. Agron. Crop Sci. 196, 38–47. https://doi.org/10.1111/j.1439-037X.2009.00394.x

Muller, J., Eschenroder, a, Diepenbrock, W., 2009. Through-flow chamber CO_2/H_2O canopy gas exchange system—Construction, microclimate, errors, and measurements in a barley (Hordeum

vulgare L.) field. Agric. For. Meteorol. 149, 214–229. https://doi.org/10.1016/j.agrformet.2008.08.007

Sacksteder, C. a, Kanazawa, A., Jacoby, M.E., Kramer, D.M., 2000. The proton to electron stoichiometry of steady-state photosynthesis in living plants: A proton-pumping Q cycle is continuously engaged. Proc. Natl. Acad. Sci. U. S. A. 97, 14283–14288. https://doi.org/10.1073/pnas.97.26.14283

Sagardoy, R., Vázquez, S., Florez-Sarasa, I.D., Albacete, A., Ribas-Carbó, M., Flexas, J., Abadía, J., Morales, F., 2010. Stomatal and mesophyll conductances to CO_2 are the main limitations to photosynthesis in sugar beet (Beta vulgaris) plants grown with excess zinc. New Phytol. 187, 145–158. https://doi.org/10.1111/j.1469-8137.2010.03241.x

Sobota, J., Pĭsl, R., Balda, P., Schlegel, M., 2013. Raspberry pi and arduino boards in control education. IFAC Proc. Vol. 10, 7–12. https://doi.org/10.3182/20130828-3-UK-2039.00024

Song, X., Li, H., 2016. Effects of building shade on photosynthesis and chlorophyll fluorescence of Euonymus fortunei. Acta Ecol. Sin. 36, 350–355. https://doi.org/10.1016/j.chnaes.2016.05.008

Stefański, P., Siedlarz, P., Matysik, P., Rybka, K., 2019. Usefulness of LED lightings in cereal breeding on example of wheat, barley and oat seedlings. Int. J. Agric. Biol. Eng. 12, 32–37. https://doi.org/10.25165/IJABE.V12I6.3646

Stuerz, S., Sow, A., Muller, B., Manneh, B., Asch, F., 2014. Yield components in response to thermal environment and irrigation system in lowland rice in the Sahel. Field Crops Res. 163, 47–54. https://doi.org/10.1016/j.fcr.2014.04.004

Szalai, I., 1968. Gibberellinsäure und Chlorophyllgehalt des Blattes von Phaseolus vulgaris L. Planta 83, 161–165.

Takai, T., Matsuura, S., Nishio, T., Ohsumi, A., Shiraiwa, T., Horie, T., 2006. Rice yield potential is closely related to crop growth rate during late reproductive period. Field Crops Res. 96, 328–335. https://doi.org/10.1016/j.fcr.2005.08.001

Thomas, M.D., Hill, G., 1937. The Continuous Measurement of Photosynthesis, Respiration, and Transpiration of Alfalfa and Wheat Growing under Field Conditions. Plant Physiol. 12, 285–307.

van Iersel, M.W., Bugbee, B., 2000. A multiple chamber, semicontinuous, crop carbon dioxide exchange system: design, calibration, and data interpretation. J. Am. Soc. Hortic. Sci. 125, 86–92.

Wang, L., Deng, F., Ren, W.J., 2015. Shading tolerance in rice is related to better light harvesting and use efficiency and grain filling rate during grain filling period. Field Crops Res. 180, 54–62.

https://doi.org/10.1016/j.fcr.2015.05.010

Wittwer, S.H., Robb, W.M., 1964. Carbon dioxide enrichment of greenhouse atmospheres for food crop production. Econ. Bot. 18, 34–56. https://doi.org/10.1007/BF02904000

Wünsche, J.N., Palmer, J.W., 1997. Portable through-flow cuvette system for measuring whole-canopy gas exchange of apple trees in the field. HortScience 32, 653–658.

Xin, M., Shuang, L., Yue, L., Qinzhu, G., 2015. Effectiveness of gaseous CO_2 fertilizer application in China's greenhouses between 1982 and 2010. J. CO2 Util. 11, 63–66. https://doi.org/10.1016/j.jcou.2015.01.005

Yamori, W., Zhang, G., 2014. Feasibility Study of Rice Growth in Plant Factories. Rice Res. Open Access 2, 1–6. https://doi.org/10.4172/jrr.1000119

Yoshida, S., Forno, D.A., Cock, J., 1971. Laboratory manual for physiological studies of rice. International Rice Research Institute, Los Baños, Laguna, Philippines.

Yoshinaga, S., Takai, T., Arai-Sanoh, Y., Ishimaru, T., Kondo, M., 2013. Varietal differences in sink production and grain-filling ability in recently developed high-yielding rice (Oryza sativa L.) varieties in Japan. Field Crops Res. 150, 74–82. https://doi.org/10.1016/j.fcr.2013.06.004

Zhu, X.-G., Long, S.P., Ort, D.R., 2008. What is the maximum efficiency with which photosynthesis can convert solar energy into biomass? Curr. Opin. Biotechnol. 19, 153–159. https://doi.org/10.1016/j.copbio.2008.02.004

Zivcak, M., Brestic, M., Balatova, Z., Drevenakova, P., Olsovska, K., Kalaji, H.M., Yang, X., Allakhverdiev, S.I., 2013. Photosynthetic electron transport and specific photoprotective responses in wheat leaves under drought stress. Photosynth. Res. 117, 529–546. https://doi.org/10.1007/s11120-013-9885-3

7. General Conclusions and Recommendations

In this research, the energy demand for light supply of a plant stand with a final dry matter of 2500 g m^{-2} by artificial LED illumination has been calculated. Uncertainties regarding the biochemistry of photosynthesis have been taken into account as well as the effect of different technical management strategies. It has been shown that the light demand of a plant stand is highly variable over a production period and that maximizing the ratio of absorbed radiation by the plant stand is the management strategy that should be focused on in further studies since it is a promising approach to reduce the energy requirement but, at the same time, technically complex. Since it is essential to measure canopy gas exchange when designing progressive light environments for future indoor production of cereals like rice, a low-cost gas-exchange measurement chamber has been designed that uses of-the-shelf material. The system is scalable and can be used in chamber-sized systems or in smaller cuvettes for single plants. Further, an experiment was carried out to investigate the responses of a super-dwarf rice variety that was proposed as a model crop for space-flight experiments to low-light conditions and different levels of nitrogen supply. It was demonstrated, that this variety shows only minor morphological adaptions too low light conditions but that yield losses under reduced illumination are high. Since a reduction in tiller number was the main contributor to yield loss, further experiments should investigate the possibility if the number of fertile heads per area under low light can be kept constant by adjusting planting density, thus keeping up a high per area yield under low light conditions. Further, studies on the reduced pigment content under reduced illumination and the overall high contribution of mesophyll resistance to photosynthetic limitations should be carried out in order to gain knowledge whether studies on this genotype can be generalized for rice and other cereals. The here developed Python tool for fitting A/C_i curves and A-g_s models can also be used for simulating leaf-level photosynthesis. As a publically available open-source tool researchers are welcomed to extend its functionality.

Acknowledgements

Eidesstattliche Versicherung gemäß § 8 Absatz 2 der Promotionsordnung der Universität Hohenheim zum Dr.sc.agr.

1. Bei der eingereichten Dissertation zum Thema
   'Photosynthesis, quantum requirements, and energy demand for crop production in controlled environments'
   handelt es sich um meine eigenständig erbrachte Leistung.
2. Ich habe nur die angegebenen Quellen und Hilfsmittel benutzt und mich keiner unzulässigen Hilfe Dritter bedient. Insbesondere habe ich wörtlich oder sinngemäß aus anderen Werken übernommene Inhalte als solche kenntlich gemacht.
3. Ich habe nicht die Hilfe einer kommerziellen Promotionsvermittlung oder -beratung in Anspruch genommen.
4. Die Bedeutung der eidesstattlichen Versicherung und der strafrechtlichen Folgen einer unrichtigen oder unvollständigen eidesstattlichen Versicherung sind mir bekannt. Die Richtigkeit der vorstehenden Erklärung bestätige ich. Ich versichere an Eides Statt, dass ich nach bestem Wissen die reine Wahrheit erklärt und nichts verschwiegen habe.

Hohenheim, 10.6.2020   Marc Schmierer

Curriculum Vitae

Personal Information

Name:	Marc Schmierer
Date of birth, place:	14.03.1980 in Stuttgart
Adress (recent):	Steinäcker 47a, 70619 Stuttgart, Germany
Email:	marc.schmierer@uni-hohenheim.com
Telephone (mobile):	0711/50458617, 0178/1335914
Marital status:	Single

Work experience

09 / 2011 – 07 / 2019	**Scientific staff**

University of Hohenheim, Stuttgart, Germany
Institute of Agricultural Sciences in the Tropics
(Hans-Ruthenberg-Institute) (490)

- Teaching in the study courses ‚Reaktionen und Anpassungen von Pflanzen unter Wasserstress ‘ and ‚Ökophysiologie und Anbau rohstoffliefernder Pflanzen der Tropen und Subtropen ‘
- Teaching in the practical courses ‘Crop Production Affecting the Hydrological Cycle’, ‘Ecophysiology of Crops in the Tropics and Subtropics’ and ‘Interdisciplinary Practical Science Training’
- Supervision of Bachelor and Master students

Education

10 / 2002 – 10 / 2011	Diplomstudiengang Agrarbiologie, University of Hohenheim, Germany Subject of the Diploma Thesis: ‚Optimierung von aeroponischen Anbausystemen für Reis‘ Title of qualification: Diplom-Agrarbiologe

10 / 2001 – 10 / 2002	Diplomstudiengang Biologie, University of Bayreuth, Germany
07 / 2000	School leaving certificate (Abitur) Geschwister Scholl-Gymnasium, Stuttgart, Germany

---

Conference oral and poster presentations

Knopf, O., Stürz, S., <u>Schmierer, M.</u>, Asch, F. (2019): Effects of P Nutrition and VPD on Rice Leaf Morphology and Photosynthesis
Filling gaps and removing traps for sustainable resources development. Conference poster presentation, Tropentag 2019, Kassel

<u>Schmierer, M.</u>, Knopf, O., Asch, F. (2018): Analysis of Yield Components and Photosynthetic Limitations of a Dwarf Rice Variety in Response to Shade
Global food security and food safety: The role of universities. Conference poster presentation, Tropentag 2018, Ghent

Johnson, K., Stürz, S., <u>Schmierer, M.</u>, Asch, F. (2018): Effects of Day and Night Temperature on Rice Photosynthesis
Global food security and food safety: The role of universities. Conference poster presentation, Tropentag 2018, Ghent

<u>Schmierer, M.</u> Knopf, O., Asch, F. (2016): Growth Dynamics and Yield Formation Related to Flag leaf Photosynthesis and PSII Fluorescence in Rice
Solidarity in a competing world -fair use of resources. Conference oral presentation, Tropentag 2016, Wien

<u>Schmierer, M.</u>, Bruguera, E., Asch, F. (2015): Response of Rice to Changes in the Green and Far-Red Light Ratio
Management of land use systems for enhanced food security: conflicts, controversies and resolutions. Conference poster presentation, Tropentag 2015, Berlin

<u>Schmierer, M.</u>, Asch, F. (2014): Whole-Plant Gas Exchange Characteristics of a Super Dwarf Rice Genotype
Bridging the gap between increasing knowledge and decreasing resources. Conference oral presentation, Tropentag 2014, Prag

Fattahi, N., <u>Schmierer, M.</u>, Asch, F. (2013): Effects of Light Quality and Direction on Growth and Development of Rice
Agricultural development within the rural-urban continuum. Conference poster presentation, Tropentag 2013, Hohenheim

Schmierer, M., Asch, F. Brueck, H. (2013): Indoor Plant Production Systems - Effects of Light Quality on Light Transmission Ratio of Rice Canopies
Agricultural development within the rural-urban continuum. Conference poster presentation, Tropentag 2013, Hohenheim

Schmierer, M., Brueck, H., Asch, F. (2012): Skyfarming – Staple Food Production in Cities – Light vs Energy Demand
Resilience of agricultural systems against crises. Conference poster presentation, Tropentag 2012, Göttingen

Hohenheim, 10. 6. 2020   **Marc Schmierer**